Universität Hamburg

Alterations of host cell physiology in the late phase of *Plasmodium* hepatocyte infection

Dissertation
zur Erlangung der Würde des Doktors der Naturwissenschaften
des Departments Biologie der Fakultät für Mathematik, Informatik
und Naturwissenschaften an der Universität Hamburg

vorgelegt von
Stefanie Gräwe
aus Detmold

Hamburg, Dezember 2010

Genehmigt vom Fachbereich Biologie
der Fakultät für Mathematik, Informatik und Naturwissenschaften
an der Universität Hamburg
auf Antrag von Prof. Dr. V. HEUSSLER
Weitere Gutachterin der Dissertation:
Prof. Dr. I. BRUCHHAUS
Tag der Disputation: 12. November 2010

Hamburg, den 28. Oktober 2010

Professor Dr. Axel Temming
Leiter des Fachbereichs Biologie

LANGUAGE CERTIFICATE

I am a native speaker, have read the present PhD thesis and hereby confirm that it complies with the rules of the English language.

Hamburg, September 14, 2010

(Dr. Kathleen Rankin)

Abstract

Malaria is one of the top three infectious diseases in the developing world. It is mostly restricted to tropical and subtropical regions and causes up to 500 million infections and 2 million deaths per year. The infectious agent that causes Malaria is the protozoan parasite *Plasmodium*, which is transmitted by female *Anopheles* mosquitoes during a blood meal. After inoculation into the vertebrate host the parasite migrates to the liver and develops within hepatocytes before it is shuttled into the blood stream within vesicles termed merosomes. Once released from these merosomes, the parasite infects erythrocytes and causes symptoms of disease. Since the parasite load is low during the apathogenic liver stage, this step of the life cycle is a convenient time period for eradication of the parasite. However, many aspects of liver stage development are still unknown.

Here, live cell imaging was employed to follow parasite and host cell structures and organelles during liver stage development and to understand how they interconnect and change. Initially, a novel red-fluorescent parasite expressing mCherry was generated. It was demonstrated that mCherry is bright and photostable when expressed in *P. berghei* and that it can be used for long-term imaging without photodamage. Using this parasite strain, it was for the first time possible to record the entire *P. berghei* liver stage development from sporozoite invasion to merosome formation in long-term live imaging studies.

An array of other fluorescent parasite strains was then generated and used to identify the origin of the membrane surrounding merosomes and to understand the changes in host cell physiology during the late liver stage. The three membranes that the merosome membrane could originate from - parasite membrane, membrane of the parasitophorous vacuole (PVM) and host cell membrane - were examined in turn. This revealed that the parasite membrane invaginates to become the merozoite membrane and that the PVM disintegrates once merozoite formation is completed. The host cell membrane, in contrast, stays intact for several hours and forms the membrane of the detached cell and of merosomes.

Once the PVM has broken down, the host cell is altered profoundly. The mitochondrial network disintegrates and most likely releases apoptotic factors. Nevertheless, the resulting death of the host cell differs from the normal apoptotic program. While protein biosynthesis is arrested and the turnover rate appears to slow down, phosphatidylserine asymmetry is retained, protecting the newly formed merozoites from the attack of phagocytes. It is proposed that the observed phenotype of detached cells is due to a premature termination of the apoptotic program because of the depletion of energy within the cell. The dismantling of the host cell under retention of the sheltering membrane hereby simultaneously marks the final step in the exploitation of the host hepatocyte by the *Plasmodium* parasite and the first step towards the blood stage.

Zusammenfassung

Malaria ist eine der am weitesten verbreiteten Infektionskrankheiten der Entwicklungsländer. Zu den endemischen Gebieten zählen vor allem tropische und subtropische Regionen, in denen es zu etwa 500 Millionen Infektionen und 2 Millionen Todesfällen pro Jahr kommt. Der verantwortliche Erreger ist der einzellige Parasit *Plasmodium*, der während der Blutmahlzeit von weiblichen *Anopheles*-Mücken übertragen wird. Nach der Inokulation in den Wirbeltierwirt wandert der Parasit zur Leber und entwickelt sich in Hepatozyten, bevor er in Vesikeln, den sogenannten Merosomen, in den Blutstrom transportiert wird. Sobald der Parasit aus diesen Merosomen entlassen wird, infiziert er Erythrozyten und erste Krankheitssymptome treten auf. Da die Parasitenlast im symptomfreien Leberstadium gering ist, bietet sich dieser Abschnitt des Lebenszyklus zur Bekämpfung der Erkrankung an. Viele Aspekte des Leberstadiums sind allerdings noch unbekannt.

Hier wurde der Ansatz der Lebendzell-Beobachtung gewählt, um Strukturen und Organellen des Parasiten und der Wirtszelle durch das Leberstadium hindurch zu verfolgen und zu verstehen wie sie sich verändern und voneinander abhängig sind. Zunächst wurde ein neuer rot-fluoreszierender Parasitenstamm generiert, der mCherry exprimiert. Es wurde gezeigt, dass mCherry bei Expression in *P. berghei* hell fluoresziert, photostabil ist und für Langzeitexperimente verwendet werden kann, ohne phototoxisch zu sein. Unter Verwendung dieses Parasitenstammes war es unter anderem das erste Mal möglich, die gesamte Leberstadienentwicklung von *P. berghei* in einer Langzeit-Lebendzellbeobachtung aufzuzeichnen, beginnend mit der Invasion der Sporozoiten und endend mit der Bildung von Merosomen.

Anschließend wurde eine Auswahl weiterer fluoreszierender Parasitenstämme generiert, um den Ursprung der Membran zu klären, die die Merosomen umgibt, und um die Veränderungen in der Physiologie der Wirtszelle während des späten Leberstadiums zu verstehen. Die drei Membranen, aus denen die Merosomenmembran entstehen könnte - Parasitenmembran, Membran der parasitophoren Vakuole (PVM) und Wirtszellmembran - wurden nacheinander untersucht. Dies zeigte, dass die Parasitenmembran sich einstülpt und zur Merozoitenmembran wird und dass die PVM sich auflöst sobald die Merozoitenbildung abgeschlossen ist. Im Gegensatz dazu bleibt die Wirtszellmembran für mehrere Stunden intakt und bildet die Membran der abgelösten Zellen und Merosomen.

Sobald die PVM zusammengebrochen ist, verändert sich die Wirtszelle erheblich. Das mitochondriale Netzwerk disintegriert und entlässt höchstwahrscheinlich proapoptotische Faktoren. Nichstdestotrotz unterscheidet sich der resultierende Wirtszelltod von einer normalen Apoptose. Während die Proteinbiosynthese zum Stillstand kommt und sich Austauschprozesse verlangsamen, bleibt die Phosphatidylserin-Asymmetrie erhalten. Dies schützt die neu gebildeten Merozoiten vor einem Angriff durch Phagozyten. Es wird vermutet, daß der beobachtete Phänotyp der abgelösten Zellen durch einen frühzeitigen Abbruch des apoptotischen Programms in Folge einer Erschöpfung der Energievorräte der Zelle zustande kommt. Die Demontage der Wirtszelle unter Erhalt der schützenden Membran stellt hierbei gleichzeitig den letzten Schritt in der Ausbeutung des Wirts-Hepatoyzten durch den *Plasmodium*-Parasiten und den ersten Schritt zum Blutstadium dar.

TABLE OF CONTENTS

LIST OF FIGURES

LIST OF TABLES

ABBREVIATIONS

%	percent
°C	degrees Celsius
α	anti
A. stephensi	*Anopheles stephensi*
ACT	artemisinin-based combination therapy
AIF	apoptosis inducing factor
AMA	apical membrane antigen
Apaf	apoptotic protease activating factor
ApoA	apolipoprotein A
ASGR	asiaglycoprotein receptor
ATP	adenosine triphosphate
AWF	advanced model wide-field microscope
bp	base pairs
BSA	bovine serum albumine
BWF	basic model wide-field microscope
CCD	coupled charge device
CD	cluster of differentiation
CDC	Centers for Disease Control
cDNA	complementary DNA
CelTOS	cell traversal protein for ookinetes and sporozoites
CIP	calf intestinal phosphatase
CLS	confocal line scanning microscope
CO_2	carbon dioxide
Cox8	subunit VIII of cytochrome c oxidase
CPS	confocal point scanning microscope
CSP	circumsporozoite protein
Cy	cyanine dye
Dapi	4, 6-diamidino-2-phenylindol
ddH_2O	double distilled water
DDT	dichlordiphenyltrichlorethan

DMSO	dimethylsulfoxide
DNA	desoxyribonucleic acid
dNTP	desoxyribonucleoside 5-triphosphate
E. coli	*Escherichia coli*
E64	L-trans-epoxysuccinyl-leucylamido-(4-guanidino)-butane
ECACC	European Collection of Cell Cultures
EDTA	ethylene diamine tetraacetic acid
EGTA	ethylene glycol tetraacetic acid
et al.	*et alii* (and others)
Exp1	exported protein 1
FBS	foetal bovine serum
FCS	foetal calf serum
g	gram; gravitational force
GAS	genetically attenuated sporozoites
GFP	green fluorescent protein
HepG2	hepatocellular carcinoma line G2
HGF	hepatocyte growth factor
hpi	hours post infection
HSPGs	heparan sulfate proteoglycans
IFN-γ	interferon gamma
IRG	interferon-inducible immunity-related GTPases
IRS	indoor residual spraying
LB	lysogeny broth
LI	laser intensity
LISP	liver-specific protein
LLINs	long-lasting insecticidal nets
LLS	late liver stage
LRP	low density lipoprotein receptor-related protein
M	mole
m	milli
MACPF	membrane attack complex/perforin
MEM	minimum essential medium
Met	mesenchymal-epithelial transition factor

MFI	mean fluorescence intensity
MHC	major histocompatibility complex
min	minute
ml	milliliter
ms	millisecond
MSP	merozoite surface protein
n	nano; number of specimen/experiments
NEB	New England Biolabs
ng	nanogram
NMRI	Naval Medical Research Institute
O_2	oxygen
OD	optical density
p	pico
P. berghei	*Plasmodium berghei*
P. chabaudi	*Plasmodium chabaudi*
P. falciparum	*Plasmodium falciparum*
P. knowlesi	*Plasmodium knowlesi*
P. malariae	*Plasmodium malariae*
P. ovale	*Plasmodium ovale*
P. vivax	*Plasmodium vivax*
P. yoelii	*Plasmodium yoelii*
pbeef1α	*Plasmodium berghei* eukaryotic elongation factor 1 alpha
PbICP	*Plasmodium berghei* inhibitor of cystein proteases
PBS	phosphate buffered saline
PCR	polymerase chain reaction
PFP	pore-forming protein
PGE_2	prostaglandin E2
pH	potential of hydrogen
pSIVA	polarity-sensitive indicator of viability and apoptosis
PVM	parasitophorous vacuole membrane
RAS	radiation-attenuated sporozoites
RBC	red blood cell
RFP	red-fluorescent protein

RNA	ribonucleic acid
RPMI	Roswell Park Memorial Institute
s	second
SAP	sporozoite asparagine-rich protein
SERA	serine repeat antigen
SERCA	sarcoplasmic/endoplasmic reticulum calcium ATPase
SLARP	sporozoite and liver stage asparagine-rich protein
SOC	super optimal broth with catabolite repression
SPATR	sporozoite protein with an altered thrombospondin domain
SPECT	sporozoite microneme protein essential for cell traversal
ssu-rRNA	small subunit ribosomal RNA
STARP	sporozoite threonine asparagine-rich protein
T. gondii	*Toxoplasma gondii*
TAE	Tris base, acetic acid, EDTA
tBHP	tert-butyl hydroperoxide
TGF-β	transforming growth factor beta
TMRE	tetramethylrhodamine ethyl ester
TRAP	thrombospondin-related adhesive protein
U	units
UIS/uis	upregulated in infectious sporozoites
UV	ultraviolet
V	volt
WHO	World Health Organization
x	times
ZEN	Zeiss Efficient Navigation
µ	micro
*µ*g	microgram
*µ*l	microliter
*µ*M	micromolar

CHAPTER 1: INTRODUCTION

1.1 Malaria

1.1.1 The causative agent, the *Plasmodium* parasite

Malaria is an infectious disease caused by the protozoan parasite *Plasmodium* which belongs to the phylum of apicomplexa. It was first discovered in blood samples in 1880 by Charles Laveran but references to infections date back as far as 2700 BC. The resulting illness was known under a variety of names including marsh fever or Roman fever before it was termed malaria. The name stems from the medieval Italian for ‚bad air' (mala aria) because the disease was associated with swamps and marshland. We now know that this is due to the fact that *Plasmodium* is transmitted by mosquitoes of the *Anopheles* species, which find ideal breeding grounds in such areas. Of the 430 known *Anopheles* strains, between 30 and 40 can transmit the parasite (CDC 2009). Transmission from human to human is rare and occurs only via blood transfusions or during birth.

There are about 200 different *Plasmodium* species which differ in their host specificity. Besides humans, they infect monkeys, chimpanzees, rodents, birds and reptiles. Four *Plasmodium* species have long been known to be pathogenic to humans. The most dangerous of them is *Plasmodium falciparum* which causes malaria tropica and is responsible for the majority of fatalities (Haldar, Murphy et al. 2007). The other three strains are characterized by their pattern of recurring fever episodes: *P. malariae* infections are also known as malaria quartana (every 72 hours) and *P. ovale* and *P. vivax* infections as malaria tertiana (every 48 hours). In addition, the simian strain *P. knowlesi* has recently been reported to infect humans; most of these cases occurred in the Asian region (Cox-Singh, Davis et al. 2008). The different *Plasmodium* species vary in their clinical course and geographical distribution.

1.1.2 Prevalence, morbidity and mortality

While malaria was quite common in Europe until the 1960s, it is nowadays mostly restricted to sub-Saharan Africa, Southeast Asia, South and Central America and parts of the Caribbean (Figure 1.1). This is mostly due to the successful application of strategies for controlling the population of the *Anopheles* vector. The infection risk in the endemic areas differs and is dependent upon seasonal and geographical conditions. Overall, two billion people are at risk (WHO 2008). Since many cases occur in rural areas of developing countries and remain undocumented, there are no exact statistics concerning the spread of malaria. The World Health Organization estimates that 300 to 500 million infections and 2 million deaths occur per year (WHO 2010). About 90% of these deaths take place in sub-Saharan Africa. In comparison, less than ten

Figure 1.1: Malaria disproportionately affects tropical and subtropical countries
Areas with a high risk for *Plasmodium falciparum* infection are shown in red. Light pink signifies unstable risk areas while areas in light grey are associated with low risk. Dated 2007. Maps taken from the Malaria Atlas Project (MAP 2007).

deaths a year are reported in Germany and most of these arise after travel to Africa (RKI 2010). Among the population groups that are most at risk are children under the age of five since they develop severe malaria more often than adults. Worldwide, every 30 seconds a child dies of malaria. About 80% of the cases and 90% of the deaths are caused by *P. falciparum* (Mendis, Sina et al. 2001).

1.1.3 Pathology, clinical symptoms and diagnosis

After transmission by an infected *Anopheles* mosquito, the *Plasmodium* parasite undergoes a variable time period of incubation. For *P. falciparum*, symptoms occur after a mean of twelve days, while the other human-pathogenic strains usually take a few days longer (Trampuz, Jereb et al. 2003). The symptoms are only caused after the parasite has reached the blood stage; the preceding liver stage is asymptomatic (see section 1.2). During the blood stage, large numbers of infected erythrocytes rupture and release their cargo of merozoites. This provokes the release of inflammatory cytokines, which ultimately results in flu-like symptoms such as fever, nausea, chills, tiredness, headaches, joint pains, diarrhea and vomiting (Kaiser, Bienz et al. 1998; Sherman 2005; Haldar, Murphy et al. 2007). If infections are not treated, symptoms worsen and include anemia, convulsions, paralysis, coma and even death (Flegel 1976).

One of the reasons why *P. falciparum* infections are the most dangerous is that the parasite inserts proteins into the erythrocyte membrane that mediate adhesion (Rowe, Moulds et al. 1997; Jensen, Magistrado et al. 2004). Infected cells can then either attach to capillary endothelium or form clusters with other infected and uninfected erythrocytes (Sherman 2005; Haldar, Murphy et al. 2007). Both strategies allow the parasite to avoid passage through the spleen where it is in danger of being eliminated. Adhering and clustering erythrocytes form major obstructions in capillaries, especially in high endothelial venules. This disturbs the distribution of oxygen and nutrients and leads to tissue hypoxia and organ damage (Kaiser, Bienz et al. 1998). Especially in the central nervous system the consequences are severe and range from neurological problems to reduced

consciousness and coma. These effects are summed up under the term cerebral malaria and result in death if untreated. Even if treated, 15 to 20 percent of cerebral malaria cases are fatal (WHO 2010).

A very basic indicator for the identification of the different *Plasmodium* species is the time period between recurring fever episodes. As already mentioned, they occur every 48 hours for *P. vivax* and *P. ovale* and every 72 hours for *P. malariae*. In *P. falciparum* infections, though, the fever pattern is irregular and since these are the most dangerous cases, an early diagnosis is vital. In addition, co-infections with different species can lead to unclear patterns. Therefore, parasites are usually examined in a blood smear for morphological identification. A thin film preserves the parasites best and allows identification while a thick film is prepared to detect parasites already at low levels of infection. This method is very sensitive but requires trained personnel. As an alternative, several antigen detection tests are available. After application of the blood sample to the test area, colored strips serve as a read-out. Typical *Plasmodium* enzymes such as *P. falciparum* lactate dehydrogenase are used as antigens. While easy to interpret, these assays only pick up on infections after a certain parasitemia threshold has been reached and do not allow an exact determination of the level of parasitemia. An extremely sensitive method is the analysis of blood samples for *Plasmodium* genetic material by PCR. However, while this is a very accurate diagnosis tool, it is relatively expensive and requires laboratory equipment that is not available in most endemic areas.

1.1.4 Impact on society and economy

Malaria infections cause significant economic damage in the developing world. The total economic impact in Africa alone has been estimated to amount to 12 billion US dollars every year (Greenwood, Bojang et al. 2005). It consolidates health care costs, loss of working and education days, loss of productivity because of brain damage from cerebral malaria and loss of tourism and investment. While the average per capita gross domestic product (adjusted for parity of purchasing power) in countries without malaria rose 2.4% per year between 1965 and 1990, it only grew by 0.4% in countries where malaria was widespread (Sachs and Malaney 2002). Estimations assume that in some countries up to 40% of health care costs and 50% of hospital visits are caused by malaria infections (WHO 2010).

All of these factors feed into a vicious cycle: the widespread poverty results in a low level of education and an insufficient infrastructure and health care system. This in turn makes it difficult to successfully prevent and treat malaria infections and results in high morbidity and mortality rates which lead to even more poverty (Gollin and Zimmermann 2007). This cycle can only be broken by a concerted effort of both the developing and industrialized countries to eradicate malaria.

1.1.5 Approaches to the eradication of malaria

1.1.5.1 Prophylaxis and treatment

The risk of contracting malaria can be greatly reduced by relatively simple means. The first line of defense is the protection from mosquito bites in endemic areas. Since *Anopheles* mosquitoes are mainly active during and after dusk, it is advisable to stay indoors at night. While being outdoors, long clothing, insect repellent and mosquito coils can help to keep the number of bites to a minimum. Beds should be draped with mosquito nets treated with long-lasting insecticidals (LLINs).

If these basic protection measures fail, several antimalarial drugs are available that can be used both preventively and for treatment. They target various steps in the parasite metabolism and often interfere with the conversion of heme to non-toxic, crystalline hemozoin during the blood stage. As a result, reactive heme accumulates and damages parasite membranes and enzymes.

Common drugs used for prophylaxis are mefloquine (sold under the brand name Lariam) and atovaquone-proguanil (brand name Malarone). The dosage used is lower than for treatment, but can nevertheless cause side effects when taken over longer time periods. Therefore and for reasons of cost and availability, chemical prophylaxis is not practical for full time residents of endemic areas. Even for short-term visitors, prophylaxis is usually only administered for travels into high-risk areas. Otherwise, carrying the necessary drugs for a stand-by therapy is sufficient.

Drug resistance against common antimalarial drugs has become widespread. To avoid further spreading of resistances, combination therapies are usually employed. The individual components need to target different molecular structures and need to have an effect against the parasite blood stages independent of each other. Since drug resistances differ from region to region, there is no common treatment regimen. Instead, drugs are chosen depending on the destination of travel. In areas where resistance has not yet spread, chloroquine is still a valid drug for therapy, but in most cases combination therapies include artemisinin or its derivates (artemisinin-based combination therapy, ACT) (WHO 2008). Artemisinin was originally extracted from the leaves of annual wormwood (*Artemisia annua*) but can now be synthesized artificially (Ro, Paradise et al. 2006). It is extremely efficient against *Plasmodium* parasites but its exact mode of action remains unclear. Theories include an inhibition of a parasite SERCA type calcium ATPase (Krishna, Pulcini et al. 2008), damaging of parasite mitochondria (Wang, Huang et al. 2010) and interference with heme detoxification (Pandey, Tekwani et al. 1999). Commonly used formulations are atovaquon-proguanil and artemether-lumefantrin.

If the infection is caused by either *P. vivax* or *P. ovale*, additional treatment with primaquine is required to eliminate dormant parasite stages in the liver (hypnozoites) and the danger of recurring infections (Adak, Sharma et al. 1998).

1.1.5.2 Vaccines

The most promising tool to eradicate malaria is a reliable vaccine producing sterile protection from infection. Several candidates are in development but so far no commercial vaccine is

available. In general they can target either liver stage parasites (pre-erythrocytic vaccines), blood stage parasites (erythrocytic vaccines) or gametocytes (transmission-blocking vaccines).

Of these three groups a successful pre-erythrocytic vaccine is most desirable because it would eliminate the parasite before the transition to the blood stage and therefore before symptoms of malaria occur. The first parasite protein found to elicit protective immune responses was the circumsporozoite protein (CSP) and therefore most vaccines are based on it. The most promising formulation up to date is the subunit vaccine RTS,S/AS02A, which is being developed by GlaxoSmithKline and currently tested in a phase three clinical trial (Walther 2006; Plebanski, Locke et al. 2008). It consists of the immunogenic S antigen of the hepatitis B virus fused to a portion of CSP that contains known epitopes for B as well as CD4 and CD8 T cells. It is administered in combination with the adjuvant AS02A. Vaccination with RTS,S/AS02A has been shown to induce a short-term protection in adults and to reduce the risk of severe malaria infections in children but its overall efficacy is not yet sufficient (Alonso, Sacarlal et al. 2004; Bejon, Lusingu et al. 2008). To further improve the vaccine, a combination with other immunogenic *Plasmodium* proteins is planned (Matuschewski 2006).

For quite some time the question remained why certain parasite proteins could induce protection when used in a subunit vaccine but not during the normal course of a malaria infection. This was compounded when tests showed that a distinct host immune response is generated during liver stage infection (Zhou, Xiao et al. 2002). The puzzle was solved when it was discovered that the resulting blood stage parasites interfered with the formation of a fully functional immune response via mechanisms that are not yet fully understood (Orjih and Nussenzweig 1979; Orengo, Wong et al. 2008). From this it concludes that liver stage infection without a subsequent blood stage should produce protective immunity. Therefore, live parasites were altered either genetically (genetically attenuated sporozoites, GAS) or through irradiation (radiation-attenuated sporozoites, RAS) to prevent their transition to the blood stage. Vaccination with these parasites elicited sterile protection in a majority of the cases (Hoffman, Goh et al. 2002; van Dijk, Douradinha et al. 2005; Jobe, Donofrio et al. 2009). While these results are promising, the use of attenuated parasites for large vaccination campaigns in developing countries is questionable since their preparation and storage is relatively expensive and requires sophisticated equipment.

It is not only the development of pre-erythrocytic stage vaccines that proves to be challenging, though. Although *P. falciparum* inserts numerous foreign proteins into the erythrocyte membrane (Foley and Tilley 1998), it escapes host immune responses due to the extreme antigenic variation of these proteins (Reeder and Brown 1996). Vaccines using proteins that show less polymorphism such as MSP (merozoite surface protein) and AMA (apical membrane antigen) have also failed to generate immunity (Genton 2008; Pinzon-Charry and Good 2008)

The mode of action of the third group of vaccines, the transmission-blocking vaccines, differs from the previous two because it is altruistic. Transmission-blocking vaccines do not protect the infected person from infection but merely stop the infection from spreading to other individuals (Carter 2001). This is achieved by interfering with the development or vitality of parasite gametocytes in the mosquito midgut and therefore preventing the formation of infectious sporozoites. While this approach is clearly beneficial, the low educational standard in endemic areas will make it complicated to explain the use of these vaccines, and therefore implementation might be difficult.

In summary, a candidate fit for widespread vaccination programs has yet to be found but ideally would be a safe, inexpensive pre-erythrocytic vaccine that is easy to store and generates a long-lasting, sterile immunity to malaria infections.

1.1.5.3 Vector control

An alternative approach to the eradication of malaria is the removal of the vector, the *Anopheles* mosquito. This technique has proven successful in Europe, where malaria is virtually extinct today. The draining of marshes and wetlands reduces the breeding grounds of *Anopheles* mosquitoes and therefore their population size. It can be further decreased by the use of insecticides such as DDT (dichlordiphenyltrichlorethan), whose use is now restricted to the control of disease vectors. For areas where resistance against DDT is spreading, the WHO has compiled a list of twelve alternative insecticides including deltamethrin (WHO 2008). On a small scale, indoor walls can be sprayed since *Anopheles* mosquitoes rest on available surfaces after feeding (indoor residual spraying of long-lasting insecticide, IRS). On a large scale, the insecticide can be used to spray whole areas of mosquito breeding grounds. As a biological alternative to chemical pesticides, *Bacillus thuringiensis israelensis* has been planted into typical breeding grounds. It develops within the mosquito larvae and destroys their intestinal lumen, thus arresting their development before hatching (Shililu, Tewolde et al. 2003).

In addition, transgenic mosquitoes are developed that are resistant to *Plasmodium* infection and can therefore not transmit the disease (Ito, Ghosh et al. 2002; Corby-Harris, Drexler et al. 2010). Once their harmlessness has been fully confirmed, they could be released into the wild. For a successful replacement of the wild-type population, the spread of transgenes needs to be driven by selfish genetic elements that favor offspring carrying the transgene (Chen, Huang et al. 2007). Combined, these measures stand a reasonable chance to eradicate a substantial portion of the insect vector and therefore to help control the incidence of malaria infections in endemic areas.

1.2 The *Plasmodium* life cycle

The life cycle of *Plasmodium* is rather complex and involves a mosquito vector and a vertebrate host (Figure 1.2). After transmission of the sporozoite form by the *Anopheles* mosquito the parasite travels to the liver and replicates within hepatocytes during the so-called liver stage. It then moves on to the blood stage where it infects reticulocytes and erythrocytes. A subset of blood stage parasites develops into sexual forms that can then be taken up by mosquitoes during a blood meal. During the subsequent mosquito stage, these sexual forms fuse and ultimately generate new sporozoites that can be transmitted to the next vertebrate host. Since sexual reproduction only takes place in the mosquito vector it is considered the main host for *Plasmodium*. In the following sections, mosquito, liver and blood stages are explained in further detail.

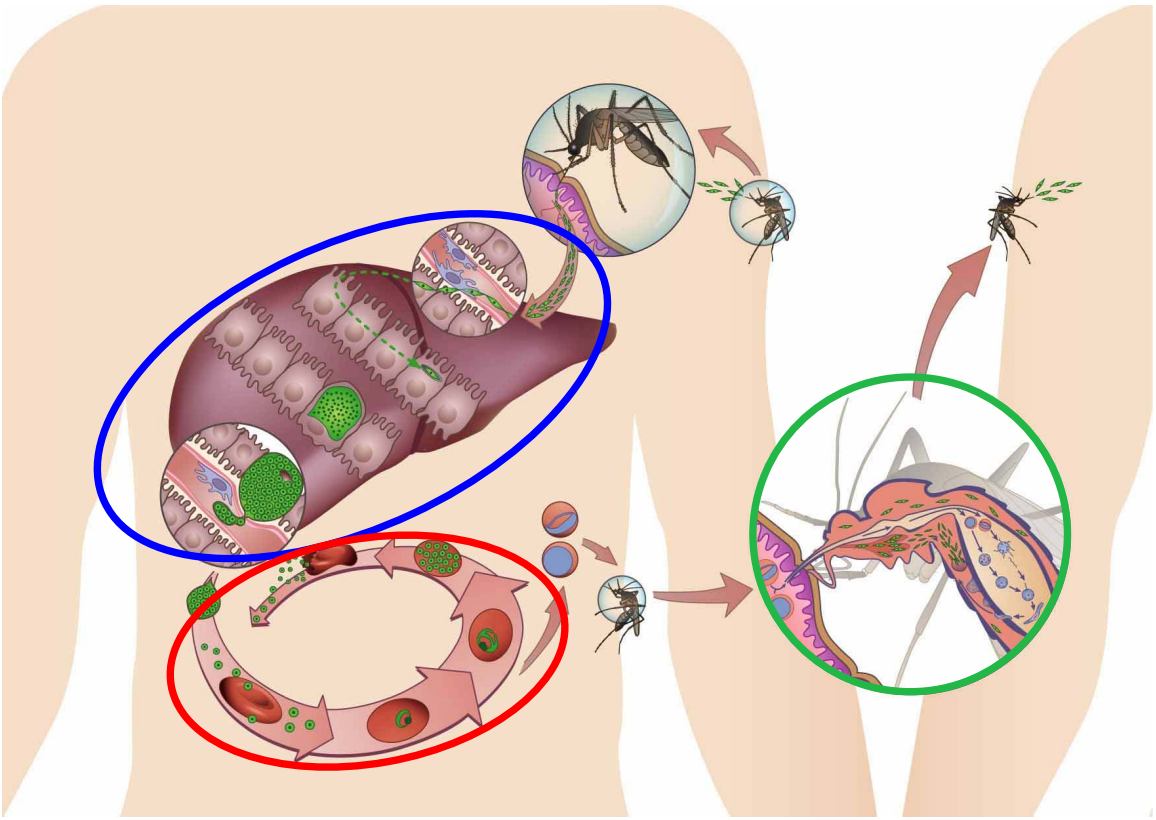

Figure 1.2: The *Plasmodium* life cycle (adapted from Sturm and Heussler 2007)
After inoculation of sporozoites into the skin of the vertebrate host, the parasite enters blood vessels, travels to the liver and invades host hepatocytes. During the liver stage (indicated in blue), it undergoes multiple rounds of nuclear divisions. Towards the end of this process, individual merozoites are formed and delivered into the bloodstream by way of membrane-wrapped vesicles (merosomes). These merosomes travel to the lung capillaries where they burst and release their cargo of merozoites, thus initiating the blood stage (indicated in red). The parasite replicates further in multiple rounds of erythrocyte infection and lysis. Some of the resulting blood stage parasites develop into sexual forms, the gametocytes. They are taken up by *Anopheles* mosquitoes during blood meals. In the following mosquito stage (indicated in green), male and female gametes fuse and transform into an oocyst. Within these oocysts, thousands of sporozoites are formed that ultimately take up residence in the mosquito‘s salivary glands, ready for injection into the next vertebrate host.

1.2.1 The mosquito stage

Male microgametocytes and female macrogametocytes are taken up by the female *Anopheles* mosquito during a blood meal from an infected vertebrate host. Once they have reached the mosquito midgut, sexual development begins. The female macrogametocytes differentiate to macrogametes, and male microgametocytes give rise to flagellated microgametes in a process called exflagellation (Kaiser, Bienz et al. 1998). The micro- and macrogametes then fuse into a motile zygote, the ookinete. This ookinete traverses the midgut epithelium and settles between it and the basal membrane of the midgut. It develops into an oocyst in which asexual reproduction proceeds (Kaiser, Bienz et al. 1998). Thousands of sporozoites are formed during sporogony and are ultimately released into the haemolymph. They are passively carried through the mosquito and take up residence in the salivary glands where they are ready for inoculation into the vertebrate host upon the next blood meal (Sherman 2005). The entire development from gametocytes to infectious sporozoites takes between eight and sixteen days depending on the *Plasmodium* strain and the ambient temperature.

1.2.2 Getting from the skin to the liver

Once sporozoites have been injected into the dermis of the vertebrate host, they actively move through the tissue. This gliding motility is powered by an actin-myosin motor (Matuschewski and Schuler 2008; Soldati-Favre 2008) and requires the interaction between sporozoite surface proteins and its environment (Stewart and Vanderberg 1991; Kappe, Bruderer et al. 1999). The overall movement has shown to be circular *in vitro* (Shorte and Frischknecht 2007) and is assumed to result in a spiralling motion *in vivo* that serves both to reach deeper layers of the dermis and to measure the size of blood vessels. Some of the inoculated sporozoites enter the lymphatic system where they are likely phagocytosed (Amino, Thiberge et al. 2006). Others remain in the skin where they, also, are thought to be taken up by phagocytic cells (Sinnis and Coppi 2007; Amino, Giovannini et al. 2008). Most, however, evade phagocytosis and enter capillaries. They circulate through the bloodstream and are arrested in the liver sinusoids by binding of their surface protein CSP to liver-specific heparan sulfate proteoglycans (HSPGs) (Ying, Shakibaei et al. 1997; Pinzon-Ortiz, Friedman et al. 2001; Pradel, Garapaty et al. 2002; Coppi, Pinzon-Ortiz et al. 2005). HSPGs are anchored on the surface of hepatocytes and thought to extend into the sinus lumen through fenestrations of the blood vessel endothelium (Pradel and Frevert 2001; Coppi, Tewari et al. 2007). Besides their function for the homing of the sporozoite to the liver, they also appear to trigger signal transduction pathways in the sporozoite that are important for the subsequent infection program (Coppi, Tewari et al. 2007).

Initially, though, the sporozoites need to cross the blood vessel endothelium to reach the layers of hepatocytes. They are thought to achieve this by traversing Kupffer cells, the resident macrophages of the liver that line the sinusoids (Pradel and Frevert 2001; Frevert, Engelmann et al. 2005). The inflammatory reaction that would usually be triggered by such traversal is suppressed by the parasite via CSP and by modulating the cell‘s cytokine profile (Usynin, Klotz et al. 2007; Klotz and Frevert 2008). Interestingly, the sporozoites are surrounded by a membrane

while crossing through Kupffer cells (Pradel and Frevert 2001). This is in contrast to the next step where the sporozoites transmigrate several hepatocytes without formation of a parasitophorous vacuole and where cell wounding is evident (Mota, Pradel et al. 2001; Mota, Hafalla et al. 2002). The mechanism of transmigration is not yet understood but some proteins have been shown to be essential since their knock-out leads to a loss of traversal activity. These include SPECT1 and 2 (sporozoite microneme protein essential for cell traversal), a surface phospholipase (formerly known as UIS10), a protein with a membrane attack complex/perforin (MACPF)-related domain and CelTOS (cell traversal protein for ookinetes and sporozoites) (Ishino, Yano et al. 2004; Kaiser, Camargo et al. 2004; Bhanot, Schauer et al. 2005; Ishino, Chinzei et al. 2005; Kariu, Ishino et al. 2006). The purpose of transmigration remains equally elusive, although some theories exist. It is believed that some host cell factors such as the intracellular potassium concentration serve to trigger the exocytosis of apical proteins that are required for infection (Mota, Hafalla et al. 2002; Kumar, Garcia et al. 2007; Ono, Cabrita-Santos et al. 2008). Also, transmigrated hepatocytes have been shown to secrete hepatocyte growth factor (HGF) (Carrolo, Giordano et al. 2003). It has been suggested that this protects neighbouring hepatocytes from apoptosis and primes them for infection (Leiriao, Albuquerque et al. 2005).

While these mechanisms might play a role, they are not essential for subsequent invasion. Knock-out sporozoites incapable of traversal can still infect hepatocytes *in vitro*. They cannot, however, reach hepatocytes *in vivo* if they are injected intradermally. Likely, the traversal activity is required for exiting the dermis (Amino, Giovannini et al. 2008) and crossing the blood vessel endothelium via Kupffer cells. If knock-out sporozoites are injected intravenously and Kupffer cells are depleted, infection proceeds as normal (Ishino, Yano et al. 2004; Kariu, Ishino et al. 2006). Interestingly, a knock-out of the surface phospholipase formerly known as UIS10 leads to a failure to exit from the dermis while Kupffer cells can still be traversed (Bhanot, Schauer et al. 2005). Apparently, different mechanisms are used for these transmigration processes. In any case, after the sporozoite has encountered and usually traversed several hepatocytes, invasion into the final host cell takes place. This step requires the sporozoite proteins Pbs36p and Pbs36 since their disruption leads to continuous traversal (Ishino, Chinzei et al. 2005).

1.2.3 The liver stage

Invasion into the hepatocyte is mostly driven by sporozoite motility and requires multiple interactions between the parasite and the host cell. Several sporozoite surface proteins have been shown to mediate binding to hepatocytes, including STARP (sporozoite threonine asparagine-rich protein), TRAP (thrombospondin-related adhesive protein), SPATR (sporozoite protein with an altered thrombospondin domain) and likely AMA-1 (apical membrane antigen) (Fidock, Bottius et al. 1994; Pasquetto, Fidock et al. 1997; Chattopadhyay, Rathore et al. 2003; Lopez, Garcia et al. 2003; Silvie, Franetich et al. 2004; Morahan, Wang et al. 2009). Among the binding sites required on the hepatocyte are Fetuin-A, CD81 and LRP (low density lipoprotein receptor-related protein) (Shakibaei and Frevert 1996; Silvie, Rubinstein et al. 2003; Jethwaney, Lepore et al. 2005). Upon successful attachment of the sporozoite, the host cell membrane invaginates and becomes the

membrane of a parasitophorous vacuole (PVM) (Meis, Jap et al. 1983; Bano, Romano et al. 2007). During and after formation, this PVM is modified extensively by the parasite; host cell proteins are removed and parasite proteins inserted. Several key players of this process have already been identified. The parasite proteins P52 and P36 are essential for the formation of the parasitophorous vacuole in general (Labaied, Harupa et al. 2007; van Schaijk, Janse et al. 2008). Once it has been formed, uis3 and 4 (upregulated in infectious sporozoites) appear to play a role during further PVM maintenance since their loss results in developmental arrest shortly after invasion (Mueller, Camargo et al. 2005; Kumar, Baxter et al. 2009). The expression of several of these proteins is controlled by a transcription factor that has been simultaneously named SAP1 (sporozoite asparagine-rich protein) and SLARP (sporozoite and liver stage asparagine-rich protein) (Aly, Mikolajczak et al. 2008; Silvie, Goetz et al. 2008). The disruption of SAP1/SLARP results in an impairment in PVM remodelling and developmental arrest early after invasion.

After successful invasion, the sporozoite settles near the host cell nucleus and a period of rapid growth and nuclear amplification begins (Bano, Romano et al. 2007). Since the development of the parasite during the liver stage is described in detail in section 1.3.1, only a brief overview is given here. The parasite begins reproduction by undergoing several rounds of nuclear division. The resulting nuclei are surrounded by both the PVM and the parasite plasma membrane. After this process is completed, the parasite membrane invaginates to form individual merozoites, which are still contained within the parasitophorous vacuole (Sturm, Graewe et al. 2009). Soon, though, the PVM ruptures and the merozoites are released into the host cell cytoplasm. The entire cell begins to detach and sets of merozoites are shuttled into the so-called merosomes, small vesicles that bud off of the host hepatocyte (Sturm, Amino et al. 2006). The length of time between invasion and formation of these merosomes depends on the *Plasmodium* species and ranges from two days for *P. berghei* to fifteen days for *P. malariae* (Kaiser, Bienz et al. 1998; Sturm, Amino et al. 2006). In *in vivo* infections, forming merosomes expand directly into blood vessels. They eventually dissociate from the main cell body and travel to the lung capillaries where they rupture and release their cargo (Baer, Klotz et al. 2007). This marks the beginning of the blood stage.

1.2.4 The blood stage

Once the infectious merozoites have been released from the merosomes, they are free within the blood stream. Depending on the *Plasmodium* strain they quickly attach to erythrocytes, reticulocytes or both. Initial attachment likely occurs by random collision followed by adhesion via specific proteins. Among the proteins involved are several members of the MSP family (Cowman and Crabb 2006). During the next step, the merozoite reorients itself until its apical pole is in contact with the surface of the RBC (red blood cell). The parasite surface protein AMA-1 has been shown to be essential for this process (Mitchell, Thomas et al. 2004).

After reorientation, the host cell is invaded. The RBC membrane invaginates as the parasite enters the cell. The driving force of this interaction is not yet understood but is assumed to involve a parasite motor complex similar to the *Toxoplasma gondii* invasion machinery (Pinder, Fowler et al. 2000). Once invasion is completed, the parasite is again surrounded by a PVM. Whether this

PVM is of host cell or parasite origin is still under debate. Likely, it is a combination of both: the RBC membrane invaginates and forms the PVM, which is then cleared of RBC membrane proteins and enriched with proteins and membrane stretches produced by the merozoite.

Within the parasitophorous vacuole, the parasite now develops first into a ring form, then into a mononuclear trophozoite and finally into a syncytic schizont similar to the liver stage (Kaiser, Bienz et al. 1998; Sherman 2005). During this growth process it obtains nutrients by taking up host cell hemoglobin and breaking it down in an acidic food vacuole (Rosenthal and Meshnick 1996). This process releases heme, which catalyzes the production of reactive oxygen species and is therefore damaging. The parasite detoxifies heme by converting it into crystalline hemozoin, which is then stored in the food vacuole (Sullivan 2002). The release of hemozoin upon parasite egress from the host cell is one of the factors triggering the fever spikes that are characteristic for malaria infections.

After nuclear division has finished, the parasite membrane invaginates and up to 36 merozoites are formed (Kaiser, Bienz et al. 1998; Sherman 2005). Then, the PVM and the host cell membrane rupture in quick succession (Salmon, Oksman et al. 2001; Wickham, Culvenor et al. 2003). The merozoites are propelled outwards and brought into contact with fresh RBCs for the next cycle of invasion and replication. The time passing between invasion and discharge of daughter merozoites depends on the *Plasmodium* strain and takes between 24 and 72 hours (Kaiser, Bienz et al. 1998). Some of the merozoites do not simply replicate within the RBC but differentiate into male microgametocytes and female macrogametocytes (Kaiser, Bienz et al. 1998; Sherman 2005). These can be taken up by an *Anopheles* mosquito during a blood meal and constitute the beginning of the mosquito stage.

1.3 A closer look at the *Plasmodium* liver stage

The liver stage is a platform of immense replication for the *Plasmodium* parasite. At the same time, it is asymptomatic and thus offers interesting possibilities for treatment and vaccine design. The following sections explain the clinical relevance of the liver stage, detail the current state of knowledge and introduce the malaria research model that was used in this study. They address the questions: why is the liver stage so important? What do we know about it so far? And how can we find out more?

1.3.1 Clinical relevance

The liver stage of the *Plasmodium* life cycle is of great interest for the worldwide effort to eradicate malaria since it offers points of attack on several levels.

Treatment of a malaria infection at this stage would have a whole range of beneficial side effects. For one, transition to the blood stage and its often disastrous symptoms would not occur

and fatalities could be avoided. At the same time, the risk of transmission would be eliminated because *Anopheles* mosquitoes can only take up parasites circulating in the blood stream. In addition, treatment at this early point of infection is more likely to succeed since the parasite load is comparatively low.

The liver stage is not only a good target for treatment, though, but also for vaccine development. It has several advantages over an erythrocytic stage vaccine. For one, while candidate proteins for erythrocytic stage vaccines are difficult to find due to extreme antigen polymorphism, the liver stage expresses a number of very stable antigens. In addition, whereas the host erythrocyte is only capable of basic functions, the liver stage host cell is fully operational and can present parasite antigen via a full set of MHC (major histocompatibility complex) molecules. This aids the mounting of a host immune response and makes the infected cells more accessible to cytotoxic T cells. Despite that, there is no natural immunity against malaria infections. Instead, only a moderately protective effect is observed in endemic areas, that mediates a partial immunity against severe malaria (Walther 2006). This is because the subsequent blood stage prevents the formation of a full immune response against the liver stage. The exact mechanisms behind this phenomenon are not yet understood but seem to involve the suppression of dendritic cells and T cells via inhibitory cytokines (Orjih and Nussenzweig 1979; Ocana-Morgner, Mota et al. 2003; Ocana-Morgner, Wong et al. 2007; Orengo, Wong et al. 2008). If the transition to the blood stage is blocked either by drugs or by using attenuated parasites, vaccination can result in sterile protective immunity (Nussenzweig 1980; van Dijk, Douradinha et al. 2005; Matuschewski 2006; Walther 2006; Jobe, Lumsden et al. 2007; Mueller, Deckert et al. 2007; Purcell, Yanow et al. 2008). Therefore, various live attenuated vaccines are currently designed to mimic or carry out liver stage infection without progression to the blood stage, thus leading to protection from malaria.

Although some of these vaccines show promise, it is clear that their efficacy and availability need to be improved. At the same time, the evolving resistance against commonly used, inexpensive drugs makes it necessary to identify novel drug targets. For both of these objectives, it is essential to understand the liver stage of *Plasmodium* parasites in as much detail as possible.

1.3.2 *Plasmodium* and host cell development in detail

Despite its importance for drug and vaccine development, surprisingly little is known about the *Plasmodium* liver stage to date. While the basic developmental steps have been identified (Figure 1.3), the underlying molecular mechanisms remain mostly unclear.

After invasion into the host hepatocyte and formation of a parasitophorous vacuole the parasite undergoes an initial period of comparatively subtle changes. As already mentioned previously, it settles in a perinuclear location and remodels its PVM. Several proteins are known to be important for this early stage since their knock-out led to an impairment in development. Among them are uis3 and 4 as well as Pb36p (Mueller, Camargo et al. 2005; Mueller, Labaied et al. 2005; van Dijk, Douradinha et al. 2005). Their exact role, however, has not yet been resolved.

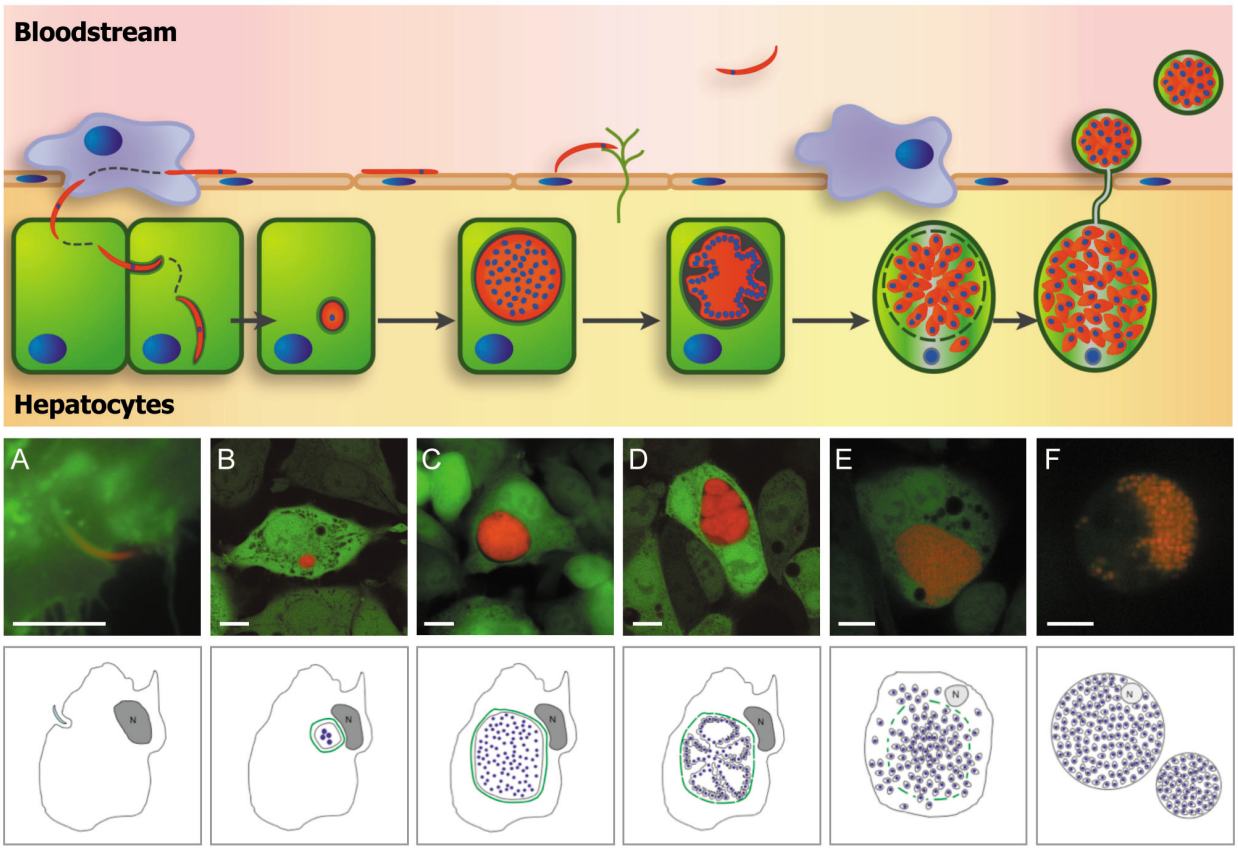

Figure 1.3: Current model of *Plasmodium* liver stage development (adapted from Sturm, Graewe et al. 2009; Rankin, Graewe et al. 2010)
The known steps of the *Plasmodium* liver stage development are shown in an illustration in biological context (top panel), in fluorescence images of HepG2-GFP cells infected with *P. berghei*-mCherry parasites (middle panel) and in corresponding schematic drawings (bottom panel). Bars = 10 μm.
After adhering to HSPGs (green), *Plasmodium* parasites (red in the upper and middle panels) glide along the blood vessel endothelium. They then enter the liver through Kupffer cells (purple in the top panel) and subsequently first transmigrate and then invade hepatocytes (green in the top and middle panels) (A). In the host cell they are surrounded by a parasitophorous vacuole membrane (indicated in green in the bottom panel). Within this vacuole, they develop into a multinucleate schizont (B and D). Once nuclear division is completed, the parasite membrane invaginates around groups of nuclei (D) and ultimately individual merozoites. The PVM ruptures and releases these merozoites into the host cell cytoplasm (E). The host cell detaches and merozoites are packaged into merosomes for transport into the blood vessels (F).

At approximately twenty hours after invasion, the parasite nucleus starts dividing repeatedly and displays one of the fastest replication rates known for eukaryotes: during the next 35 hours up to 29.000 nuclei are generated (Baer, Klotz et al. 2007; Bano, Romano et al. 2007). At the same time, the parasitophorous vacuole extends in size to accommodate the growing parasite. During blood stage replication, the parasite is known to take up hemoglobin from its host cell and to digest it in a food vacuole (Rosenthal and Meshnick 1996). So far no similar structure has been described in the liver stage. It is therefore still unknown how the parasite manages to obtain the resources necessary for its immense reproduction effort within the hepatocyte. Apart from the endoplasmatic reticulum, which gathers around the parasite, there appears to be no association to host cell organelles (Bano, Romano et al. 2007). It has been speculated that the parasite inserts transport channels designed for nutrient uptake into the PVM (Bano, Romano et al. 2007; Sturm, Graewe et al. 2009).

So far only few parasite proteins have been identified that might orchestrate liver stage growth. One of them is the protein ApoA1 that was found to localize to the parasitophorous vacuole around 24 hours after invasion. It might interact with uis4 and is speculated to play a role in the synthesis of additional membrane during the enlargement of the vacuole (Prudencio, Rodriguez et al. 2006).

Interestingly, during its growth to a syncytic schizont the parasite suppresses the apoptotic program in its host cell (van de Sand, Horstmann et al. 2005). It is not yet understood how exactly this resistance to apoptosis stimuli is conferred but at least initially HGF/Met-signalling has been suggested to play a role (Leiriao, Albuquerque et al. 2005). A number of proteins that influence host cell behaviour are known to be secreted during the blood stage (Foley and Tilley 1998). For the liver stage, though, such proteins are mostly still unknown. A recently identified cysteine protease inhibitor, PbICP (*Plasmodium berghei* inhibitor of cystein proteases), is the first definite candidate suspected to play a role in the suppression of host cell death (Rennenberg, Lehmann et al. 2010).

After parasite growth and nuclear division are completed, the parasite membrane begins to invaginate around groups of nuclei. This forms the cytomere stage, which continues on to the merozoite stage through further invagination of the parasite membrane around invididual nuclei and organelle sets (Sturm, Graewe et al. 2009). It is unclear how parasite organelles are distributed to each merozoite. Recent studies have revealed that both mitochondria and apicoplasts grow as a branched network which ultimately subdivides into individual organelles (Stanway, Witt et al. 2009; personal communication). The mechanisms driving and controlling this subdivision, however, are still elusive. It seems, though, that incomplete distribution of parasite organelles to merozoites results in developmental arrest of the parasite.

After the formation of merozoites, they are clustered within the parasitophorous vacuole. Soon after, the PVM is thought to break down and release merozoites into the host cell cytoplasm (Sturm, Amino et al. 2006; Sturm, Graewe et al. 2009). It is unknown which signals trigger and which proteins execute PVM breakdown. It has been shown, though, that the general cysteine protease inhibitor E64 prevents breakdown and therefore cysteine proteases are suspected to play a role (Sturm, Amino et al. 2006). This would be a parallel to the blood stage where different sets of proteases are involved in the destabilization of the PVM and the host cell membrane before parasite release (Wickham, Culvenor et al. 2003). A protein that has recently been implicated in PVM breakdown is the liver-specific protein 1 (LISP1) but mechanistic details are still unknown (Ishino, Boisson et al. 2009).

Once the PVM has broken down, the host cell begins to detach. In *in vivo* infections, it remains within the liver tissue, whereas in *in vitro* infections it floats in the culture supernatant. Small vesicles bud off that contain a variable number of merozoites. *In vivo*, these so-called merosomes are released directly into blood vessels (Sturm, Amino et al. 2006). Through these they travel to the lung capillaries where they rupture and release the infectious merozoites to initiate the blood stage (Baer, Klotz et al. 2007).

During this last stage of development, the host cell undergoes an atypical cell death (Sturm, Amino et al. 2006). It exhibits some features of apoptosis such as cytochrome c release and nuclear condensation but lacks most of its effector mechanisms. Neither activation of the caspase cascade nor DNA fragmentation are observed. Furthermore, the phosphatidylserine asymmetry of the outer membrane is conserved, which ensures that the cell remains inconspicuous to the immune system. It has been speculated that the parasite employs the host cell membrane in a

Trojan horse strategy. Merosomes are believed to be surrounded by it on their way to the lung, thus masking the merozoites and protecting them from being recognized by the host immune system. Final proof of this theory is still lacking, though, since attempts to stain the membrane of merosomes for typical hepatocyte surface markers have failed (Baer, Klotz et al. 2007). It is also unclear how the atypical host cell death in general is orchestrated to suit the needs of the parasite.

1.3.3 *Plasmodium berghei*, a rodent malaria model system

A main reason for the relative ignorance about *Plasmodium* liver stage development is the difficulty associated with studying *P. falciparum* during this stage. Until recently *P. falciparum* liver stages could only be cultured in primary human hepatocytes which were difficult to obtain and could not be kept in culture over longer time periods. Meanwhile, a human hepatoma cell line has been identified that can serve as a host cell for *P. falciparum* liver stage development (Karnasuta, Pavanand et al. 1995). However, this system does not allow the investigation of more complex interactions, e.g. between the parasite and the host immune system. Only an animal model can provide these settings and help to answer fundamental questions.

In addition, the culture of *P. falciparum* liver stages is difficult because it requires the presence of infected mosquitoes. Since these mosquitoes could also transmit malaria to humans, their keeping calls for special security measures that are only met in a safety level three insectary. Only few laboratories possess the equipment necessary for this. In contrast, safety level two conditions which are needed for the culture of strains that are only pathogenic to animals can be found in many research facilities.

A commonly chosen animal model is the rodent model since many cellular processes closely resemble the human system. Several rodent *Plasmodium* strains display similar morphology, physiology and symptoms as human-pathogenic strains (Carter and Diggs 1977). Among them are *P. berghei*, *P. chabaudi* and *P. yoelii*. The strain used in this study is *P. berghei* which was initially described by Vincke and Lips in 1948 (Vincke and Lips 1948). Its natural host is the thicket rat *Gramnomys surdaster* from Central Africa. Unfortunately, *Gramnomys surdaster* is unfit for laboratory purposes for several reasons: it is difficult to breed and to manipulate genetically. Also, close to no antibody reagents for staining of the host cell are available. Therefore, the NMRI mouse model was chosen as the vertebrate host.

Female *Anopheles stephensi* mosquitoes served as the insect vector during the *P. berghei* life cycle. They were allowed to feed on an infected mouse and after an incubation period *P. berghei* sporozoites could be dissected from the salivary glands. These sporozoites were then used to infect hepatocytes *in vivo* or the hepatoma cell line HepG2 *in vitro*. While it would be preferable to perform all studies about parasite development in an *in vivo* setting, this is near impossible due to its inaccessibility for analysis. Therefore, *in vitro* models are invaluable to gain insights into the parasite liver stage. To the best of current knowledge, the liver stage of the *Plasmodium* parasite in *in vitro* model systems does not differ significantly from *in vivo* development.

1.4 Project introduction

It is obvious from section 1.3.2 that the specifics of the *Plasmodium* liver stage development are mostly unknown. In addition, major gaps remain in the current knowledge of even the basic developmental steps.

As with any complex system, it is often difficult to find a starting point to understand the mechanisms at play. The observation of specimen by microscopy has been used as an elegant solution for this problem for a long time and recent advances in molecular biology and technology open whole new worlds of imaging. Parasites can now be genetically modified to express fluorescent proteins either cytosolically or targeted to specific organelles (Janse, Ramesar et al. 2006). At the same time, the development of more and more sophisticated microscopy hard- and software allows the acquisition of high-quality confocal images of such specimen over time. This enables us to follow parasite and host cell structures and organelles during liver stage development and to understand how they interconnect and change.

Obviously, this requires bright, photostable fluorescent proteins that can be imaged at minimal laser intensity to avoid photodamage to the specimen. Therefore, the first objective of this study was to find a suitable red-fluorescent protein that could be expressed in *P. berghei* parasites and used for imaging throughout the whole liver stage.

The second objective was to identify the origin of the membrane surrounding merosomes. In principle, there were three candidate membranes: the parasite membrane, the membrane of the parasitophorous vacuole and the host cell membrane. Each of these membranes should be made visible for confocal fluorescence imaging either by staining or by transgenic expression of fluorescent proteins. The fate of all three membranes during late liver stage parasite development should then be observed live.

The third objective of this study was to shed light on the changes in host cell physiology during the late liver stage. Several aspects such as mitochondrial activity and protein distribution should be observed in live imaging setups to further the understanding of the parasite-dependent host cell death that is observed towards to end of liver stage parasite development.

CHAPTER 2: MATERIALS AND METHODS

2.1 Materials

2.1.1 Technical and mechanical devices

Table 2.1: Technical and mechanical devices

Type	Model	Manufacturer/Distributor
Agarose gel electrophoresis chamber	Horizon® 58 PerfectBlue™	Gibco, Karlsruhe PEQLAB, Erlangen
Analytical scale	KERN 410	Kern & Sohn GmbH, Balingen-Frommern
Basic fluorescence microscope	Leitz DM RB	Leica, Bentheim
Basic fluorescence microscope	Axiovert 200	Zeiss, Hamburg
Binocular	KL 1500LCD	Zeiss, Hamburg
Cell culture incubator	B5060EK-C02 B6200	Heraeus, Hannover Heraeus, Hannover
Centrifuges	5415C 5417 4K10 1-15K Minifuge T J2-H5 J2-21	Eppendorf, Hamburg Eppendorf, Hamburg Sigma, Steinheim Sigma, Steinheim Heraeus, Hannover Beckmann, Krefeld Beckmann, Krefeld
Digital camera	C4742-95	Hamamatsu, Herrsching
Fluorescence binocular	SMZ 800	Nikon, Duesseldorf
Light microscope	Axiovert 25	Heraeus, Hannover
Magnetic stirrer	RET basic	IKA Labortechnik, Hamburg
Microscopes - light - basic model wide-field - advanced model wide-field - confocal point scanning - confocal line scanning	 Axiovert 25 Axiovert 200 Observer Z.1 FluoView 1000 LSM5 Live	 Zeiss, Jena, Germany Zeiss, Jena, Germany Zeiss, Jena, Germany Olympus, Hamburg, Germany Zeiss, Jena, Germany
Microwave	R-208	Sharp Electronics, Hamburg, Germany
Mosquito incubator	Climacell-707	MMM-Group, Graefelfing, Germany
PCR machines	MJ Mini™ T3000	Bio-Rad, Munich, Germany Biometra, Goettingen, Germany

continued on next page

Type	Model	Manufacturer/Distributor
pH meter	pH Level 1	InoLab, Weilheim, Germany
Photometer	Bio-Photometer	Eppendorf, Hamburg, Germany
Pipetting aid	Pipetus®-akku	Hirschmann, Eberstadt, Germany
Power supplies	Consort E835 Consort EV231 EPS 3500	Consort, Turnhout, Belgium Consort, Turnhout, Belgium Amersham Biosciences, Freiburg, Germany
Scale	TP-3002	Denver Instrument, Goettingen, Germany
Shaker	Innova™ 4400 KS250 Basic	New Brunswick, Nuertingen, Germany IKA Labortechnik, Hamburg, Germany
Sterile benches	BSB 6A Herasafe	Gelaire Flow Laboratories, Opera, Italy Heraeus Instruments, Osterode, Germany
Thermo incubators	Thermomixer 5436 Thermomixer compact Thermomixer comfort	Eppendorf, Hamburg, Germany
Transfection device	Nucleofector II	Amaxa biosystems, Cologne, Germany
Tweezers	neoLab-Dumont Pinzette Inox Nr. 5	neoLab Migge Laborbedarf-Vertriebs GmbH, Heidelberg, Germany
UV transilluminator	UV-Flächenstrahler	Konrad Bender, Wiesloch, Germany
Vortex	VF2 Vortex Genie 2	IKA Labortechnik, Hamburg, Germany Scientific Industries Inc, New York, USA
Water bath	FBH 604 SW 20	Fisherbrand®, Schwerte, Germany Julabo, Seelbach, Germany

2.1.2 Labware and disposables

Table 2.2: Labware and disposables

Type	Specification	Manufacturer/Distributor
Cell culture flasks	250 ml	Sarstedt, Nuernbrecht-Rommelsdorf, Germany
Cell culture plates	24-well	Greiner, Solingen-Wald, Germany
Coverslips	round 13 mm	Menzel&Glaser, Braunschweig, Germany
Cuvettes	Halbmikro-Einmalkuevette 1.5-3 ml	Eppendorf, Hamburg, Germany
Falcon tubes	15 ml and 50 ml	Sarstedt, Nuernbrecht-Rommelsdorf, Germany
Glass bottom dishes	Willco®Dish	WillCo Wells BV, Amsterdam, NO
Microscope slides	SuperFrost® Polysine slides	Roth, Karlsruhe, Germany Mentel GmBH, Braunschweig, Germany

continued on next page

Type	Specification	Manufacturer/Distributor
Mounting medium	Dako Fluorescent mounting medium	Dako Cytomation, Hamburg, Germany
Needles	Sterican	Braun, Melsungen, Germany
Parafilm	Parafilm „M“®	American Can Company, Greenwich, Great Britain
Pasteur pipets	---	Brand, Wertheim, Germany
Petri dishes	9 cm	Sarstedt, Nuernbrecht-Rommelsdorf, Germany
Plastic pipet tips	10µl / 200µl / 1000 µl	Sarstedt, Nuernbrecht-Rommelsdorf, Germany
Plastic pipets	5 ml / 10 ml / 25 ml	Sarstedt, Nuernbrecht-Rommelsdorf, Germany
Reaction tubes	1.5 ml / 2 ml 1.5 ml Nerbe PCR Softtubes 0.2 ml CryoTube™ vials	Eppendorf, Hamburg, Germany Nerbe plus, Winsen/Luhe, Germany Biozym, Oldendorf, Germany Nunc, Roskilde, Denmark
Surgical scissors	13 cm	Hauptner, Zurich, Switzerland
Syringes	BD-Micro-Fine 0.5 ml	BD Medical, Franclin Lakes, USA

2.1.3 Chemicals and biological reagents

Table 2.3: Chemicals and biological reagents

Chemical or biological reagent	Manufacturer/Distributor
2-(*N*-morpholino)ethanesulfonic acid (MES)	Roth, Karlsruhe, Germany
Accutase	PAA Laboratories GmbH, Pasching, Austria
Agarose	Bio&Sell, Nuernberg, Germany
Alsever‘s solution	Sigma, Steinheim, Germany
Amaxa® Human T Cell Nucleofector® kit	Lonza, Cologne, Germany
Amphotericin	PAA Laboratories GmbH, Pasching, Austria
Ampicillin	Sigma-Aldrich, Taufkirchen, Germany
Antibodies	see 2.6.2
Aqua ad iniectabilia Delta Select	Delta Select GmbH, Pfullingen, Germany
Bromephenol blue sodium salt	Merck, Darmstadt, Germany
Calcium chloride	Sigma-Aldrich, Taufkirchen, Germany
Calf intestinal phosphatase (CIP)	New England Biolabs, Frankfurt, Germany

continued on next page

Chemical or biological reagent	Manufacturer/Distributor
Chloramphenicol	Sigma-Aldrich, Taufkirche, Germany
Cycloheximide	Sigma-Aldrich, Taufkirche, Germany
Dako Fluorescent Mounting Medium	Dako, Cambridgeshire, UK
Dimethylsulfoxide (DMSO)	Sigma, Steinheim, Germany
dNTP-Mix	Roth, Karlsruhe, Germany
Domitor®	Pfizer GmbH, Karlsruhe, Germany
Dulbecco‘s phosphate buffered saline (PBS, 1x)	Invitrogen™, Karlsruhe, Germany
EDTA sodium salt (ethylene diamine tetraacetic acid)	Biomol, Hamburg, Germany
EGTA sodium salt (ethylene glycol tetraacetic acid)	Roth, Karlsruhe, Germany
Ethanol (100%)	Roth, Karlsruhe, Germany
Ethidiumbromide (1%)	Biomol, Hamburg, Germany
Foetal Bovine/Calf Serum (FBS/FCS)	PAA Laboratories GmbH, Pasching, Austria
Formaldehyde	Merck, Darmstadt, Germany
Gentamicin-ratiopharm®80 SF	Ratiopharm GmbH, Ulm, Germany
Glucose	Roth, Karlsruhe, Germany
Glutaraldehyde	Sigma-Aldrich, Taufkirchen, Germany
Glycerol	Roth, Karlsruhe, Germany
Hank‘s buffered saline solution	PAA Laboratories GmbH, Pasching, Austria
Heparin-Sodium-25000	Ratiopharm GmbH, Ulm
Hoechst 33342 (BisBenzimide H33342 trihydrochloride)	Molecular Probes, Leiden, Netherlands
Hydrochloric acid (37%)	Roth, Karlsruhe, Germany
Hyperladder DNA markers	Bioline, Luckenwalde, Germany
Isopropanol	Roth, Karlsruhe, Germany
Kanamycin	Sigma-Aldrich, Taufkirche, Germany
Ketavet® (100 mg/ml)	Pfizer GmbH, Karlsruhe, Germany
L-glutamine (100x)	PAA Laboratories GmbH, Pasching, Austria
LB-Agar (Lennox)	Roth, Karlsruhe, Germany
LB-Media (Lennox)	Roth, Karlsruhe, Germany
Live/Dead reduced biohazard cell viability kit #1	Molecular Probes, Leiden, Netherlands
LysoTracker® Red DND-99	Molecular Probes, Leiden, Netherlands

continued on next page

Chemical or biological reagent	Manufacturer/Distributor
Lysozyme (from hen egg white)	Roche Diagnostics, Mannheim, Germany
Magnesium chloride	Roth, Karlsruhe, Germany
Magnesium sulfate	Roth, Karlsruhe, Germany
Mangane chloride	Sigma-Aldrich, Taufkirchen, Germany
MEM with Earle‘s salts withouth L-glutamine	PAA Laboratories GmbH, Pasching, Austria
Methanol	Roth, Karlsruhe, Germany
MidRange polymerase	Peqlab Biotechnologie GmbH, Erlangen, Germany
MitoTracker® Green FM	Molecular Probes, Leiden, Netherlands
MOPS solution	Sigma-Aldrich, Taufkirchen, Germany
MyBudget PCR Aufreinigungskit	BioBudget Technologies GmbH, Krefeld, Germany
Nucleofector V solution	Amaxa biosystems, Cologne, Germany
NucleoSpin® Blood QuickPure	Macherey&Nagel, Dueren, Germany
NucleoSpin® Extract II	Macherey&Nagel, Dueren, Germany
NucleoSpin® Plasmid	Macherey&Nagel, Dueren, Germany
Nycodenz	AXIS-SHIELD Poc AS, Oslo, Norway
Paraformaldehyde	Fluka, Steinheim, Germany
Penicillin/Streptomycin-Mix (100x)	PAA Laboratories GmbH, Pasching, Austria
Phalloidin 488/568	Molecular Probes, Leiden, Netherlands
Phusion™ High Fidelity DNA polymerase	Finnzymes/New England Biolabs, Frankfurt am Main, Germany
Potassium acetate	Sigma-Aldrich, Taufkirchen, Germany
Potassium chloride	Roth, Karlsruhe, Germany
Propidium iodide	Sigma-Aldrich, Taufkirche, Germany
pSIVA	kindly provided by Yujin Kim, USC, USA
Pyrimethamine	Sigma, Steinheim, Germany
Restriction enzyme buffers	New England Biolabs, Frankfurt, Germany
Restriction enzymes	New England Biolabs, Frankfurt, Germany
Rompun (xylazine, 2%)	Bayer, Leverkusen, Germany
RPMI 1640	PAA Laboratories GmbH, Pasching, Austria
Saccharose	Sigma, Steinheim, Germany
Silicone oxide	Sigma, Steinheim, Germany
Sodium acetate	Biomol, Hamburg, Germany

continued on next page

Chemical or biological reagent	Manufacturer/Distributor
Sodium borohydride	Roth, Karlsruhe, Germany
Sodium chloride	Roth, Karlsruhe, Germany
Sodium iodide	Roth, Karlsruhe, Germany
T4 DNA ligase	New England Biolabs, Frankfurt am Main, Germany
Taq polymerase (GoTaq)	Promega, Mannheim, Germany
tBHP	Sigma-Aldrich, Taufkirchen, Germany
Tetracycline	Sigma-Aldrich, Taufkirchen, Germany
Tetramethylrhodamine ethyl ester, perchlorate (TMRE)	Molecular Probes, Leiden, Netherlands
Tris	Biomol, Hamburg, Germany
Tris-HCl	Biomol, Hamburg, Germany
Triton X-100	Sigma, Steinheim, Germany
Trypan blue	Merck, Darmstadt, Germany
Trypton	Biomol, Hamburg, Germany
Vybrant DiO cell labeling solution	Molecular Probes, Leiden, Netherlands
Wright‘s stain	Sigma, Steinheim, Germany
Xylene Cyanol FF	Sigma-Aldrich, Taufkirchen, Germany
Yeast extract	Biomol, Hamburg, Germany

2.1.4 Stock solutions, buffers and media

Table 2.4: Stock solutions, buffers and media

Solution	Composition
Ampicillin stock solution (1000x)	100 mg/ml in dH_2O, add one drop of NaOH to dissolve; store at -20°C
Anesthetic for mice - for blood meals - for intravital imaging	 12.5 µl Domitor, 27 µl Ketavet, 159 µl PBS pH 7.4; make fresh, 100 µl/ 22 g body weight 40 µl Rompun, 80 µl Ketavet, 120 µl PBS pH 7.4; make fresh, 100 µl/ 22 g body weight
Blocking buffer for immunofluorescence analysis	10% (v/v) FCS in PBS (pH 7.4); short-term storage at 4°C, long-term storage at -20°C
Chloramphenicol stock solution (1000x)	34 mg/ml in ethanol; store at -20°C
Cytoskeletal buffer	150 mM NaCl, 5 mM EGTA, 5 mM $MgCl_2$, 5 mM Glucose, 10 mM MES in dH_2O; pH 6.1

continued on next page

Solution	Composition
Cytoskeletal fixation buffer (1% glutaraldehyde)	1% glutaraldehyde in cytoskeletal buffer
Cytoskeletal fixation buffer (0.25% glutaraldehyde)	0.25% glutaraldehyde, 0.25% triton X in cytoskeletal buffer
Cytoskeletal postfixation buffer	1% $NaBH_4$ in cytoskeletal buffer
DNA loading buffer (6x)	60% (v/v) glycerol, 0.25% (w/v) bromephenol blue sodium salt, 0.25% (w/v) xylene cyanol FF; store at 4°C
Freezing solution for blood stabilates	Alsever‘s solution with 10% glycerol; make fresh or store at -20°C
HepG2 culture medium	500 ml Minimal Essential Medium with Earle‘s salts, 10% (v/v) FCS, 2 mM L-glutamine, 100 U/ml Penicillin, 100 µg/ml Streptomycin; store at 4°C
Infection medium	HepG2 culture medium, 10% amphotericin; store at 4°C for no longer than four days
Kanamycin stock solution (1000x)	50 mg/ml in dH_2O; store at -20°C
LB agar for plates	35 g/L LB agar in dH_2O, autoclave, add antibiotics when lukewarm, pour plates; store plates at 4°C
Lysozyme stock solution	10 mg/ml lysozyme in dH2O
New Wash buffer	50% ethanol, 5 mM EDTA sodium salt, 5 mM Tris-HCl, 50 mM NaCl, pH 7.5; storage for several months at 4°C, long-term storage at -20°C
Paraformaldehyde (4%)	100 ml PBS, 4 g paraformaldehyde, pH 7.4; short-term storage at 4°C, long-term storage at -20°C
Pyrimethamine (100x)	7 mg/ml pyrimethamine in DMSO; store at 4°C
Schizont transfection medium	100 ml RPMI 1640, 25 ml FCS, 150 µl Gentamicin-Ratiopharm® 80SF; make fresh
Silicone suspension	30 g silicone oxide in 250 ml dH20, stir for several hours, sediment over night at room temperature, remove 220 ml of the supernatant, add 300 µl 37% HCl, aliquot and autoclave; short-term storage at 4°C, long-term storage at -20°C
SOC medium	2% trypton, 0.5% yeast extract, 10 mM NaCl, autoclave 2.5 mM KCl, 5 mM $MgCl_2$, 5 mM $MgSO_4$, 0.4% glucose, filter sterilize; store at -20°C
Sodium iodide solution (6 M)	89,6 g NaI in 100 ml dH2O; store at 4°C in the dark
Staining buffer for immunofluorescence analysis	10% (v/v) FCS in PBS (pH 7.4); short-term storage at 4°C, long-term storage at -20°C
STET buffer	8% saccharose, 50 mM Tris-HCl, 1 mM EDTA sodium salt, 5% Triton X-100, pH 8.0; storage for several months at 4°C, long-term storage at -20°C

continued on next page

Solution	Composition
TAE buffer	0.4 M Tris, 0.2 M sodium acetate, 0.01 M EDTA sodium salt, pH 8.0; store at room temperature
Tfb1 buffer	30 mM potassium acetate, 50 mM mangane chloride, 100 mM potassium chloride, 10 mM calcium chloride, 15% glycerol; autoclave solutions before combining, store at -20°C
Tfb2 buffer	10 mM MOPS/NaOH pH 7.0, 10 mM potassium chloride, 75 mM calcium chloride, 15% glycerol; autoclave solutions before combining, store at -20°C
Wright‘s staining solution	1 mg/ml Wright stain in methanol; store at room temperature

2.1.5 Software programs and databases

Table 2.5: Software programs and databases

Program/Database	Version	Used for
Zeiss Efficient Navigation (ZEN)	2008, 2009	Acquisition of confocal line scanning images, measurement of fluorescence intensity and photostability, editing of time lapse videos, image enhancement, time stamping, scaling
Axiovision	4.7.1	Acquisition of wide-field images, measurement of fluorescence intensity and photostability, editing of time lapse videos, image enhancement, time stamping, scaling
Microsoft Excel	2004, 11.5.5	Calculations
GraphPad Prism	1.0	Graphs, statistical calculations (student‘s t test)
Openlab	5.0.2	Acquisition of wide-field images, image enhancement, scaling
QuickTime Player	7.6.3, Pro	Editing of time lapse videos
Microsoft PowerPoint	2004, 11.5.5	Figures, contrast and brightness adjustion of fluorescence images
Adobe Illustrator	CS2, 12.0.0	Illustrations
Adobe Photoshop	CS, 8.0	Clipping of images, image enhancement, overlays
ImageJ	1.43u	Editing of time lapse videos, image enhancement
FluoView	1.7b	Acquisition of confocal point scanning images, scaling
MacVector™	7.2.3	DNA sequence alignments, plasmid maps

2.2 Culture of *P. berghei*

The *P. berghei* strain used in this study is the ANKA strain described by Vincke and Lips in 1948 (Vincke and Lips 1948). Transgenic strains were generated by transfecting the ANKA wild type strain.

2.2.1 Blood stage

2.2.1.1 Infection of mice from blood stabilates

Blood stabilates prepared as described in 2.2.1.3 were thawed and injected intraperitoneally into six- to eight-week-old NMRI mice.

2.2.1.2 Determination of parasitemia via blood smears

The parasitemia of infected mice was determined by taking a small blood sample from the tail vein and smearing it on a microscope slide. After drying the sample was stained with ten drops of Wright's staining solution for one minute. Ten drops of ddH_2O were added and after two minutes the slide was rinsed with tab water. The slide was examined under a light microscope and the number of infected versus non-infected erythrocytes and reticulocytes was counted. The parasitemia was then calculated as infected cells/non-infected cells*100.

2.2.1.3 Blood stabilates

At a parasitemia of 5 - 15%, aliquots of 100 µl blood were mixed with 200 µl freezing solution (see 2.1.5) and rapidly frozen in liquid nitrogen.

2.2.2 Mosquito stage

2.2.2.1 Breeding of mosquitoes

In this study, *Anopheles stephensi* mosquitoes were used as the invertebrate host of *P. berghei*. They were kept at 27°C and 80% humidity with a 12-hour circadian rhythm and fed via cotton balls soaked in 10% glucose solution. Once a week, female mosquitoes were collected and given a blood meal to enable egg production. Donated human blood was mixed in equal ratios with FCS, warmed to 37°C and fed to the mosquitoes through a parafilm membrane. Soaked filter paper was provided to the mosquitoes and laid eggs were collected two days after the blood meal. The eggs were kept in water and hatching larvae fed with fish food. After ten days pupae were separated from the larvae and kept in water in a mosquito cage until hatching of the adults occurred.

2.2.2.2 Infection of mosquitoes

For the infection of mosquitoes with *P. berghei* parasites, an NMRI mouse was infected with a blood stabilate (see 2.2.1.1). When the parasitemia had reached 10-15% and mature gametocytes

were present in the blood, 100-150 mosquitoes were transferred into infection cages without a food source. The mouse was anesthetized with Ketavet/Domitor and placed on the infection cage for 30 minutes to allow a blood meal. Afterwards, the anesthetized mouse was sacrificed by cervical dislocation. The mosquitoes were subsequently kept at 21°C and 80% humidity for optimal development of the *Plasmodium* parasites.

2.3 *In vitro* infection model for the liver stage

2.3.1 Culture and seeding of HepG2 cells

For *in vitro* infection, HepG2 cells were obtained from the European Collection of Cell Cultures (ECACC). The cell line is derived from a human hepatocellular carcinoma, has an epithelial morphology and adheres to the culture surface. HepG2 cells were kept in 20 ml culture medium in 250 ml cell culture flasks at 37°C and 5% CO_2. Twice a week, cells were washed with sterile PBS and treated with 2 ml accutase for 10 minutes at 37°C. Fresh medium was added to stop the enzymatic reaction and cells were spun down at 200 g for 5 minutes. The pellet was resuspended in 5 ml, and 1 ml was reseeded into a culture flask with fresh medium. For infection experiments, the cell number was determined using a Neubauer counting chamber and dilutions appropriate for seeding into culture dishes were prepared. Between 0.4 and $1x10^5$ cells were seeded either on coverslips in 24-well plates, directly into 24-well plates or into glass bottom dishes.

2.3.2 Preparation of sporozoites

Between days 18 and 26 after a blood meal, infected *A. stephensi* mosquitoes were caught and anesthetized with chloroform. They were dipped briefly into ethanol for surface sterilization and then rinsed with PBS. To prevent dehydration, they were then stored on paper towels soaked in distilled water. The salivary glands were dissected from the thorax under a binocular using 20 - 50x magnification. They were placed in infection medium and disrupted using either needles or a micro mortar. The presence of sporozoites was confirmed microscopically under 400x magnification and their number was either estimated or counted using a Neubauer chamber. Sporozoites were then immediately used for infection of HepG2 cells.

2.3.3 Infection of HepG2 cells

Cells were seeded 12 hours prior to infection and kept in culture medium at 37°C and 5% CO_2. If the cells were also transfected (see 2.6.1), transfection took place one day prior to infection. For glass bottom dish infection, the sporozoites from four to five infected salivary glands were then added in 200 μl infection medium. For 24-well plate and coverslip infections, the sporozoites from one to three infected salivary glands were added to each well. The cells were incubated with the sporozoites for two hours under culture conditions. Then, the infection medium was replaced with 1 ml of fresh culture medium and cells were again kept at 37°C and 5% CO_2 until the respective time point after infection. During this time, the medium was changed twice a day.

2.4 Generation of transgenic parasite strains

To generate transgenic parasite strains, the respective fusion constructs were created and cloned into *Plasmodium* expression plasmids. Expression plasmids carried one of two promoters: pbeef1α for constitutive expression of the transgene or the promoter of the gene Pb103464.00.0 (Aurrecoechea 2008) for expression of the transgene only during late liver stages. Then, *P. berghei* blood stage schizonts were transfected with plasmid DNA by electroporation and immediately injected intravenously into mice. Resistance markers on the expression plasmids allowed the selection of transfected schizonts. Once a sufficient parasitemia had been reached, infected blood was transferred intraperitoneally into a second mouse that subsequently served as a blood meal for mosquitoes. Sporozoites were prepared from the infected mosquitoes and used to infect HepG2 cells. Resulting detached cells were collected and separated. Mice were injected intravenously with one detached cell or merosome each to obtain a clonal parasite strain. At an appropriate parasitemia, blood was collected from the infected mice and the genomic DNA was extracted. The expression plasmids carried sequences to allow stable integration into the parasite DNA and clones were tested for successful integration by PCR.

2.4.1 Cloning of plasmids and preparation for transfection

2.4.1.1 General procedure

Gene fragments of interest were amplified using specific PCR primers that added relevant restriction sites. They were purified either via an agarose gel or a column and then restricted and purified again. Subsequently, they were ligated into restricted expression plasmids and transformed into *E. coli* bacteria. In some cases, ligation of the restricted insert into the expression vector proved difficult for reasons that were not entirely clear but likely related to the restriction sites and process. The insert was then initially ligated into the pGEM-T easy vector for analysis and subsequently restricted for ligation into the expression plasmid. Plasmid DNA was extracted from *E. coli* single colony cultures by a silicone-based method and resulting DNA was tested for the correct integration of the transgene by restriction analysis. The plasmid DNA of two to three clones that tested positive was then isolated from a second batch of culture using an extraction kit and sequenced. A clone with the correct DNA sequence was selected and linearized for transfection into *P. berghei* blood stage schizonts.

2.4.1.2 Polymerase chain reaction (PCR)

Gene fragments were amplified using either MidRange polymerase or Phusion™ High Fidelity DNA polymerase.

All primers were designed to have a melting temperature of 50 to 65°C and ordered from Operon Biotechnologies GmbH (Cologne, Germany). They were stored as stock solutions of 100 pmol/µl in DNAse-free, distilled water (aqua ad iniectabilia Delta Select) at -20°C. For use, the stock solutions were diluted 1:10. Individual primer sequences can be found in sections 2.4.1.13 and 2.4.2.2.

Table 2.6: PCR reaction mix for MidRange and Phusion polymerases

component	MidRange	Phusion
DNA template	50-200 ng	50-200 ng
Reaction buffer (5x)	10 µl	10 µl
dNTPs (10 mM each)	1 µl	1 µl
sense primer (10 pmol/µl)	2.5 µl	2.5 µl
anti-sense primer (10 pmol/µl)	2.5 µl	2.5 µl
polymerase	1 µl (5 U)	1 µl (2 U)
$MgCl_2$ (50 mM)	1.5 µl	---
dH_2O	ad 50 µl	ad 50 µl

Table 2.7: PCR programs for MidRange and Phusion polymerases

step	MidRange			Phusion		
	Temperature	Time	Cycles	Temperature	Time	Cycles
DNA denaturation	94°C	3 min	1x	98°C	2 min	1x
DNA denaturation	94°C	1 min	30x	98°C	0.5 min	30x
annealing	55°C	1 min		55°C	1 min	
elongation	68°C	2.5 min		72°C	2 min	
final elongation	68°C	10 min	1x	72°C	10 min	1x
storage	4°C	indefinitely	1x	4°C	indefinitely	1x

2.4.1.3 Restriction of DNA

Plasmids and PCR products were restricted with the appropriate enzymes for 1 hour at 37°C in a thermocycler. Depending on the enzymes used, BSA was either added to the reaction or not.

Table 2.8: Restriction reaction mix

component	amount
DNA	1-2 µg
restriction enzyme	10 U
buffer (10x)	2 µl
BSA (2 mg/ml)	2 µl
dH_2O	ad 20 µl

If only one enzyme was used for plasmid restriction digest, the resulting linearized vector was dephosphorylated with calf intestinal phosphatase (CIP) for 30 minutes at 37°C to avoid religation of the vector. If the restriction digest had taken place in a buffer other than NEB3, the vector was first purified via a MyBudget column according to the manufacturer‘s instructions and eluted in dH_2O.

Table 2.9: CIP reaction mix

component	amount
vector	2 µg
NEB3 buffer	3 µl
CIP (10 U)	1 µl
dH_2O	ad 30 µl

2.4.1.4 Agarose gel electrophoresis

Agarose gel electrophoresis was used to purify DNA fragments and to determine the size of vectors and DNA fragments. Samples were mixed with loading buffer containing bromephenol blue and xylene cyanol FF, which behave like 300 bp and 4000 bp fragments, respectively. Depending on their size, gels were run in TAE buffer at 80 to 110 V for 20 to 45 minutes. For fragments below 1500 bp, a 1.5% TAE agarose gel was used; for larger fragments, a 1% agarose gel. The intercalating chemical ethidiumbromide (0.1 *µ*g/ml) was added to gels at a ratio of 1:10,000. Therefore, DNA fragments could be visualized under UV illumination and compared to a size marker. For smaller fragments, 5 *µ*l HyperLadder IV (100 - 1000 bp) per lane were used, for larger fragments 5 *µ*l HyperLadder I (200 - 10,000 bp).

2.4.1.5 Extraction of DNA fragments

DNA fragments from agarose gels were purified using the kit NucleoSpin Extract II according to the manufacturer‘s instructions, DNA fragments from PCR reactions using the MyBudget PCR product purification kit according to the manufacturer‘s instructions. Subsequent agarose gel electrophoresis of an aliquot of the eluted DNA served to confirm the purification and to determine the concentration of the DNA.

2.4.1.6 Measuring DNA concentration by photometer

Concentration and purity of DNA samples was also determined using a photometer. An aliquot of DNA was diluted 1:50 in dH_2O and its extinction was measured at 260 and 280 nm. The 260 nm value indicated the concentration of the sample at 50 *µ*g/ml for an extinction of 1. The ratio of the 260 value to the 280 value gives an impression of the purity of the sample and should be close to 1.8.

2.4.1.7 Ligation of DNA fragments into expression plasmids or the pGEM-T easy vector

For a ligation, 50-100 ng restricted vector were used. The restricted insert was added in threefold molar excess and the required amount calculated as follows: 50-100 ng vector * x bp of insert * 3 / y bp of vector = z ng insert.

The ligation reaction was incubated for at least 4 hours at room temperature or overnight.

Table 2.10: Ligation reaction mix

component	volume
T4 ligase	1 µl (400 U)
ligase buffer (10x)	1 µl
insert	x µl
vector (50-100 ng)	y µl
dH_2O	ad 10 µl

In some cases, prior ligation into the pGEM-T easy vector was necessary, which possesses an overhang of multiple thymidines at its 3‘-end. Therefore, simple A-tailing of the insert, that is the addition of several desoxyadenosines to the blunt 3‘-end via the Taq polymerase, makes it available for ligation into the vector. A-tailing took place at 70°C for 30 minutes immediately before ligation at 4°C overnight.

Table 2.11: A-tailing reaction mix

component	volume
PCR product	5 µl
Taq polymerase buffer (10x)	1 µl
$MgCl_2$ (25 mM)	1 µl
dATPs (1 mM)	2 µl
Taq polymerase (GoTaq)	1 µl

Table 2.12: pGEM-T easy ligation mix

component	volume
rapid ligation buffer	5 µl
pGEM-T easy	1 µl
ligase	1 µl
A-tailing reaction mix	3 µl

2.4.1.8 Generation of and transformation into competent E. coli bacteria

Ligated vector-insert DNA was transformed into competent *E. coli* XL1 blue bacteria. To generate competent bacteria, a 5 ml LB medium liquid culture with 15 µg/ml tetracycline was grown overnight. The following morning, 1 ml of the culture were added to 100 ml of LB medium with antibiotics and grown until an OD600 of 0.5 was reached. Then, the bacteria were pelleted at 800g for 15 minutes at 4°C and resuspended in 30 ml ice-cold Tfb1 buffer. They were incubated on ice for 2 hours and occasionally inverted. After centrifugation at 800g and 4°C for 15 minutes they were resuspended in 5 ml ice-cold Tfb2 buffer. Aliquots of 50 or 100 µl were then frozen down immediately in liquid nitrogen and stored at -70°C.

When needed, aliquots were thawed on ice immediately prior to use. Five µl of the ligation reaction mix were added to 50 µl of competent bacteria and incubated on ice for 30 minutes followed by a

heat shock at 42°C for 45 seconds. Samples were cooled on ice for 2 minutes before 950 µl prewarmed SOC medium were added. The bacteria were shaken for 1 hour at 37°C and then plated on LB agar plates containing antibiotics to select for the transformed plasmid. To account for varying transformation success and therefore growth density, different volumes of the mixture were plated. First, two plates with either 50 µl mixture and 150 µl SOC medium or 200 µl mixture were prepared. The remaining mixture was spun down at 2150 g for 8 minutes. All but 200 µl of the supernatant were removed and the pellet was resuspended and plated. Agar plates were incubated at 37°C overnight.

2.4.1.9 Small-scale extraction of plasmid DNA

For initial analysis of single clone colonies, plasmid DNA was extracted using a silicone-based method that exploits the specific binding of DNA to silicone in the presence of high salt concentrations. Single colonies from plates of transformed *E. coli* were picked, transferred into 5 ml LB selection medium and shaken over night at 37°C. The following morning 4 ml of the culture were pelleted at 6,000 g for 5 minutes. The bacteria pellet was resuspended in 250 µl STET buffer before addition of 10 µl lysozyme stock solution and incubation on ice for 10 minutes. The solution was then heated to 95°C for 90 seconds. The resulting bacterial lysate was kept on ice for 3 minutes and then centrifugated at 12,000g and room temperature for 15 minutes. The supernatant was added to 500 µl of a 6 M sodium iodide solution and 10 µl silicone suspension and lightly shaken at 37°C for 5 minutes to allow binding of the DNA to the silicone particles. The suspension was then spun down at 12,000 g for 1 minute and the sediment was washed once with 1 ml New Wash buffer. After removal of the wash buffer, the sediment was kept at 56°C for 5 minutes to remove excess ethanol. It was then resuspended in 50 µl DNAse-free dH_2O (aqua ad iniectabilia Delta Select) and incubated for 5 minutes at 56°C to release the DNA from the silicone particles. The silicone particles were sedimented and DNA aliquots could be taken from the supernatant to measure their concentration photometrically. The DNA-silicone solutions were stored at -20°C.
For subsequent sequencing, plasmid DNA was extracted from a second culture batch and isolated using the NucleoSpin® Plasmid kit according to the manufacturer‘s instructions. The amount of purified DNA is comparable to the silicone-based method but is much purer (OD260/280 ≈ 1.8).

2.4.1.10 Large-scale extraction of plasmid DNA

E. coli XL1 blue bacteria were transformed and grown over night on LB selection plates. A clone was transferred into 50 to 100 ml LB selection medium and grown in liquid culture overnight at 37°C. The bacteria were spun down and their plasmid DNA was extracted using the Nucleobond® Plasmid PC100 kit according to the manufacturer‘s instructions.

2.4.1.11 DNA sequencing

DNA samples were sequenced by AGOWA GmbH (Berlin).

2.4.1.12 Linearisation for transfection

The concentration of the plasmid DNA from a large-scale extraction was measured and a volume equaling 30 µg was digested with SacII and ApaI which recognize sites within the integration sequence. The reaction mix was first incubated at room temperature for 30 minutes to allow optimal digestion with ApaI and then moved to 37°C for 1 hour for SacII restriction. If the insert

contained either an ApaI or SacII restriction site, only one enzyme was used for linearization. If both sites were present, the restriction enzyme PshAI was used. The linearized plasmid was purified via the NucleoSpin® Extract II kit and the concentration was measured in an agarose gel. As a final concentration, 5 to 10 µg DNA were needed in a volume of 10 µl.

2.4.1.13 Specific cloning strategies

Table 2.13, Part I: Cloning strategy specifics for individual constructs

Final parasite strain	vector	promoter	insert	amplification primer pair 5‘-3‘ (internal reference number)
Pb-mCherry	pL0017	pbeef1α, constitutive	mCherry cDNA	ATCGGGATCCATGGTGAGCAAGGGCGAG (forward, 914) ATGCTCTAGACTACTTGTACAGCTCGTCC (reverse, 915)
Pb-tdTomato	pL0017	pbeef1α, constitutive	tdTomato cDNA	GGGATCCTGTACGACGATGACG (forward, 948) GCTCTAGAGCTTTGTTAGCAGCCGGATC (reverse, 986)
Pb-Display-mCherry	pL0017	pbeef1α, constitutive	Display-mCherry cDNA	TTGGATCCATGGAGACAGACACACTCCTGC (forward, 1542) TTTCTAGACTAACGTGGCTTCTTCTGCCAAAGC (reverse, 1543)
Pb-LLS-Exp1-mCherry	pL17.1.1 Ch	of gene Pb103464.00.0 (PlasmoDB), late liver stage-specific	Exp1 cDNA	--- (not obtained by PCR amplification but by direct restriction of plasmid)

Table 2.13, Part II: Cloning strategy specifics for individual constructs

Final parasite strain	via pGEM	restriction sites used	linearization enzymes	strategy and result	subcloned
Pb-mCherry	no	BamHI, XbaI	ApaI, SacII	replacement of GFP with mCherry, cytosolic expression during all developmental stages	yes
Pb-tdTomato	no	BamHI, XbaI	ApaI, SacII	replacement of GFP with tdTomato, cytosolic expression during all developmental stages	yes
Pb-Display-mCherry	yes	BamHI, XbaI	PshAI	replacement of GFP with Display-mCherry, visualization of parasite membrane during all developmental stages	no
Pb-LLS-Exp1-mCherry	---	BamHI	ApaI, SacII	fusion of Exp1 to mCherry, visualization of the PVM during late liver stages	no

2.4.2 Transfection of *P. berghei* schizonts

Apart from some minor changes, *P. berghei* parasites were transfected as described previously by Janse et al, 2006 (Janse, Ramesar et al. 2006). The method is briefly outlined below.

2.4.2.1 P. berghei schizont culture and isolation

Female NMRI mice 6 to 8 weeks of age were infected with *P. berghei* wild type parasites. One mouse will yield enough blood stage schizonts to transfect 4 to 5 constructs. Mice were sacrificed at a parasitemia of 1 to 3 % and their blood was collected via heart puncture. It was immediately mixed with 300 µl heparin and 5 ml prewarmed transfection medium. The suspension was spun down for 8 minutes at 450 g in a swinging bucket centrifuge and red blood cells were resuspended in 50 ml prewarmed transfection medium. The suspension was added dropwise to 50 ml transfection medium in a 250 ml cell culture flask. Air in the flask was replaced with a 90% N2 / 5% CO_2 / 5% O_2 mixture. The culture was incubated stationary for 15 minutes at 37°C and then shaken over night at 37°C and 5% CO_2. This led to an enrichment of schizonts in the culture since *P. berghei* blood stage schizonts do not rupture *in vitro*. The presence of a sufficient amount of schizonts was confirmed by blood smearing on the following morning.

The schizonts were separated from other stages and uninfected cells by Nycodenz gradient centrifugation. 27.5 ml Nycodenz stock solution were mixed with 22.5 ml PBS. The schizont culture was divided into three aliquots of 30 to 35 ml and underlayered with 10 ml Nycodenz-PBS mixture. The suspension was centrifugated in a swinging bucket centrifuge for 20 minutes at 450 g with moderate acceleration and without brakes. The schizonts could then be seen as a brownish ring between the Nycodenz and the medium layer and could be collected using a pasteur pipet. They were transferred into a 50 ml reaction tube, and 40 ml transfection medium were added to remove residual traces of Nycodenz during the subsequent centrifugation step at 450 g for 8 minutes. The schizont pellet was resuspended in 1 ml transfection medium per transfection and aliquoted into 1.5 ml reaction tubes for transfection.

2.4.2.2 Transfection procedure and monitoring

A volume of linearized plasmid DNA equaling 5 to 10 µg in a maximum of 10 µl were added to 100 µl Nucleofector™ solution from the Human T Cell Nucleofector® kit. The 1 ml schizont culture aliquot was spun down for 5 seconds at 11,000 g and the pellet was resuspended in the DNA-Nucleofector solution mixture. The suspension was transferred into an electroporation cuvette and program U33 on the Amaxa Nucleofector™ transfection device was executed. Immediately afterwards, 100 µl transfection medium were added and the entire mixture was transferred first into a reaction tube and then into an insulin syringe. It was then injected intravenously into the tail vein of an NMRI mouse.

Since the vectors used for transfection carried a gene transferring resistance to pyrimethamine, it could be used to select for transfected parasites. One day after transfection, mice were given 7 mg/l pyrimethamine as part of their drinking water. All wild type parasites die, resulting in negative blood smear readings until day 7 to 14 after transfection when the transgenic parasites have replicated sufficiently.

2.4.3 Subcloning of parasite lines by single merosome injection

To allow comparative studies of certain parasite lines, such as the brightness and photostability of *P. berghei*-mCherry and -tdTomato, they were subcloned. Other parasite lines, such as *P. berghei*-LLS-Exp1-mCherry were not subcloned to make sure that the observed phenotype is not aberrant behavior shown by a single clone but a general phenomenon.

The method used here for subcloning is described at length in Stanway/Graewe et al (Stanway, Graewe et al. 2009) and makes use of the naturally occurring parasite replication step during the liver stage. A single sporozoite infects a hepatocyte and develops into several thousand merozoites which are therefore by definition clonal. Injection of these merozoites into a mouse reliably leads to a blood stage infection and the resulting subcloned parasite can easily be stored and analyzed.

Briefly, HepG2 cells were infected with sporozoites isolated from the salivary glands of an infected *A. stephensi* mosquito and at 65 hours post infection, detached cells and merosomes were collected. They were examined under a microscope and single detached cells or merosomes that carried rapidly moving merozoites were isolated using a 10 µl pipet. If the transgene encoded a fluorescent protein expressed during the late liver stage, presence of the fluorescence signal was checked to confirm that the merozoites within the selected detached cell or merosome were transgenic. The detached cell or merosome was transferred to a 10 µl drop of HepG2 culture medium on a Petri dish. It was subsequently passaged through 3 to 5 droplets to remove potential contaminations with free merozoites. Eventually, 150 µl of sterile PBS with a pH of 7.4 were added to the last droplet and, using an insulin syringe, the entire mixture was injected into the tail vein of an NMRI mouse. To account for accidental loss of the detached cell or merosome during the injection procedure and for parasites carrying the transgene episomally, three mice were injected with one detached cell or merosome each. The parasitemia was monitored by blood smearing and parasites were typically visible at 8 to 14 days after injection.

2.4.4 Control of gene integration into target locus by site-specific PCR

The plasmids used for *P. berghei* transfection carried sequences targeting the transgene for integration into the genomic DNA of the parasite. Due to their high extent of homology, integration can occur either into the c- or the d-ssu-rRNA locus. After extraction from blood stage parasites, the genomic DNA of individual subclones can be tested for integration of the transgene by PCR.

2.4.4.1 Extraction of gDNA from erythrocytic P. berghei stages

The blood of an infected NMRI mouse with a parasitemia of at least 10% was collected via heart puncture and immediately mixed with heparin to avoid clotting. It was centrifugated at 2000 g and 4°C for 2 minutes and then repeatedly washed with ice-cold PBS (pH 7.4) until the supernatant remained clear. The sedimented cells were then resuspended in 2.5 times their volume of 0.05 % saponin solution and incubated on ice for 10 minutes. Afterwards they were spun down at 2800 g and 4°C for 10 minutes and washed repeatedly with PBS until the supernatant was clear. The parasite pellet was then either stored at -20°C or gDNA was extracted directly using the NucleoSpin® Blood QuickPure kit according to the manufacturer‘s instructions.

2.4.4.2 Primer probes

To test samples for integration of the transgene, two sets of three primers were used in different combinations (see Figure 3.1).

Table 2.14: Primer probes for the control of gene integration

Primer number from figure 3.2	sequence 5‘ - 3‘ (internal reference number)	testing locus
1	GTGTAGTAACATCAGTTATTGTGTG (forward, 654)	c-ssu-rRNA wild type with 655 c-ssu-rRNA integration with 653
2	ATACTGTATAACAGGTAAGCTGTTATTGTG (forward, 652)	d-ssu-rRNA wild type with 655 d-ssu-rRNA integration with 653
3	TTTCCCAGTCACGACGTTG (reverse, 653)	c-ssu-rRNA integration with 654 d-ssu-rRNA integration with 652
4	CTTAGTGTTTTGTATTAATGTCGATTTG (reverse, 655)	c-ssu-rRNA wild type with 654 d-ssu-rRNA wild type with 652

2.5 Evaluation of newly generated parasite strains

2.5.1 Viability

The viability of all newly generated parasite strains was defined as their ability to complete all stages of the parasite life cycle without visible effects. The presence of parasitemia after a transfection proved the capability to go through the blood stage. Subsequent infection of mosquitoes via a blood meal, the presence of oocysts and the development of infectious sporozoites marked completion of the mosquito stage. Finally, success of liver stage development was measured by the formation of detached cells and merosomes carrying rapidly moving merozoites, which have been shown to lead to a blood stage infection when injected intravenously into mice (Stanway, Graewe et al. 2009).

2.5.2 Brightness

The brightness of the newly generated red-fluorescent parasite lines *P. berghei*-mCherry and *P. berghei*-tdTomato was compared to that of the existing *P. berghei*-RedStar line (Sturm, Graewe et al. 2009) in both *in vitro* live and intravital imaging setups.

2.5.2.1 Brightness in an in vitro live imaging setup

To examine the brightness of *P. berghei* liver stage parasites in an *in vitro* imaging setup, $1x10^5$ HepG2 cells were seeded into glass bottom dishes and infected with *P. berghei*-RedStar, -mCherry or -tdTomato sporozoites (see 2.3). At 48 hours post infection, the parasite liver stages were exposed to wide-field or confocal line scanning illumination exciting red fluorescence (see 2.10). In the wide-field setup, their brightness was measured in Grey using the Axiovision software. In the

confocal setup, brightness was measured on a 256-grey scale using the ZEN software. For each *P. berghei* strain, 15 to 22 parasites were examined.

2.5.2.2 Brightness in an intravital imaging setup

To measure the brightness of *P. berghei* liver stage parasites intravitally, $4x10^5$ to $8x10^5$ *P. berghei*-RedStar, -mCherry or -tdTomato sporozoites were collected and injected intravenously into female NMRI mice. The mice were anesthetized with rompun/xylazine at 44 hours post infection and prepared for imaging of the liver as described by Thiberge et al (Thiberge, Blazquez et al. 2007). Then, the brightness of liver stage parasites was determined as described in 2.5.2.1.

2.5.3 Photostability

P. berghei-RedStar, -mCherry and -tdTomato were also compared in terms of their photostability, both in *in vitro* live and intravital imaging setups.

2.5.3.1 Photostability in an in vitro live imaging setup

Parasite liver stages were prepared as described in 2.5.2.1. They were then exposed to 90 seconds of constant wide-field or confocal line-scanning illumination. The mean red fluorescence intensity was measured every 2 seconds, in Grey for wide-field imaging and on a 256-grey scale for confocal imaging. The initial mean fluorescence intensity (MFI) was set to 100% and all other values were calculated in relation to this value. The drop in intensity was then shown as a graph of time against relative fluorescence intensity.

2.5.3.2 Photostability in an intravital imaging setup

The intravital imaging setup was prepared as described in 2.5.2.2 and the subsequent measurement of photostability was performed as described in 2.5.3.1.

2.6 Indirect immunofluorescence analysis of adherent HepG2 cells

2.6.1 Fixation

Between $4x10^4$ and $8x10^4$ HepG2 cells were seeded on coverslips in 24-well plates and infected with *P. berghei* sporozoites. At the indicated time points after infection, the culture medium was removed and cells were fixed according to the respective protocol described below.

2.6.1.1 Fixation for regular immunofluorescence staining

Cells were fixed in 300 µl 4% paraformaldehyde for 20 minutes at room temperature. They were then washed three times with PBS. For further permeabilization, 300 µl ice-cold methanol were added for an incubation period of 10 minutes at -20°C before cells were again washed three times with PBS.

2.6.1.2 Fixation for staining with the anti-α-tubulin antibody

Cells were fixed first in 300 µl 0.25 % glutaraldehyde cytoskeletal fixation buffer for 1 minute at room temperature, and then in 300 µl 1 % glutaraldehyde cytoskeletal fixation buffer for 10 minutes at room temperature. To minimize autofluorescence, the aldehyde groups of glutaraldehyde needed to be reduced before staining and analysis. Therefore, a postfixation step followed. Cells were incubated in 300 µl cytoskeletal postfixation buffer for 30 minutes at room temperature. Afterwards, cells were washed three times with PBS.

2.6.1.3 Fixation for phalloidin staining

Cells were fixed in 300 µl 4% paraformaldehyde in cytoskeletal buffer for 15 minutes at 37°C and then washed three times with PBS.

2.6.2 Staining procedure

After fixation cells were incubated in 10% FCS/PBS for 1 hour at room temperature to block unspecific binding sites. A staining chamber was prepared by placing wet paper towels into a plastic box to create a humid atmosphere that prevents evaporation of the antibody solutions. The box was wrapped in aluminium foil to exclude light and a strip of parafilm was placed on top of the paper towels. Primary antibodies were diluted in 10% FCS/PBS and 50 µl drops of antibody dilution were pipetted on to the parafilm strip. The coverslips were then removed from the blocking buffer and put upside down into the antibody solution. After incubation at room temperature for 2 hours, the coverslips were placed back into 24-well plates and washed three times with PBS for five minutes each. Secondary antibodies and fixed cell stains were also diluted in 10% FCS/PBS and put dropwise on to a fresh strip of parafilm. Coverslips were incubated in the secondary antibody solution for 1 hour at room temperature. They were again washed three times with PBS for 5 minutes each and then briefly dipped into dH_2O. Excess liquid was removed by tipping the edges of the coverslips on to a paper towel before they were mounted on microscope slides using Dako Fluorescent Mounting Medium. The microscope slides were then stored at 4°C overnight to allow the mounting medium to solidify. Afterwards, slides could be stored at 4°C for several weeks.

2.6.3 Antibodies and fixed cell stains

All primary antibodies used for indirect immunofluorescence staining of HepG2 cells can be found in Table 2.15, secondary antibodies and fixed cell stains in Table 2.16.

Table 2.15: Primary antibodies

Antibody	species	dilution	clone	Manufacturer/Distributor
anti-GFP	mouse	1:1000	7.1+13.1	Roche, Grenzach-Wyhlen, Germany
anti-Exp1	chicken	1:250	chicken 91/egg 8.2	Heussler Lab, BNI, Hamburg, Germany
anti-GFP	rabbit	1:1000	A6455	Invitrogen, Karlsruhe, Germany

continued on next page

Antibody	species	dilution	clone	Manufacturer/Distributor
anti-RFP	rat	1:1000	5f8	Chromotek, Planegg-Martinsried, Germany
anti-MSP1 (*P. yoelii*)	mouse	1:1000	251	Anthony Holder, MRC National Institute for Medical Research, London, UK
anti-α-tubulin	mouse	1:500	DM1A	Sigma-Aldrich, Taufkirchen, Germany

Table 2.16: Secondary antibodies and fixed cell stains

Antibody	species	dilution	clone	Manufacturer/Distributor
anti-chicken Cy2	goat	1:400	polyclonal	Dianova, Hamburg, Germany
anti-chicken Cy5	donkey	1:4000	polyclonal	Dianova, Hamburg, Germany
anti-mouse Alexa Fluor® 488	goat	1:5000	687621	Invitrogen, Karlsruhe, Germany
anti-mouse Alexa Fluor® 594	goat	1:5000	polyclonal	Invitrogen, Karlsruhe, Germany
anti-mouse Cy5	donkey	1:200	polyclonal	Dianova, Hamburg, Germany
anti-rabbit DyLight™ 488	goat	1:1000	polyclonal	Cell Signaling, Frankfurt/ Main, Germany
anti-rat Alexa Fluor® 594	goat	1:5000	49440A	Invitrogen, Karlsruhe, Germany
Dapi	---	1:100	---	Sigma-Aldrich, Taufkirchen, Germany
Phalloidin 488	---	1:150	---	Molecular Probes, Invitrogen, Karlsruhe, Germany
Phalloidin 568	---	1:150	---	Molecular Probes, Invitrogen, Karlsruhe, Germany

2.6.4 Antibody combinations used for specific immunofluorescence analysis experiments

Table 2.17: Antibody combinations used for specific experiments

Figure	primary antibodies	secondary antibodies
8C	chicken anti-Exp1 antibody mouse anti-MSP1 antibody rat anti-RFP antibody	anti-chicken Cy2 anti-mouse Cy5 anti-rat Alexa Fluor® 594

continued on next page

Figure	primary antibodies	secondary antibodies
9	chicken anti-Exp1 antibody mouse anti-MSP1 antibody rat anti-RFP antibody	anti-chicken Cy2 anti-mouse Cy5 anti-rat Alexa Fluor® 594
10B	chicken anti-Exp1 antibody rat anti-RFP antibody	anti-chicken Cy2 anti-rat Alexa Fluor® 594
13C	rat anti-RFP antibody mouse anti-GFP (chicken anti-Exp1 antibody)	anti-rat Alexa Fluor® 594 anti-mouse Alexa Fluor® 488 (anti-chicken Cy5)
17A	mouse anti-GFP antibody	anti-mouse Alexa Fluor® 488
17B	mouse anti-α-tubulin antibody	anti-mouse Alexa Fluor® 594

2.7 Transfection and chemical treatments of HepG2 cells

2.7.1 Transfection of HepG2 cells

2.7.1.1 Transfection method

HepG2 cells in a cell culture flask were washed with sterile PBS and treated with 2 ml accutase for 7 minutes. At least 3 ml prewarmed FCS were added to the cell solution and cells were counted using a Neubauer counting chamber. For each transfection a volume equivalent to $2x10^6$ cells was pipetted into a 15 ml falcon tube and cells were spun down at 200 g for 5 minutes. Then the supernatant was removed quantitatively and 100 µl Nucleofector V solution were added. The cell pellet was carefully resuspended using a 1000 µl pipet tip and the resulting solution was added to an aliquot of the transfection plasmid. For GFP-coding plasmids, 3 µg plasmid DNA were used and for mCherry- or dsRed-coding plasmids 5 µg plasmid DNA. The Nucleofector-cell-DNA solution was then transferred into an Amaxa cuvette and placed into the electroporation device. Program T-28 was executed and immediately afterwards 500 µl prewarmed RPMI 1640 medium were added. The cell-RPMI mixture was then transferred into an 1.5 ml reaction tube using an Amaxa plastic pipet and incubated at 37°C and 5% CO_2 for at least 15 minutes. Afterwards, an appropriate volume of the solution was diluted with fresh medium and seeded into culture dishes. For glass bottom dishes, 100 µl were used and for 24-well plates 25 µl.

2.7.1.2 Transfected constructs

Table 2.18: Plasmids used for transfection of HepG2 cells

Name	Promoter	Expressed protein	Used for	Provided by
pDisplay-mCherry	CMV	Display-mCherry	labelling of membranes in mammalian cells	Isabelle Tardieux

continued on next page

Name	Promoter	Expressed protein	Used for	Provided by
pDsRed1-N1-Cox8	CMV	Cox8-dsRed	labelling of mitochondria in mammalian cells	Leonie Hecht Christina Deschermeier Frauke Bach
pEGFP-N1-Cox8	CMV	Cox8-GFP	labelling of mitochondria in mammalian cells	Leonie Hecht Christina Deschermeier Frauke Bach

2.7.2 Chemical treatments of HepG2 cells

2.7.2.1 Cycloheximide treatment

To assess the effect of cycloheximide on detached cell and merosome formation $8x10^4$ HepG2 cells were seeded into 24-well plate wells and infected with *P. berghei*-mCherry or -GFP sporozoites. The cells were then treated with 5 µg/ml cycloheximide for different time periods during infection, 36-44 hpi, 60-68 hpi or 36-70 hpi. The medium containing cycloheximide was changed twice daily during treatment. At 70 hpi, the cell culture supernatants were collected, stained with Hoechst 33342 and detached cells and merosomes were counted. Their number was set in relation to the amount of detached cells and merosomes resulting from an untreated control infection and graphed.

For staining with the Live/Dead reduced biohazard cell viability kit #1, cells were seeded as for the infection experiment and treatment was timed so it took place during the time period corresponding to 36-70 hpi.

2.7.2.2 Tert-butyl hydroperoxide treatment

$4x10^4$ HepG2 cells were seeded into 24-well plate wells. 12 hours after seeding, they were treated with 155 µM tert-butyl hydroperoxide (tBHP) for four hours.

2.8 Staining of cell components for microscopic analysis of living cells

In general, to stain living cells the culture medium was removed and fresh culture medium with the diluted stain was added for the indicated amount of time. Usually, when staining adherent cells, the staining medium was removed after the incubation period and fresh medium was added. When staining detached cells, the staining solution was diluted by adding an equal amount or more of fresh medium before imaging.

Table 2.19: Staining concentrations and conditions for used live stains

Name	concentration	time	temperature	medium change	target organelle
Hoechst 33342	1 µg/ml	10 min	37°C	no	nuclei

continued on next page

Name	concentration	time	temperature	medium change	target organelle
Live/Dead reduced biohazard cell viability kit #1	1 µl A + 1 µl B in 0.5 ml HBSS	15 min	21°C	yes, wash and keep in HBSS	cytosol (green), nuclei (red)
LysoTracker® Red DND-99	75 nm	30 min	37°C	yes	lysosomes
MitoTracker® Green FM	300 nM	30 min	37°C	yes, 3x wash with medium	mitochondria, staining retained upon loss of membrane potential
propidium iodide	2 ng/µl	15 min	21°C	diluted with equal amount of medium	nuclei when membrane is not intact
pSIVA	20 µg/ml	1 h	37°C	diluted with equal amount of medium	phosphatidylserine in the outer membrane leaflet
TMRE	25 nM	30 min	37°C	no	mitochondria, staining lost upon loss of membrane potential
Vybrant DiO (for detached cells)	10 µl/ml	1 h	37°C	diluted with equal amount of medium	membranes
Vybrant DiO (for adherent cells)	5 µl/ml	1 h	37°C	yes	membranes

2.9 Live imaging preparation and setup

2.9.1 Time point imaging

Between 4x10^4 and 1x10^5 HepG2 cells were seeded into glass bottom dishes and infected with *P. berghei* sporozoites. At the time point after infection that was of interest, cells were first stained with the relevant live stains or imaged directly. Then, single images of several parasites from the sample were taken under the settings described for the individual microscopes in 2.10.

2.9.2 Time lapse imaging

Between 4x10^4 and 1x10^5 HepG2 cells were seeded into glass bottom dishes and infected with *P. berghei* sporozoites. Since all time lapses were planned to observe the process of PVM breakdown and cell detachment, imaging began at 55-62 hours post infection. Cells were either stained with live stains or imaged directly using the confocal line scanning microscope. General image acquisition parameters were set as described in 2.10.2. Images of both the red and green fluorescence channels were taken every 5 to 15 minutes for 3 to 30 hours.

The ZEN MultiTime module was used to acquire images of multiple parasites in different locations during a time lapse experiment. To keep phototoxicity to a minimum, between 10 and 35 locations were imaged in time lapses lasting 6 hours or less and 10 to 15 locations in longer time lapses.

2.10 Microscopes and imaging settings

Images were acquired using four different microscopes. Which microscope was used is indicated in each figure legend by a three-letter code that is detailed below.

2.10.1 Confocal point scanning microscope (CPS)

In a confocal point scanning microscope, the excitation laser light illuminates the sample at a single point and moves over the entire specimen dot by dot. This minimizes phototoxicity and bleaching but is a relatively slow process that is best suited for fixed cells or live samples where little movement is expected. In addition, this microscope was used for samples that were stained with Hoechst 33342 because it was the only available confocal microscope equipped with an UV-laser.

The microscope is built around an Olympus IX81 base and images were acquired with the Olympus Fluoview software version 1.7b. It is equipped with an incubator chamber that was used to keep live cells at 37°C and 5% CO_2 during the imaging process. Depending on the size of the structures to be observed, either an Olympus 60x Plan-Apochromat 1.35 Oil or an Olympus 100x UPlanSApo 1.4 Oil objective were used. The fluorescence of fluorophores was excited by activating the relevant lasers (see Table 2.19). The laser intensity was kept as low as possible and varied from sample to sample, overall ranging from 3 to 60%. While an intensity of 60% is comparatively high and not to be recommended for time lapse imaging or sensitive specimens, it was possible for imaging single time points in our infection model. Emitted fluorescence light is detected via photomultiplier tubes. The sensitivity of the photomultiplier tubes was not raised past 800 during scanning of the sample at x4 focus, and activation of the autoHV function served to adapt these settings when the image was acquired under normal settings. All images were acquired in a 512 x 512 pixel format. The pinhole size was set automatically, and offset and gain were set to zero and one, respectively. The pixel dwell time was set to 20 μs and the image was averaged three times linewise.

As an exception, images of detached cells and merosomes were not averaged and the pixel dwell time was set to only 10 μs/pixel because the movement of merozoites was fast enough to significantly blur the image under the conditions detailed above.

For four-color immunofluorescence analysis, a virtual channel scan had to be set up because the microscope is only equipped with three photomultiplier tubes. The fluorescence signals for Cy2, Dapi and Alexa Fluor 594 were detected in the first phase and Cy5 fluorescence in the second.

Table 2.20: Laser lines of the confocal point scanning microscope

Laser	Manufacturer	Used for excitation of
405 nm diode	Olympus, Hamburg, Germany	Dapi, Hoechst 33342
488 nm argon	Olympus, Hamburg, Germany	GFP, Alexa Fluor 488, DyLight 488, Cy2, Vybrant DiO, MitoTracker® Green FM, Phalloidin 488
559 nm diode	Olympus, Hamburg, Germany	RFP, Alexa Fluor 594, Phalloidin 568, TMRE
635 nm diode	Olympus, Hamburg, Germany	Cy5

2.10.2 Confocal line scanning microscope (CLS)

In a confocal line scanning microscope, the excitation laser light is bundled into a sheet that illuminates an entire line of the sample at once. The excitation line is swept over the sample, which makes it possible to acquire images at very high speed. However, in sensitive probes this might lead to increased photobleaching and -toxicity, requiring an added amount of caution when interpreting results. Confocal line scanning microscopy is best suited for multi-color live imaging of moving objects because the time gap between the acquisition of the red- and green-fluorescence channel images is minimal.

The microscope is built around an inverted Zeiss Observer Z.1 base and images were acquired using the Zeiss Efficient Navigation 2008 and 2009 software. An incubation chamber served to keep cells at 37°C and 5% CO_2 for the duration of the experiments. For all images, a Zeiss 63x Plan-Apochromat 1.4 Oil objective was used. Fluorophore fluorescence was excited by activating the relevant lasers (see Table 2.20). The intensity of the laser light was kept as low as possible. For intravital imaging, it was occasionally necessary to raise it to as much as 8%. During normal *in vitro* live time lapse imaging it was always kept below 3.5% and preferably below 1.5%. Emission light passed first through a 505-nm longpass filter and then through a 575-nm longpass filter before detection via a CCD line detector. The detector master gain was usually kept below 30 and only raised further if the fluorescence signal was very weak; it was, however, always kept below 35. Images were acquired in a 512 x 512 pixel format. The pinhole was set to 1 Airy unit, and the offset was set to zero. The pixel dwell time was set to 307.51 μs and images were not averaged.

Table 2.21: Laser lines of the confocal line scanning microscope

Laser	Manufacturer	Used for excitation of
488 nm diode (Sapphire™)	Coherent, USA	GFP, Vybrant DiO, MitoTracker® Green FM
561 nm diode (Compass™)	Coherent, USA	RedStar, mCherry, tdTomato, TMRE, LysoTracker® Red DND-99

2.10.3 Basic model wide-field microscope (BWF)

In wide-field microscopes, fluorophores are not excited specifically by activating different laser lines but the sample is illuminated by excitation light ranging across the whole spectrum. Specificity is generated by passing the light through different filter sets before excitation and detection (see

Table 2.7). Wide-field images are usually not as detailed as confocal images and without deconvolution also cannot deliver any information about colocalization. However, the entire imaging setup is much less complicated than in confocal imaging and the start-up time is often much shorter, allowing the user to quickly examine a specimen. Also, in many cases the amount of information obtained by confocal imaging is not necessary to answer the question posed. Therefore, wide-field microscopes were used here to quickly image general features whose exact localization or colocalization did not need to be known. For this, two different microscope setups were employed, a basic and an advanced model.

The basic wide-field microscope is built around an Axiovert 200 base and images were acquired using the Openlab software. For all images, a Zeiss 20x LD A-Plan objective was used. Excitation light is emitted from an X-Cite® 120 Fluorescence Illumination System (EXFO, Mississauga, Canada) and passed through different filter sets depending on the fluorophore to be observed (see table 2.21). The binning was set to 1x and the offset to zero. The exposure time was set automatically. Images were taken using a FAST1394 QICam camera (QImaging, Surrey, Canada).

Table 2.22: Filter sets of the basic model wide-field microscope

Filter set	Manufacturer	Used for excitation of
Chroma F64-395	AHF Analysentechnik AG, Tuebingen, Germany	Hoechst 33342, Dapi
Chroma F64-485	AHF Analysentechnik AG, Tuebingen, Germany	GFP, Vybrant DiO, pSIVA
Chroma F64-560	AHF Analysentechnik AG, Tuebingen, Germany	mCherry, propidium iodide

2.10.4 Advanced model wide-field microscope (AWF)

The advanced model wide-field microscope is in general similar to the basic model. However, since it is a much more sophisticated version, its software can perform several operations that the basic model cannot, such as brightness and photostability measurements.

It is built around an inverted Zeiss Observer.Z1 base and images were acquired using the Axiovision software version 4.6. The microscope is fitted with an incubation chamber that kept cells at 37°C and 5% CO_2 during experiments. For all images, a Zeiss 63x Plan-Apochromat 1.4 Oil objective was used. Excitation light was generated by a Kuebler Codix HXP120 lamp (Leistungselektronik Jena, Germany) and passed through filter sets fitting the fluorophore to be examined (see table 2.22). The exposure time was set automatically. Images were taken by a QuantEM:512SC EMCCD camera (Spectra Services, USA).

Table 2.23: Filter sets of the advanced model wide-field microscope

Filter set	Manufacturer	Used for excitation of
49 (488049-0000)	Zeiss, Jena, Germany	Hoechst 33342
38 (1031-346)	Zeiss, Jena, Germany	GFP
43 (1114-101)	Zeiss, Jena, Germany	RedStar, mCherry, tdTomato

2.11 Image processing and analysis

2.11.1 General processing (Scaling, time stamps)

Scale bars and time stamps were added to images using the program they had been acquired with, that is either Fluoview, Axiovision, Openlab or ZEN.

2.11.2 Export into commonly readable file formats

To make images and movies widely readable and easily transferable, they were exported from the specific imaging formats of their acquisition software into either .tif or .avi files using the software they had been acquired with (Openlab, ZEN, Axiovision or Fluoview).
Movies were exported without the use of a codec and without compression at 3 frames per second. Images from the Openlab, ZEN and Fluoview softwares were exported uncompressed.

2.11.3 Tone correction, false-coloring and clipping

In general, image enhancement was kept to a minimum. Images were only enhanced as a whole and only in a way that did not change the information relayed by the image.
Wide-field images acquired with the Openlab software were contrast enhanced within the software. Clippings were also made using the Openlab software.
All wide-field images acquired with the Axiovision software were used for brightness and photostability measurement and therefore were not enhanced in any way.
Confocal point-scanning images taken with the Fluoview software were tone corrected and overlayed using Adobe Photoshop. Clipping as well as additional false-coloring were then done using Photoshop as well.
Confocal line scanning single time point images and stills from movies acquired with the ZEN software were also tone corrected in Adobe Photoshop before clipping. In some cases, contrast and brightness were additionally adjusted in PowerPoint.
Movies of confocal line scanning images taken with the ZEN software were edited to the relevant length using the ZEN software. Contrast and brightness were then adjusted using the ZEN and/or ImageJ software.

2.11.4 Fluorescence intensity and photostability

Fluorescence intensities of confocal line scanning images were measured using the ZEN software. Bleaching curves were also done using the ZEN software.
Fluorescence intensities of wide-field images were measured with the Axiovision software. Since it cannot calculate bleaching curves, these were prepared manually by measuring the fluorescence intensity at different time points and entering these data into the Prism software.

2.11.5 Fluorescence profiles

Fluorescence profiles were created using the ZEN software.

CHAPTER 3: RESULTS

3.1 Generation and evaluation of new red-fluorescent *P. berghei* strains

With the development of methods to transfect *P. berghei* parasites (Janse, Ramesar et al. 2006), it has become possible to generate transgenic strains expressing fluorescent proteins. While parasites previously needed to be fixed and stained for detailed microscopic analysis, they can now be observed live, avoiding the risk of artifacts introduced by the fixation procedure. In addition, while staining of fixed samples only allows single time point analysis, parasites expressing fluorescent proteins can be imaged over time to reveal interactions between the parasite and its host cell.

A *P. berghei* strain expressing the red-fluorescent protein RedStar was generated by Janse et al (Janse, Ramesar et al. 2006; Sturm, Graewe et al. 2009). The protein localizes to the cytosol and therefore allows imaging of the entire parasite. Here, HepG2 cells expressing GFP were infected with *P. berghei*-RedStar sporozoites. At various time points after infection, cells were additionally stained with Hoechst 33342 to visualize nuclei (Figure 1). The parasite developed from a sporozoite into a schizont before dividing into individual merozoites that were eventually contained within the detached cell. During all stages, the RedStar protein exhibited adequate fluorescence and confirmed recent observations concerning the development of the *P. berghei* liver stage (Sturm, Graewe et al. 2009). Clearly, it was well suited for microscopic analysis at fixed time points. However, imaging of this parasite strain required rather high illumination light intensity and exposure time, which potentially causes both photobleaching and phototoxicity. *P. berghei*-RedStar was thus less than ideal for long-term time-lapse imaging.

Recently, though, novel red-fluorescent proteins were developed that are reported to be much brighter and more photostable than conventional RFPs (Shaner, Campbell et al. 2004). Transgenic *P. berghei* parasite strains were created that express the most promising of these proteins, tdTomato and mCherry.

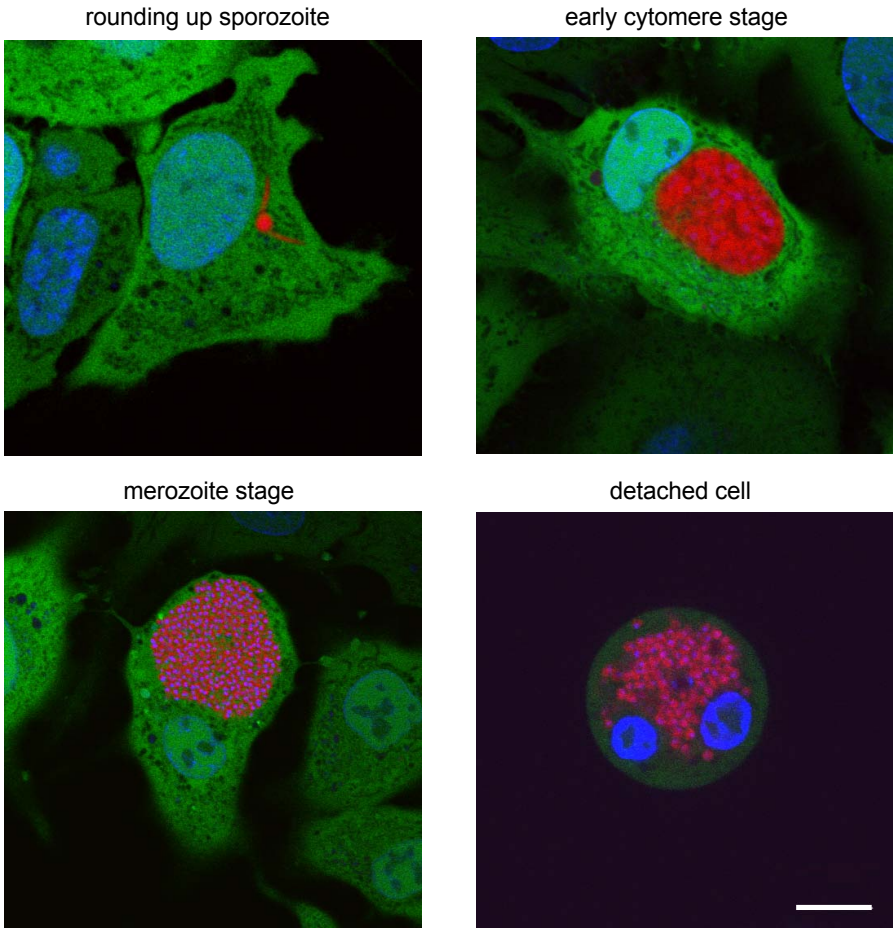

Figure 3.1: Fluorescent *P. berghei* parasite strains proved to be excellent tools to image liver stage development (Graewe, Retzlaff et al. 2009)
HepG2-GFP cells (green) were infected with *P. berghei*-RedStar parasites (red). At different time points after infection, both the host cell and parasite DNA was stained with Hoechst 33342 (blue) and confocal images were taken. The different developmental stages of the parasite were easily recognizable due to cytosolic expression of the red-fluorescent protein. Bars = 10 µm, CPS.

For this, the *Plasmodium* expression plasmid pL0017 was modified by replacing the coding sequence of GFP with that of either of the two red-fluorescent proteins (Figure 2A). The pL0017 plasmid carries sequences for integration of the transgene into the parasite genome at either the c- or d-ssu-rRNA locus. After transfection of the transgene and subcloning of the parasite by single-merosome injection (Stanway, Graewe et al. 2009), genomic DNA was extracted from blood stage parasites and tested for integration of the transgene (Figure 2B). For each locus, one primer pair was used that could only yield a PCR product if the transgene had not integrated; if it had, the primers were too far apart for the amplicon to be finished during the elongation step of the PCR program. In addition, for each locus a second primer pair was used with the forward primer binding to the parasite gDNA in front of the integration site and the reverse primer to a sequence within pL0017. Therefore the primers were only close enough together to generate a PCR product if integration had taken place. In both the *P. berghei*-tdTomato and the -mCherry clone, the transgene integrated into the c-ssu-rRNA locus (Figure 2B, bottom).

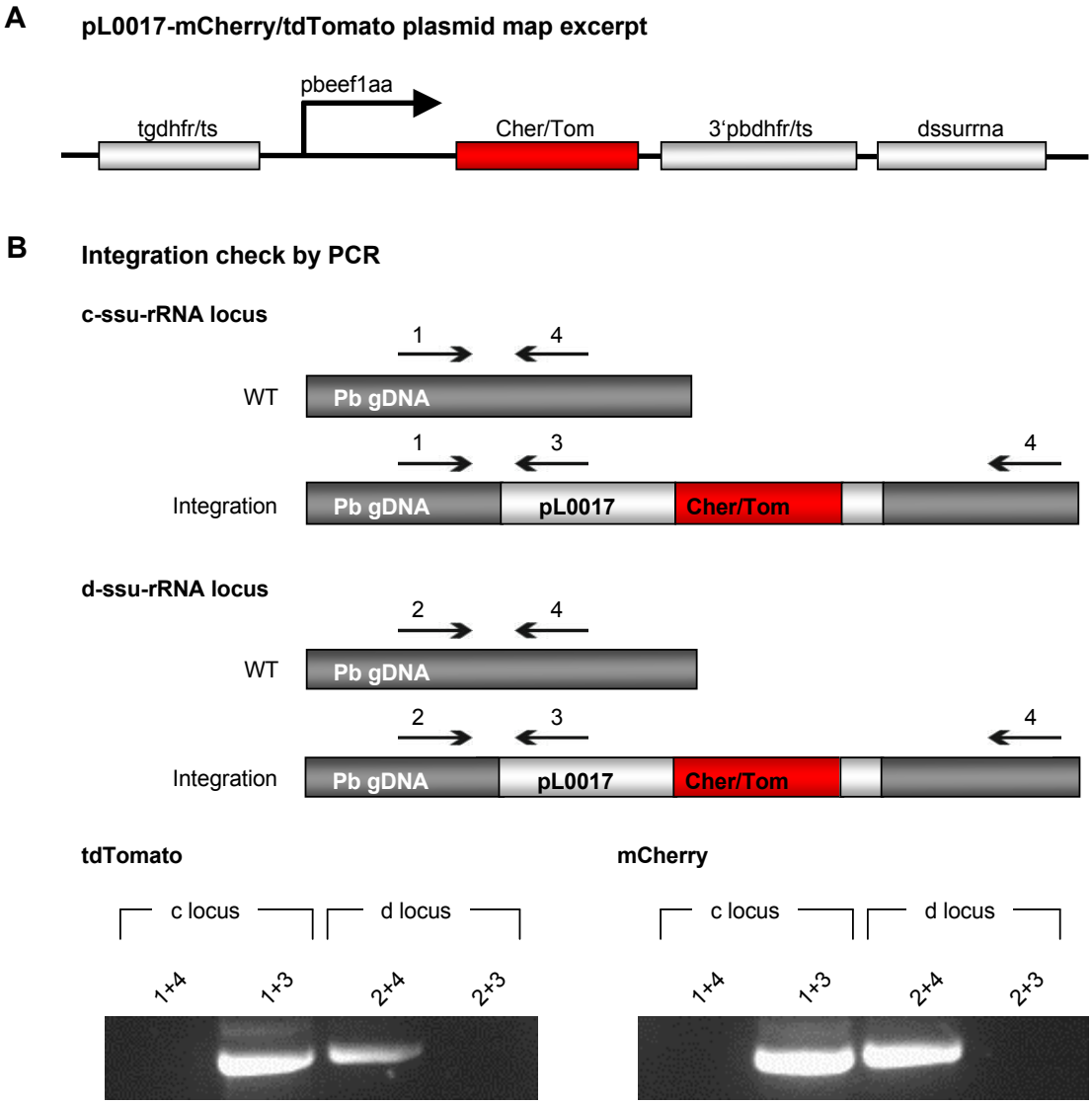

Figure 3.2: The tdTomato and mCherry expression constructs successfully integrated into the *P. berghei* genomic DNA (adapted from Graewe, Retzlaff et al. 2009)
A In the pL0017 *Plasmodium* expression plasmid, the coding sequence of GFP was replaced with the coding sequence of either tdTomato or mCherry. The transgene was expressed constitutively and localized to the cytosol.
B After transfection, integration of the transgenes into either the c- or d-ssu-rRNA locus was tested by PCR. If either of the primer pairs 1/3 or 2/3 resulted in an amplicon, integration had taken place. For both the *P. berghei*-tdTomato and the *P. berghei*-mCherry clone, integration into the c-ssu-rRNA locus had occurred.

While going through the transfection and cloning process, the newly generated parasite lines had already proven to be capable of completing all stages of the life cycle. As a first step in evaluating their specific use for fluorescence imaging, their brightness was tested in comparison to *P. berghei*-RedStar. HepG2 cells were infected with the respective sporozoites and imaged 48 hpi at 561 nm with different laser intensities (LIs) (Figure 3A). At 0.5% LI both tdTomato and mCherry exhibited fluorescence sufficient for imaging the parasite, while RedStar was hardly detectable. When imaged at 3%, RedStar was suitably excited but tdTomato and mCherry were drastically overexposed. Measurement of the mean red fluorescence intensity on a 256-grey scale additionally revealed that even when imaged at 3% LI, RedStar is considerably less bright than

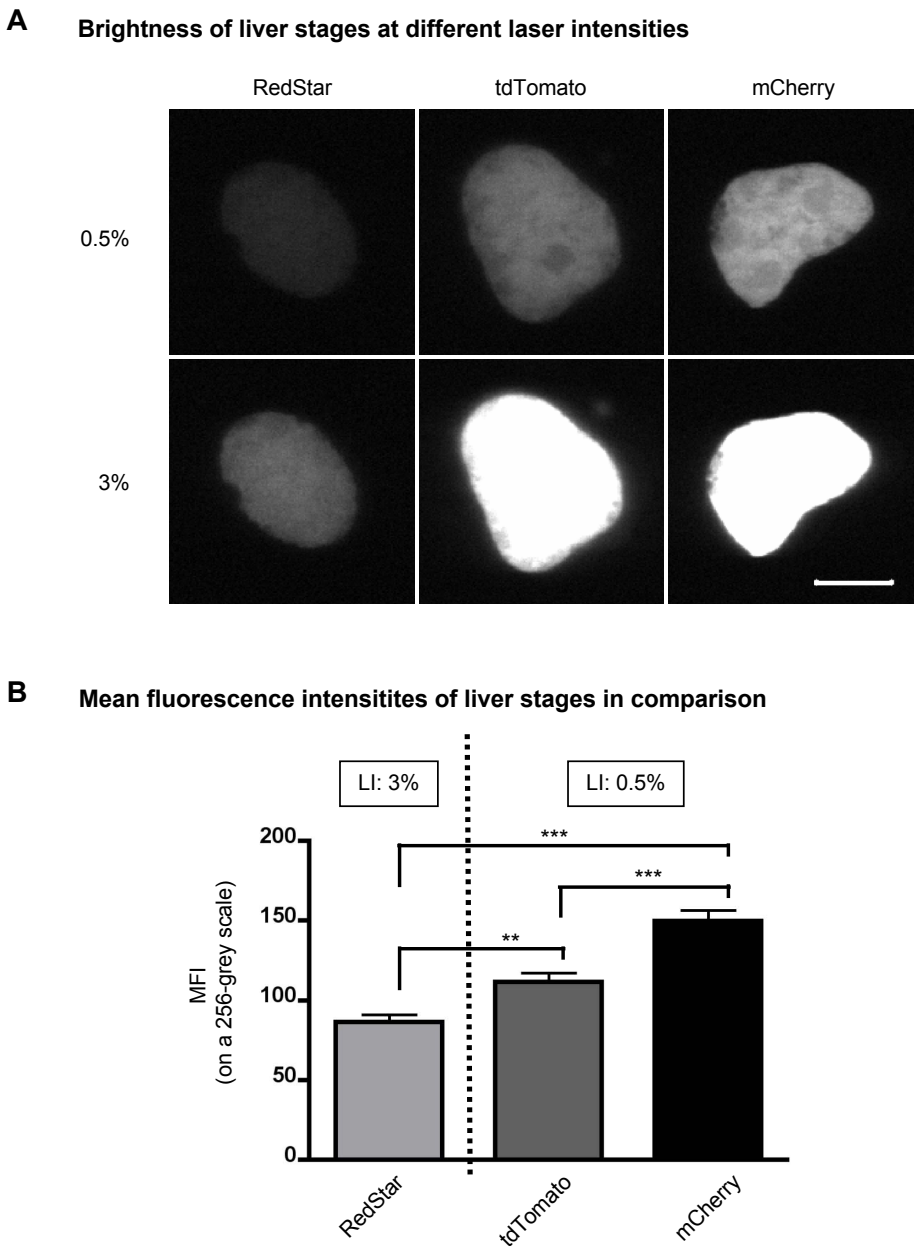

Figure 3.3: *P. berghei*-mCherry required only moderate laser intensities to excite bright fluorescence (Graewe, Retzlaff et al. 2009)
HepG2 cells were infected with *P. berghei*-RedStar, -tdTomato or -mCherry sporozoites. At 48 hpi, parasites were imaged at either 0.5% or 3% laser intensity. CLS.
A Representative images of the red-fluorescent parasites at both laser intensity settings are shown. While mCherry and tdTomato exhibited sufficient fluorescence after excitation with 0.5% laser intensity, RedStar was hardly visible. Bar = 10 µm.
B The mean + SEM fluorescence intensity of the red-fluorescent parasites when imaged at their optimal laser intensity (LI) setting is shown. At a low LI (0.5%) mCherry was significantly brighter than tdTomato and also than RedStar at a higher LI (3%). n=15, ** $p<0.005$, *** $p<0.0001$

tdTomato and mCherry imaged at 0.5% LI (Figure 3B). Of the two newly generated red-fluorescent parasite strains, *P. berghei*-mCherry proved to be the brighter one.

Brightness and the resulting short exposure times, however, are only one of the aspects important for long-term imaging. Even more important is the photostability of the fluorescent protein. Since intravital imaging has proven to be the setup most prone to photobleaching, it was chosen to test the photostability of the newly generated *P. berghei* strains. NMRI mice were

infected with *P. berghei* sporozoites and at 44 hpi the liver was prepared for confocal intravital imaging. Infected cells were illuminated constantly for 90 seconds and the mean red fluorescence intensity of the parasite was measured every 2 seconds. Due to their different levels of brightness it was not feasible to use the same imaging settings for all three strains. Instead, the settings were adapted to each strain with the aim of exciting a similar fluorescence intensity. Again, *P. berghei*-RedStar required a much higher laser intensity than tdTomato and mCherry. Imaging parameter details can be found in Table 3.1.

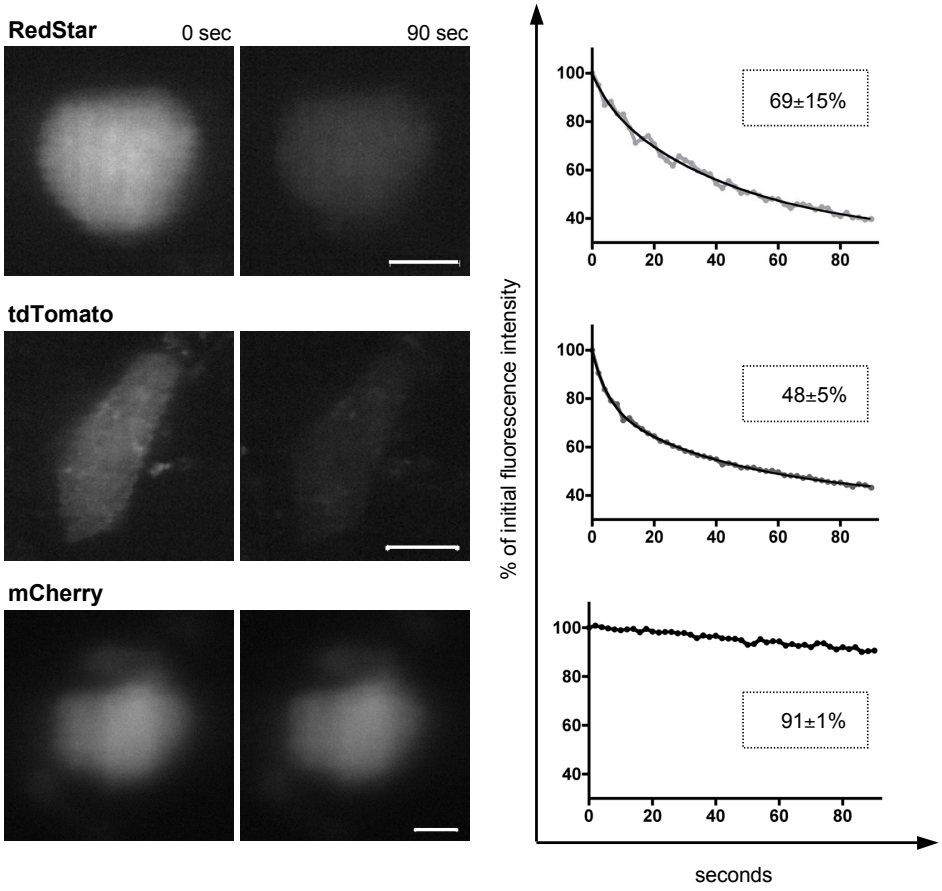

Figure 3.4: The newly generated *P. berghei*-mCherry strain possessed superior photostability in intravital imaging setups (Graewe, Retzlaff et al. 2009)
NMRI mice were injected intravenously with *P. berghei*-RedStar, -tdTomato or -mCherry sporozoites. After 44 hours, the liver was prepared for intravital imaging and the red-fluorescent parasites were imaged confocally at laser intensities optimal for the respective fluorescent protein. They were constantly illuminated for a period of 90 seconds and the mean red fluorescence intensity was measured every 2 seconds. The first and the last image of a representative parasite are shown (left panel). The mean fluorescence intensity was determined for each time point, calculated in relation to the initial intensity and plotted against time. A representative graph and the mean and SEM of all imaged parasites is shown (right panel). A curve fit was done (indicated by a thin black line) and the bleaching behavior of *P. berghei*-RedStar and -tdTomato was found to fit a biphasic exponential decay (R^2=0.9906 and R^2=0.9978, respectively). *P. berghei*-mCherry proved to be the most photostable strain. For n please refer to Table 3.1. Bars = 10 µm, CLS.

Table 3.1: Mean fluorescence intensities and settings for confocal and wide-field intravital and in vitro live imaging of red-fluorescent P. berghei liver stages (adapted from Graewe, Retzlaff et al. 2009)

Setup	Parasite strain	absolute MFI[a, b]		relative MFI after 90 s[c]	Laser power[d] [%]	Exposure time[e] [ms]	Number of parasites examined
		0 s	90 s				
Confocal							
in vitro live	RedStar	92 ± 22	48 ± 9	52 ± 4	3	100	20
	tdTomato	111 ± 20	77 ± 13	70 ± 3	0.5	100	17
	mCherry	150 ± 25	138 ± 24	92 ± 2	0.5	100	15
intravital	RedStar	74 ± 25	48 ± 6	69 ± 15	3.5-5	1000	6
	tdTomato	64 ± 13	30 ± 4	48 ± 5	3	1000	4
	mCherry	73 ± 13	67 ± 12	91 ± 1	1.8-3	400-830	3
Setup	**Parasite strain**	**absolute MFI[a] [Grey]**		**relative MFI after 90 s[c]**	**HXP120 intensity setting[f]**	**Exposure time[e] [ms]**	**Number of parasites examined**
		0 s	**90 s**				
Wide-field							
in vitro live	RedStar	17154 ± 3168	16825 ± 3104	98 ± 1	1	300	20
	tdTomato	18249 ± 3963	17479 ± 3826	96 ± 1	1	100	20
	mCherry	20090 ± 4499	19144 ± 4394	95 ± 1	1	150	15
intravital	RedStar	14874 ± 1338	8771 ± 2321	59 ± 17	4	160-630	4
	tdTomato	16151 ± 719	9300 ± 1018	57 ± 4	4	580-620	4
	mCherry	18213 ± 3853	16958 ± 3353	93 ± 2	4	270-380	4

a) mean fluorescence intensity; b) on a 256-grey scale; c) remaining percentage of initial fluorescence intensity; d) 561 nm diode pumped laser; e) per image taken; f) 1 = lowest, 4 = highest
Please note that the MFIs in confocal and wide-field setups are measured in different units and cannot be compared directly.

The observed *P. berghei*-RedStar parasites could be divided into two groups. The first group bleached only moderately but showed very weak fluorescence. The second group exhibited brighter fluorescence but bleached rapidly after the onset of illumination (Figure 4, top panel). This bleaching process appeared to be biphasic since most of the fluorescence disappeared quickly until only a low level remained that was then lost at a much slower rate. This resembled the bleaching behavior described for tagRFP, an RFP that is derived from *Entacmaea quadricolor* (Merzlyak, Goedhart et al. 2007). Reasons for the difference in brightness between the two groups might be variations of expression levels or the location in different focal planes. In any case, neither was suitable for long-term intravital imaging experiments.

Surprisingly, tdTomato did not fare much better, even though it had been reported to have enhanced photostability (Shaner, Campbell et al. 2004). It exhibited low fluorescence at the start of imaging and nearly 50% of this initial fluorescence intensity were lost after the 90 second illumination period (Figure 4, middle panel). Like *P. berghei*-RedStar, *P. berghei*-tdTomato showed a biphasic bleaching behavior.

In contrast, mCherry was bright enough for easy detection at low laser intensities and retained more than 90% of its fluorescence intensity (Figure 4, bottom panel). *P. berghei*-mCherry was also evaluated in further setups (confocal *in vitro* live imaging, wide-field *in vitro* live imaging and wide-field intravital imaging) and the results confirmed its superior brightness and photostability (Figure 5). For *in vitro* live analysis, HepG2 cells were infected with the respective parasite strain and imaged at 48 hpi as described for the intravital setup. The photostability assay for wide-field

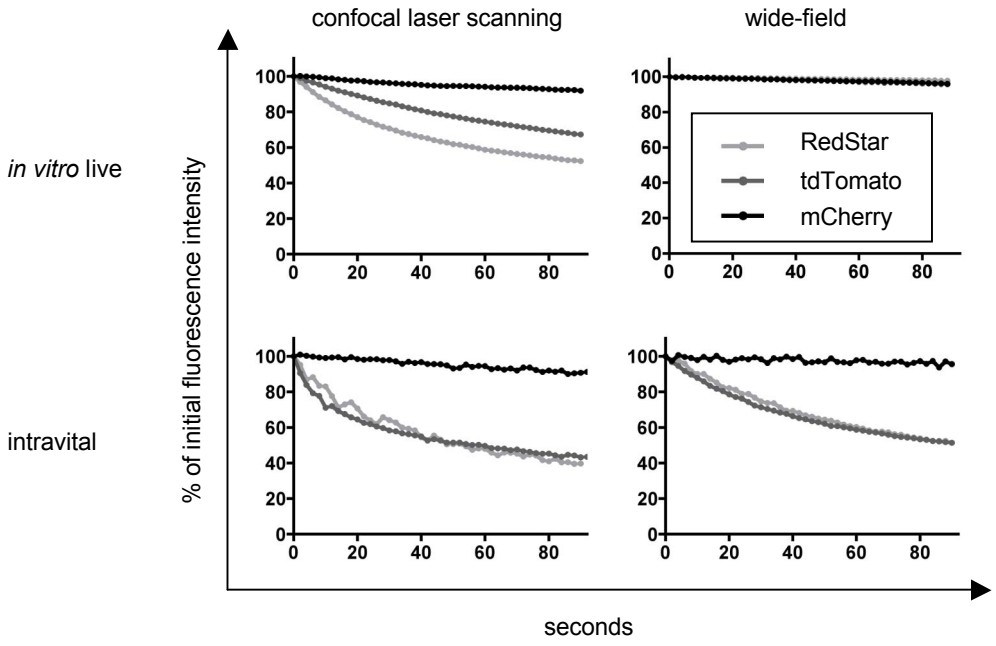

Figure 3.5: *P. berghei*-mCherry also possessed superior photostability in confocal *in vitro* live and wide-field imaging setups (adapted from Graewe, Retzlaff et al. 2009)
P. berghei-RedStar, -tdTomato and -mCherry parasites were prepared for *in vitro* live and intravital imaging (for details please refer to the Materials and Methods chapter). They were exposed to 90 seconds of constant confocal laser scanning or wide-field illumination and the mean red fluorescence intensity was measured every 2 seconds. It was calculated as the percentage of the initial fluorescence intensity and plotted against time. Representative graphs are shown. For n please refer to Table 3.1.

illumination was performed as for confocal illumination, only with a different excitation light source. Details for individual settings can be found in Table 3.1.

Taken together, of the three red-fluorescent parasite strains tested *P. berghei*-mCherry was the best choice for live observation: it could be imaged at as little as a sixth of the laser intensity required for *P. berghei*-RedStar and retained its high fluorescence intensity over long periods of illumination.

This assessment was confirmed in a long-term *in vitro* live time-lapse of liver stage development. HepG2-GFP cells were infected with *P. berghei*-mCherry sporozoites and imaged confocally every 15 minutes starting at 55 hpi (Figure 6). The parasite fluoresced brightly during the entire observation period and completed the developmental process without signs of photodamage. The sequence of events fit the current model of the late liver stage: the parasite transitioned from the schizont to the cytomere stage before separation into individual merozoites occurred. These were then released into the host cell cytoplasm before detachment of the entire cell. In addition, several surprising details were revealed that had remained hidden in previous single time point examinations. The loss of the barrier between the parasite and the host cell cytoplasm occurred much quicker than expected (within a single 15 minute time interval). Also,

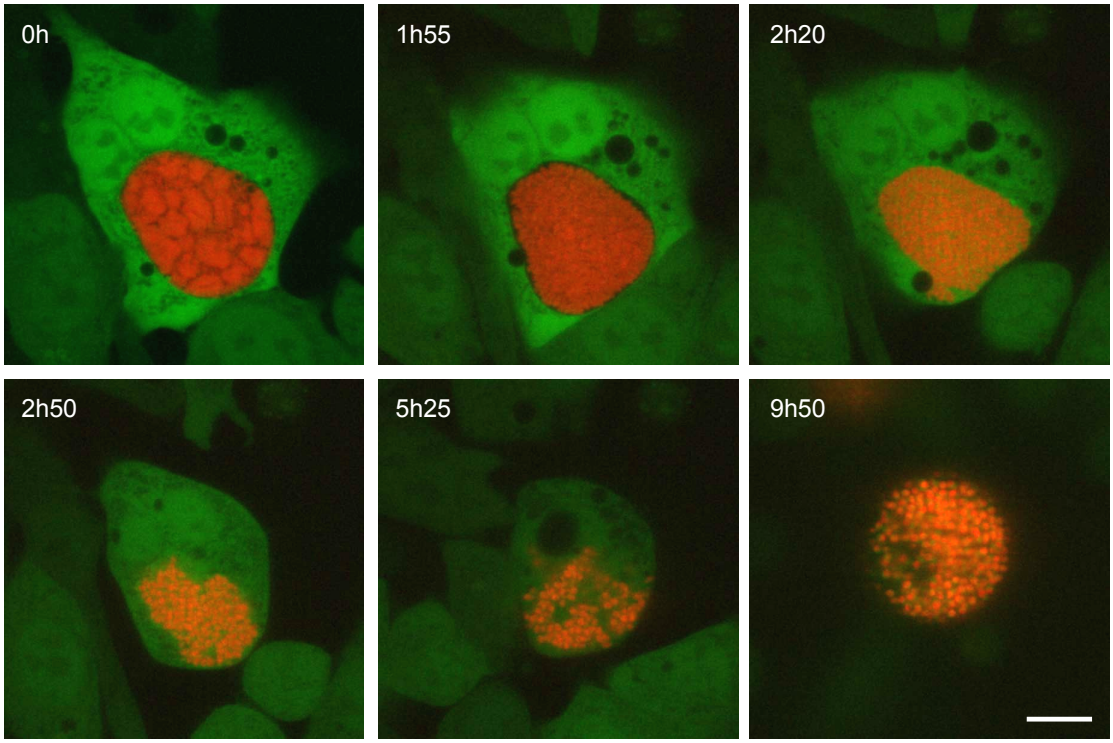

Figure 3.6: *P. berghei*-mCherry were well-suited for long-term time-lapse imaging of *Plasmodium* liver stage development and confirmed present model of liver stage development (Rankin, Graewe et al. 2010)
HepG2-GFP cells (green) were infected with *P. berghei*-mCherry sporozoites (red). At 55 hpi, infected cells were imaged every 15 minutes. Images of a representative parasite at different time points (indicated in the top left corner of each image) are shown. *P. berghei*-mCherry exhibited bright red fluorescence throughout the entire development process, beginning with the cytomere stage (0h), moving through merozoite formation (1h55), PVM breakdown (2h20), detachment (2h50 and 5h25) and concluding in the detached cell (9h50). This confirmed the present understanding of the developmental process which had so far only been observed at individual time points, not in a time-lapse. n=4 from 2 independent experiments, bar = 10 µm, CLS.

detachment of the cell began immediately after the loss of the barrier and therefore much earlier than previously assumed.

This confirmed the importance of time-lapse live imaging for a full understanding of the parasite liver stage development. In the following sections, this technique was employed to fill several crucial gaps in our knowledge concerning both parasite and host cell physiology, beginning with determining the origin of the membrane that surrounds detached cells and merosomes.

3.2 Origin of the membrane surrounding detached cells and merosomes

Towards the end of liver stage development, the parasite has divided into individual merozoites. In *in vivo* infections, they soon fill the entire host cell, which slowly detaches but is held in place by neighboring cells. From the detached cells, small vesicles, the merosomes, bud off into blood vessels. Merosomes eventually separate completely from the detached cell and carry the merozoites to the lung for initiation of the blood stage (Baer, Klotz et al. 2007). In *in vitro* infections, towards the end of the liver stage, detaching cells are freely moving in the supernatant and can be observed as floating spheres filled with merozoites. Merosomes split off these detached cells. They are clearly distinguishable from detached cells since they do not contain a host cell nucleus. Since both *in vivo* and *in vitro* merosomes derive directly from detached cells, they share the same membrane. Therefore, it was not differentiated between detached cells and merosomes during the characterization of their surrounding membrane. Care was taken, though, to confirm that there was indeed no phenotypic difference between both types.

The first step was a general characterization of the membrane in question. HepG2 cells were infected with fluorescent *P. berghei* parasites and detached cells and merosomes were collected at an early and a late time point after formation. They were incubated with Hoechst 33342 in combination with several other live stains and then subjected to wide-field imaging and quantification. The general membrane marker Vybrant DiO confirmed the presence of a surrounding membrane in both early and late merosomes and detached cells (Figure 7, top panel). The presence of phosphatidylserine in the outer membrane leaflet, which is a marker of apoptosis, was checked using pSIVA (Kim, Chen et al. 2009). In contrast to traditional annexin-based phosphatidylserine stains it can be used under growth media conditions, which minimizes the risk of artifacts. Initially, the vast majority of detached cells and merosomes was negative for phosphatidylserine but over time phosphatidylserine asymmetry was slowly lost (Figure 7, middle panel). Similarly, the surrounding membrane was intact in newly detached cells and merosomes but became permeable with time, as observed through propidium iodide staining (Figure 7, bottom panel). To summarize, upon formation the membrane of detached cells and merosomes was intact and maintained phosphatidylserine asymmetry but both of these features were lost upon aging.

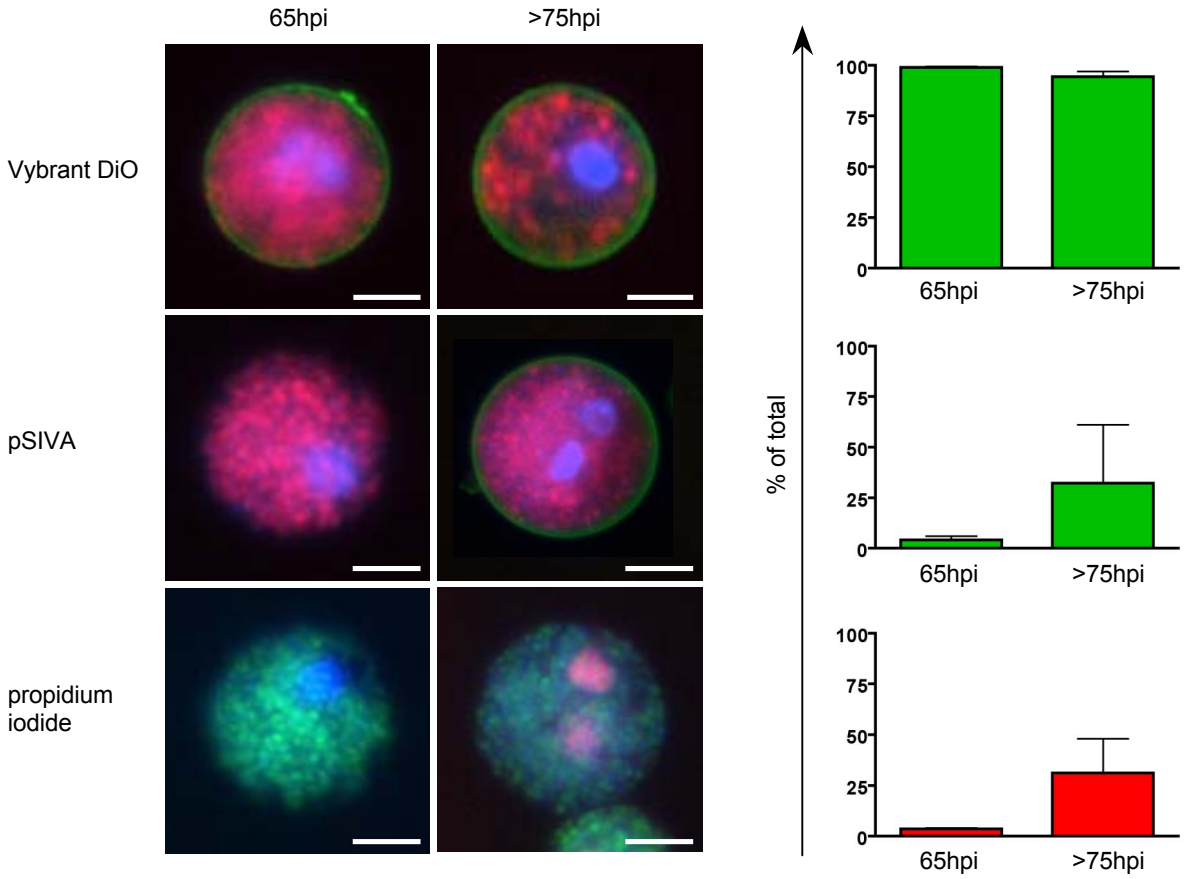

Figure 3.7: Newly formed detached cells and merosomes were surrounded by a membrane that was intact and retained phosphatidylserine asymmetry (© S. Gräwe)
HepG2 cells were infected with either *P. berghei*-mCherry or -GFP sporozoites. At 65 and >75 hpi, detached cells and merosomes were collected from the cell culture supernatant. They were treated with the nuclear stain Hoechst 33342 (blue) and additional live stains to obtain more information about the nature of the surrounding membrane. Wide-field images were taken and representative images are shown. The existence of a membrane in general was shown by staining cells infected with *P. berghei*-mCherry parasites (red) with Vybrant DiO (green, top panel). Staining of cells infected with *P. berghei*-mCherry parasites (red) with pSIVA (green) demonstrated that the membrane initially possessed phosphatidylserine asymmetry but lost it over time (middle panel). Alike, staining of cells infected with *P. berghei*-GFP (green) with propidium iodide (red) revealed that the surrounding membrane was initially intact but lost integrity as the detached cells and merosomes aged (bottom panel). The quantification shown on the left is the mean + SEM of three independent experiments. Total n for 65hpi - Vybrant DiO: 712, pSIVA: 1483, PI: 1291. Total n for 75hpi - Vybrant DiO: 899, pSIVA: 874, PI: 1564. Bars = 10 µm, BWF.

Theoretically, there are three membranes from which the membrane surrounding merosomes and detached cells could originate: the parasite membrane, the parasitophorous vacuole membrane and the host cell membrane. In the following, each possibility was examined during the late liver stage, beginning with the parasite membrane. A transgenic parasite strain was generated that expressed mCherry fused to a targeting sequence for secretion and a transmembrane domain to anchor it in the parasite membrane upon secretion (Figure 8A). The *P. berghei*-Display-mCherry parasite strain was viable and completed all life cycle stages normally. To observe the fate of the parasite membrane live, HepG2-GFP cells were infected with *P. berghei*-Display-mCherry sporozoites and imaged from 55 hpi onwards (Figure 8B). The Display-mCherry protein was initially visible as an outline of the parasite and within the invaginations of the cytomere. Later, it

appeared to surround individual merozoites. Both of these observations fit with the expectations for a localization to the parasite membrane. However, the fluorescence signal was very weak, which made a definite assessment impossible. Potential reasons for the low fluorescence level might be insufficient protein expression or quick deterioration of the fusion protein. To exclude mistargeting of Display-mCherry, infected HepG2 cells were fixed and stained for immunofluorescence analysis

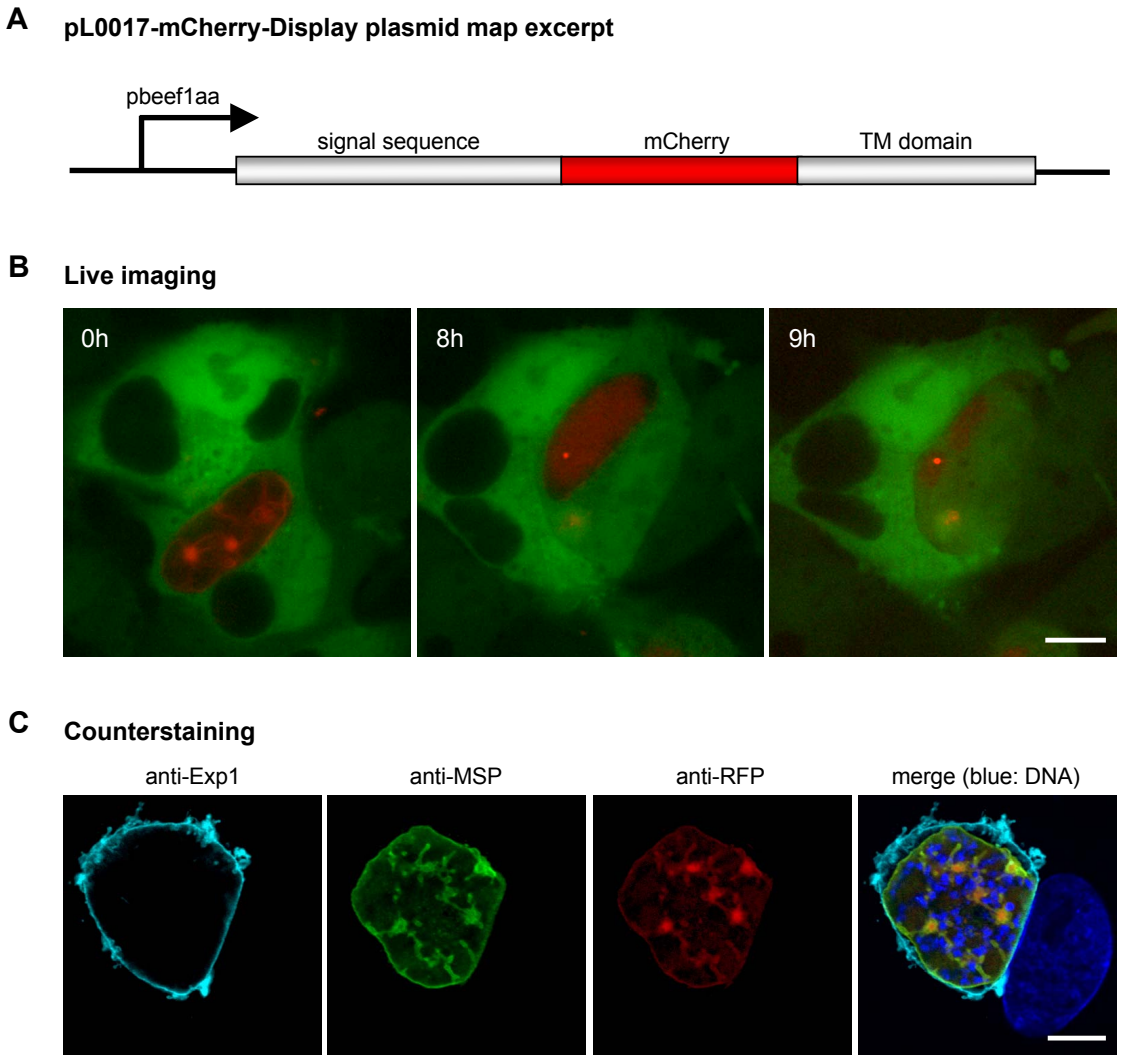

Figure 3.8: A transgenic fusion protein for live imaging of the parasite membrane localized correctly but showed only a weak fluorescence signal (© S. Gräwe)
A The coding sequence of GFP in the pL0017 *Plasmodium* expression plasmid was replaced with the Display-mCherry cassette, which contains a targeting sequence for secretion and a transmembrane domain. The fusion protein was expressed constitutively.
B HepG2-GFP cells (green) were infected with *P. berghei*-Display-mCherry sporozoites. At 55 hpi, infected cells were imaged confocally every 15 minutes in a time-lapse. The distribution of the Display-mCherry protein (red) initially followed the outline of the cytomere stage parasite (0h) before appearing to surround individual merozoites (8h and 9h). However, the weak fluorescence signal made detailed observation impossible. Bar = 10 µm, CLS.
C HepG2 cells were infected with *P. berghei*-Display-mCherry sporozoites. At 55hpi, infected cells were fixed, stained for immunofluorescence analysis and imaged confocally. Anti-Exp1 antibody served to stain the PVM (cyan) and Dapi to stain both parasite and host cell nuclei (blue). The Display-mCherry protein (red) was stained by anti-RFP antibody and the parasite membrane (green) by a monoclonal anti-MSP1 antibody. The overlay image showed colocalization of the red and green fluorescence signals, thereby confirming that the Display-mCherry protein localized to the parasite membrane. Bar = 10 µm, CPS.

with anti-RFP and anti-MSP1 antibodies (Figure 8C). Since MSP1 is a parasite membrane protein, the overlay of the anti-RFP signal with it demonstrated that Display-mCherry was indeed incorporated into the parasite membrane. However, even when amplified through immunofluorescence staining, the fluorescence level of the red signal remained low. In conclusion, the generated *P. berghei*-Display-mCherry parasite strain was not suitable for analyzing the fate of the parasite membrane in detail.

Therefore, a static setup was chosen. HepG2 cells were infected with *P. berghei*-mCherry parasites and fixed at different time points after infection. The parasite membrane (via MSP1), the membrane of the parasitophorous vacuole (via Exp1), the parasite cytoplasm (via mCherry) and the nuclei were stained for immunofluorescence analysis and confocal images were taken (Figure 9). A detailed listing of the primary and secondary antibodies used for staining can be found in section 2.6.3 in the Materials and Methods chapter. For easier detection of the different membranes, the images were false-colored: while nuclei were correctly shown in blue and the

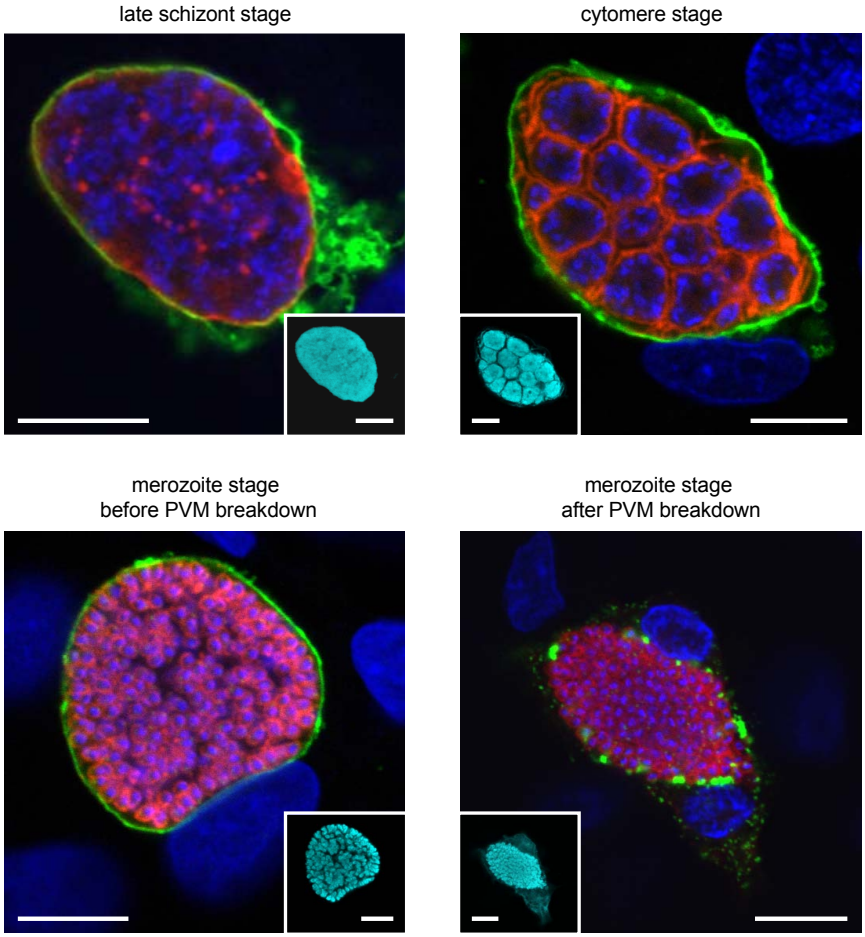

Figure 3.9: The parasite membrane became the merozoite membrane during the late liver phase (© S. Gräwe)
HepG2 cells were infected with *P. berghei*-parasites, fixed at different time points after infection and stained for immunofluorescence analysis before confocal imaging. Parasite and host cell nuclei (blue) were stained with Dapi and the PVM (green) with anti-Exp1 antibody. The anti-MSP1 antibody was used to visualize the parasite membrane (red) and anti-RFP antibody to visualize the parasite cytoplasm via transgenically expressed mCherry protein (cyan, insets). Representative images were false-colored to make colocalization of the parasite and PV membranes easier to detect. While the parasite membrane surrounded the parasite as a whole during the late schizont stage and even overlapped with the PVM at some points, it began to invaginate around groups of nuclei during cytomere formation. Eventually it surrounded individual merozoites both before and after PVM breakdown. Bars = 10 µm, CPS.

PVM in green, the parasite membrane is shown in red and the parasite cytoplasm in cyan. Initially, the PVM and the parasite membrane surrounded the schizont stage parasite and were in close contact in some areas (Figure 9, upper left). During the late liver stage, though, the parasite membrane began to invaginate around groups of nuclei to form the cytomere stage (Figure 9, upper right). Invagination proceeded until the parasite membrane surrounded individual merozoites (Figure 9, lower left). Once this process was completed, the PVM disintegrated as could be seen by the loss of a coherent Exp1 staining pattern and the distribution of parasite protein throughout the host cell (Figure 9, lower right). Detachment was now about to begin but parasite membrane could only be observed around individual merozoites, discounting it as the membrane surrounding the detached cell and merosomes.

The next candidate to be considered was the PVM. Although the previous figure already indicated that it disintegrates before detachment of the cell, a closer examination was necessary to fully validate this observation. To exclude that the breakdown was an artifact caused by the fixation and staining procedure, a transgenic parasite strain was generated for live observation. It expressed mCherry fused to the PVM protein Exp1 (Figure 10A). An attempt to express the fusion protein under a constitutive promoter failed because the parasite arrested early on during liver stage development. Therefore, expression was controlled by the promoter of the gene Pb103464.00.0 (Aurrecoechea 2008), that is only active in late liver stages (LLS). The resulting *P. berghei*-LLS-Exp1-mCherry strain completed all stages of the life cycle successfully.

To confirm the localization of the Exp1-mCherry fusion protein to the PVM, HepG2 cells were infected with *P. berghei*-LLS-Exp1-mCherry parasites, fixed at 48 hpi and stained for immunofluorescence analysis. The fusion protein was visualized via anti-RFP and anti-Exp1 antibody. The anti-Exp1 antibody additionally detected endogenous Exp1, thus ensuring staining of the PVM even if Exp1-mCherry were mistargeted. Confocal images of all fluorescence channels were taken and overlaid (Figure 10B). The anti-Exp1 and the anti-RFP signal show almost complete colocalization. Endogenous Exp1 protein will not costain with anti-RFP antibody, leading to some areas that are positive only for the anti-Exp1 antibody signal. Also, part of the fusion protein appears to release the fluorescent mCherry domain since we see anti-RFP antibody staining within the PV that does not counterstain with anti-Exp1 antibody. However, the majority of the fusion protein localizes to the PVM, which makes *P. berghei*-LLS-Exp1-mCherry a suitable tool for live imaging of the PVM during the late liver stage.

Therefore, HepG2-GFP cells were infected with *P. berghei*-LLS-Exp1-mCherry parasites and imaged in a confocal time-lapse starting at 62 hpi (Figure 10C). Imaging live parasites in a time-lapse is a delicate setup since illumination light can damage the parasite and cause artifacts. Therefore, many individual infected cells need to be examined to make sure the phenomenon observed is veritable. The sequence of events described below was consistently observed in six independent experiments for all parasites that completed liver stage development. The images shown are representative. In the first still, merozoite formation was already completed and merozoites could be seen in negative. They were surrounded by the intact PVM, but were released into the host cell cytoplasm as it ruptured, as shown in the next image. Further disintegration of the PVM was visible at the next two time points shown.

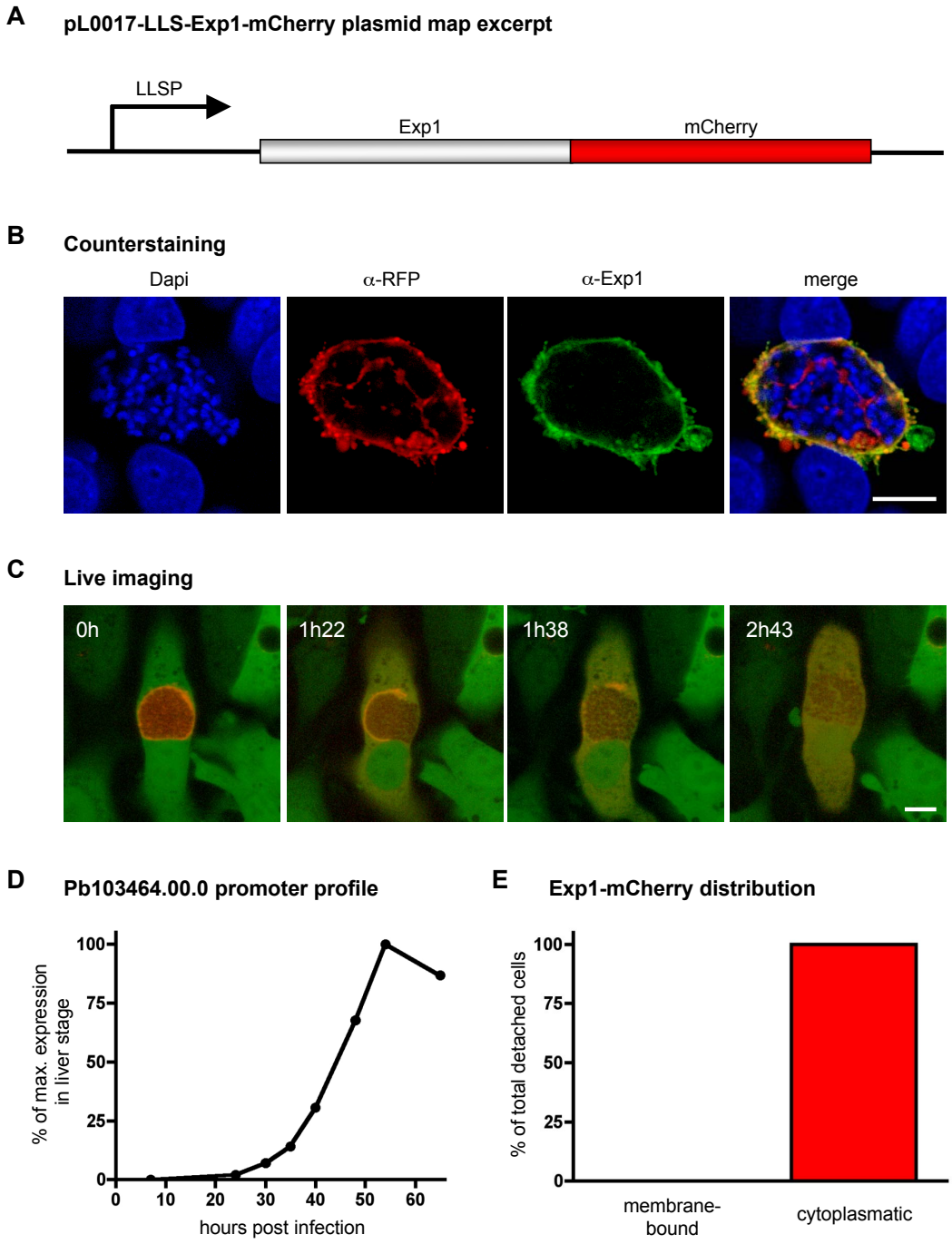

Figure 3.10: Live imaging of the PVM showed that it broke down completely (© S. Gräwe)
A The coding sequence of mCherry was fused to the coding sequence of the Exp1-protein which localizes to the PVM. Expression of the transgenic fusion protein is driven by the late liver stage-specific promoter (LLSP) of the gene Pb103464.00.0 (PlasmoDB).
B HepG2 cells were infected with *P. berghei*-LLS-Exp1-mCherry sporozoites, fixed at 48 hpi and stained for immunofluorescence analysis. Nuclei (blue) were stained with Dapi and mCherry (red) with anti-RFP antibody. Both transgenic and endogenous Exp1 (green) was visualized by anti-Exp1 antibody. The overlay image showed almost complete colocalization of the green and red fluorescence signals and thereby confirmed that the Exp1-mCherry protein localized to the PVM. Bar = 10 µm, CPS.
C HepG2-GFP cells (green) were infected with *P. berghei*-LLS-Exp1-mCherry sporozoites. At 62 hpi, infected cells were imaged every 15 minutes in a confocal time-lapse setup. Representative images are shown. Initially, the PVM (red) was intact and enclosed the cluster of merozoites (0h). It then ruptured and the merozoites were released into the host cell cytoplasm (1h22). Subsequently, the PVM disintegrated
continued on next page

further (1h38) until the Exp1-mCherry protein was distributed evenly throughout the host cell (2h43). n=20 from six independent experiments, bar = 10 µm, CLS.
D The promoter of the gene Pb103464.00.0 (PlasmoDB) was used to drive expression of a luciferase gene within the parasite, and resulting luciferase activity levels were measured at different time points during the liver stage. The maximum activity level was set to 100% and the other levels were calculated in relation to it. Expression lasted throughout the entire late liver stages, beginning around 24 hpi and reaching a maximum around 55hpi before declining slightly. Data kindly provided by Susanne Helm (Bernhard Nocht Institute for Tropical Medicine, Hamburg).
E HepG2 cells were infected with *P. berghei*-LLS-Exp1-mCherry. At 68 hpi, detached cells and merosomes were collected from the supernatant and examined microscopically to assess the distribution of the Exp1-mCherry protein. In all detached cells and merosomes examined, mCherry-fluorescence was wholly cytosolic, confirming the breakdown of the PVM. The mean + SEM of three independent experiments is shown. Total n=672.

Endogenous Exp1 expression would have abated before detachment of the host cell but, as already mentioned above, expression of the transgenic fusion protein was controlled by the promoter of the gene Pb103464.00.0 (Aurrecoechea 2008). The activity pattern of this promoter was assessed by Susanne Helm (Bernhard Nocht Institute for Tropical Medicine, Hamburg, Germany) by driving expression of a luciferase gene within the parasite and measuring the levels of luciferase activity at different time points after infection. The highest value was set to 100% and other levels were set in relation to it and graphed against time (Figure 10D). Starting at 24 hpi, the promoter of the gene Pb103464.00.0 was active throughout the whole late liver stage with a maximum around 55 hpi. Genes under the control of this promoter were still expressed in detached cells and merosomes, which made it possible to confirm the absence of the PVM. At no time point after PVM breakdown did any of the Exp1-mCherry protein localize to a distinct membraneous structure; instead, it was always uniformly distributed throughout the host cell cytoplasm for the remaining liver stage. For quantification, HepG2 cells were infected with *P. berghei*-LLS-Exp1-mCherry parasites and detached cells and merosomes were collected 68 hpi. In all cases, the distribution of Exp1-mCherry protein was solely cytosolic (Figure 10E).

The breakdown of the PVM could also be observed when following the distribution of a cytosolic host cell protein over time. HepG2-GFP cells were infected with *P. berghei*-mCherry sporozoites and imaged in a confocal time-lapse starting at 55 hpi (Figure 11A, from the green channel of Figure 6). A fluorescence profile throughout the host cell showed the distribution of GFP at an earlier and a later time point. At the earlier time point, GFP was only found in the host cell cytosol and was excluded from the parasitophorous vacuole by the PVM. Later, though, it was evenly distributed throughout both the host cell cytosol and the PV lumen, confirming the loss of the PVM barrier.

The same effect could also be seen in reverse, because at the same time that host cell protein entered the PV lumen, parasite components transitioned into the host cell cytoplasm. When examining the fluorescence of *P. berghei*-mCherry in the experimental setup described above, it was initially confined to a densely packed area of merozoites within the PV (Figure 11B). At a later time point, though, the fluorescence peaks were much more evenly distributed. The merozoites had spread throughout the host cell and appeared to move more freely and much faster. As already mentioned, live imaging is delicate and care needs to be taken to ensure that the imaged specimen has not suffered photodamage. In all live imaging experiments performed, the rapid

merozoite movement described here served as a marker of parasite viability after completion of the

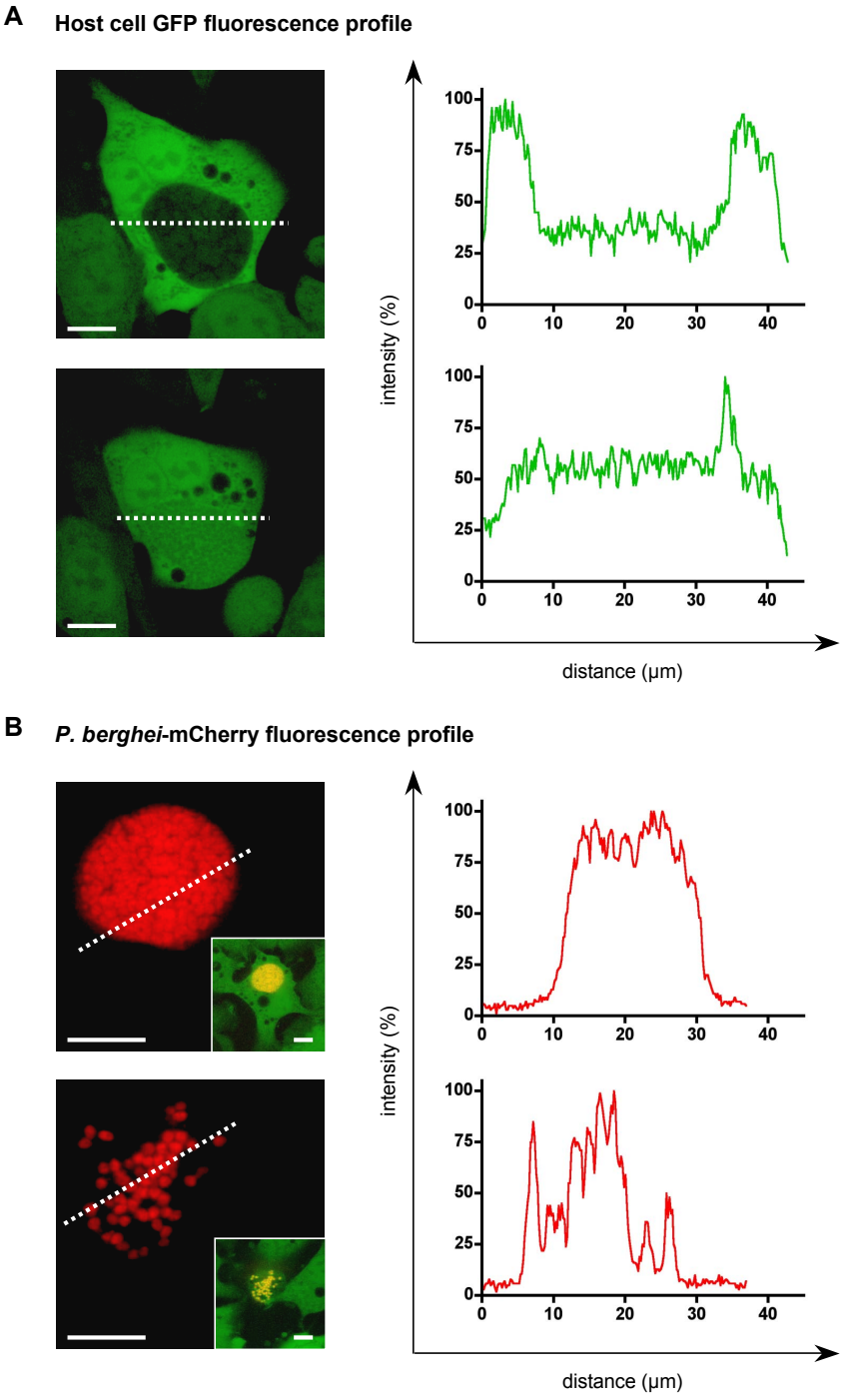

Figure 3.11: The breakdown of the PVM could also be observed through the influx of host cell protein and a changed pattern in the movement of merozoites (© S. Gräwe)
HepG2-GFP cells were infected with *P. berghei*-mCherry parasites. At 55 hpi, infected cells were imaged confocally in a time-lapse setup. Representative images before and after PVM breakdown are shown. Bars = 10 µm, CLS.
A The distribution of host cell GFP (green) along the dashed line was shown in a fluorescence profile. While GFP was initially excluded from the PVM lumen (top), the loss of the PVM barrier led to a uniform distribution (bottom). Images from the green channel of Figure 6.
B The distribution of parasite mCherry along the dashed line was shown in a fluorescence profile. For easier orientation, the insets show the parasite (red) within the host cell (green). Initially, the merozoites were tightly packed and occupied a defined area within the host cell (top). Breakdown of the PVM was marked by freer movement and a random distribution of the merozoites (bottom).

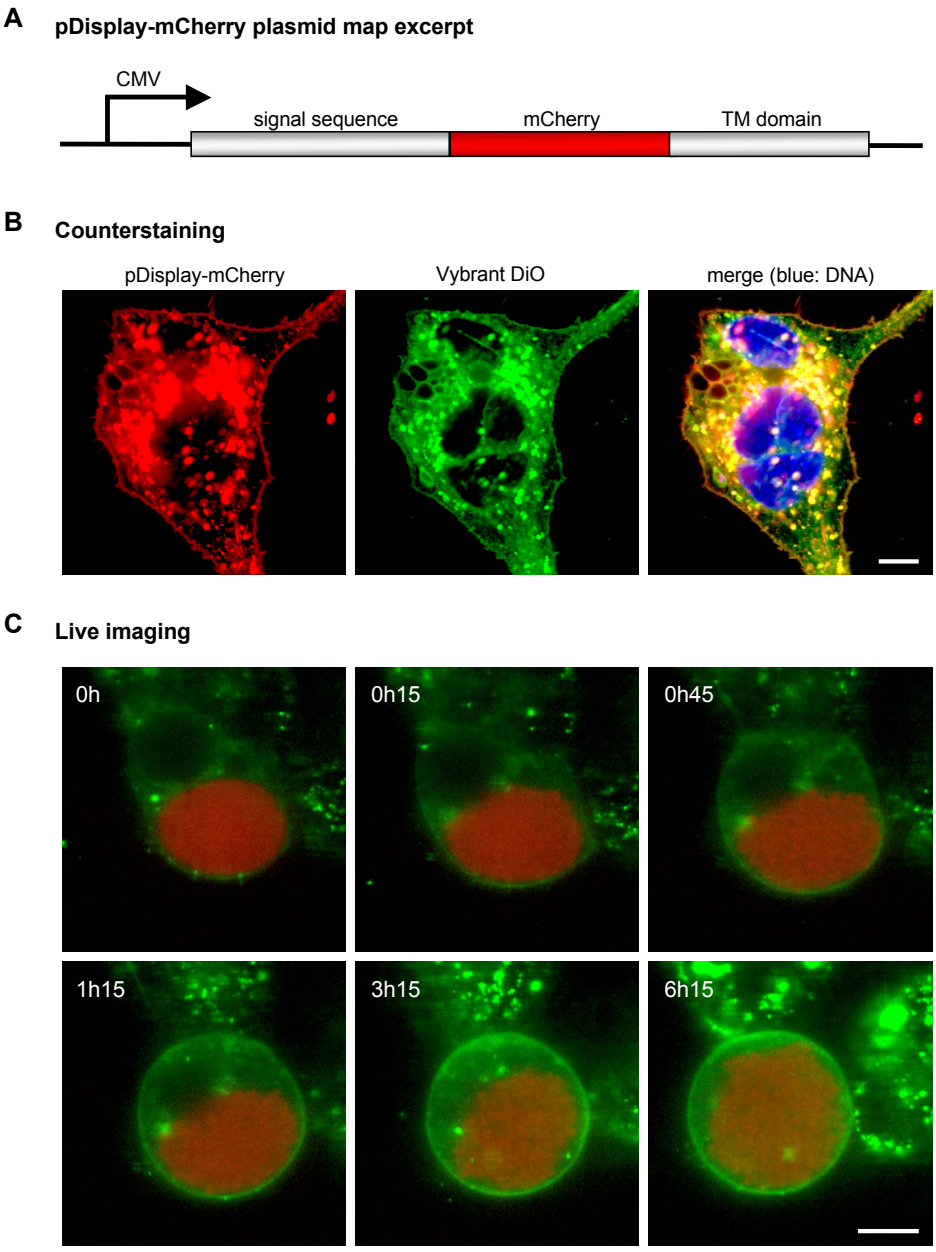

Figure 3.12: Live imaging showed that the host cell membrane became the membrane of the detached cell (© S. Gräwe)
A In the mammalian expression plasmid pDisplay-mCherry, mCherry was fused to a sequence targeting it for secretion and a transmembrane domain, resulting in its localization to the host cell membrane and intracellular vesicles. Expression was controlled by the constitutive CMV promoter. Kindly provided by Prof. Isabelle Tardieux (Institut Cochin, Universite Paris Descartes, Paris, France).
B HepG2 cells were transfected with pDisplay-mCherry (red) and stained with Vybrant DiO (green) and Hoechst 33342 (blue) before confocal images were taken. The overlay of the green and red fluorescence signals showed almost complete colocalization, confirming that Vybrant DiO stains intracellular vesicle membranes and the host cell plasma membrane. Bar = 10 µm, CPS.
C HepG2 cells were infected with *P. berghei*-mCherry sporozoites (red). At 62 hpi, infected cells were stained with Vybrant DiO (green) and imaged every 15 minutes in a confocal setup. Initially, the parasite resided within the PVM in its host cell (0h). After PVM breakdown the host cell began to detach (0h15). During the detachment process it became obvious that the Vybrant DiO-stained host cell membrane was the membrane surrounding the cluster of merozoites (0h45). Following detachment, the merozoites spread throughout the entire cell while the VybrantDiO-staining grew brighter (1h15 - 6h15). n=34 (of which 10 covered the whole development from PVM breakdown to complete detachment) from 11 independent experiments, bar = 10 µm, CLS.

liver stage. It was shown previously that the injection of detached cells or merosomes carrying such rapidly moving merozoites into mice reproducibly led to blood stage infections (Stanway, Graewe et al. 2009).

In conclusion, the PVM was shown by various means to disintegrate before and during detachment of the host cell and it therefore could be excluded as the membrane surrounding detached cells and merosomes. This left the host cell membrane, which was from the start a likely candidate because it would save the parasite the effort to build up a membrane that is only needed for the brief transport in the bloodstream, and also because it would hide the parasite from the host immune system. Previous attempts to prove this by staining the membrane of detached cells and merosomes for hepatocyte surface markers were unsuccessful (Baer, Klotz et al. 2007). Therefore, a different approach was chosen by staining not for specific markers but for the host cell membrane in general using Vybrant DiO.

As a first step, it was confirmed that Vybrant DiO indeed labelled the hepatocyte membrane. To this aim, HepG2 cells were transfected with the mammalian expression plasmid pDisplay-mCherry which encodes mCherry fused to a signal sequence for secretion and a transmembrane domain (Figure 12A). Cells were then stained with Vybrant DiO and Hoechst 33342 and imaged confocally (Figure 12B). Vybrant DiO and the Display-mCherry protein colocalized in the hepatocyte membrane, verifying the suitability of Vybrant DiO for the experimental setup.

HepG2 cells were infected with *P. berghei*-mCherry sporozoites and imaged in a time-lapse. Representative confocal images are shown (Figure 12C). During and after PVM breakdown the host cell slowly rounded up and began detaching. The Vybrant DiO staining revealed that the membrane surrounding the final detached cell was indeed the host cell membrane and that it stayed intact for an extended time (at least 3 hours). This raised the question why the membrane failed to stain positive for hepatocyte surface markers. The physiology of the infected cell likely underwent distinct changes around the breakdown of the PVM and the experiments in the following section were designed to gain more information about the nature of these changes.

3.3 Changes in host cell physiology around the breakdown of the PVM

As a first step the absence of hepatocyte surface markers on the host cell-derived membrane of detached cells and merosomes was addressed. Live imaging was used to observe a transgenically expressed fluorescent membrane protein during the late liver phase. HepG2 cells were transfected with the pDisplay-mCherry plasmid (Figure 12A) and infected with *P. berghei*-GFP sporozoites. At 62 hpi, infected cells were imaged in a confocal time-lapse setup. The sequence of events detailed below was observed in all infected cells that showed an initial membrane localization of the Display-mCherry protein and whose parasites completed liver stage development. The confocal images shown are representative (Figure 13A). Initially, the Display-mCherry protein could be

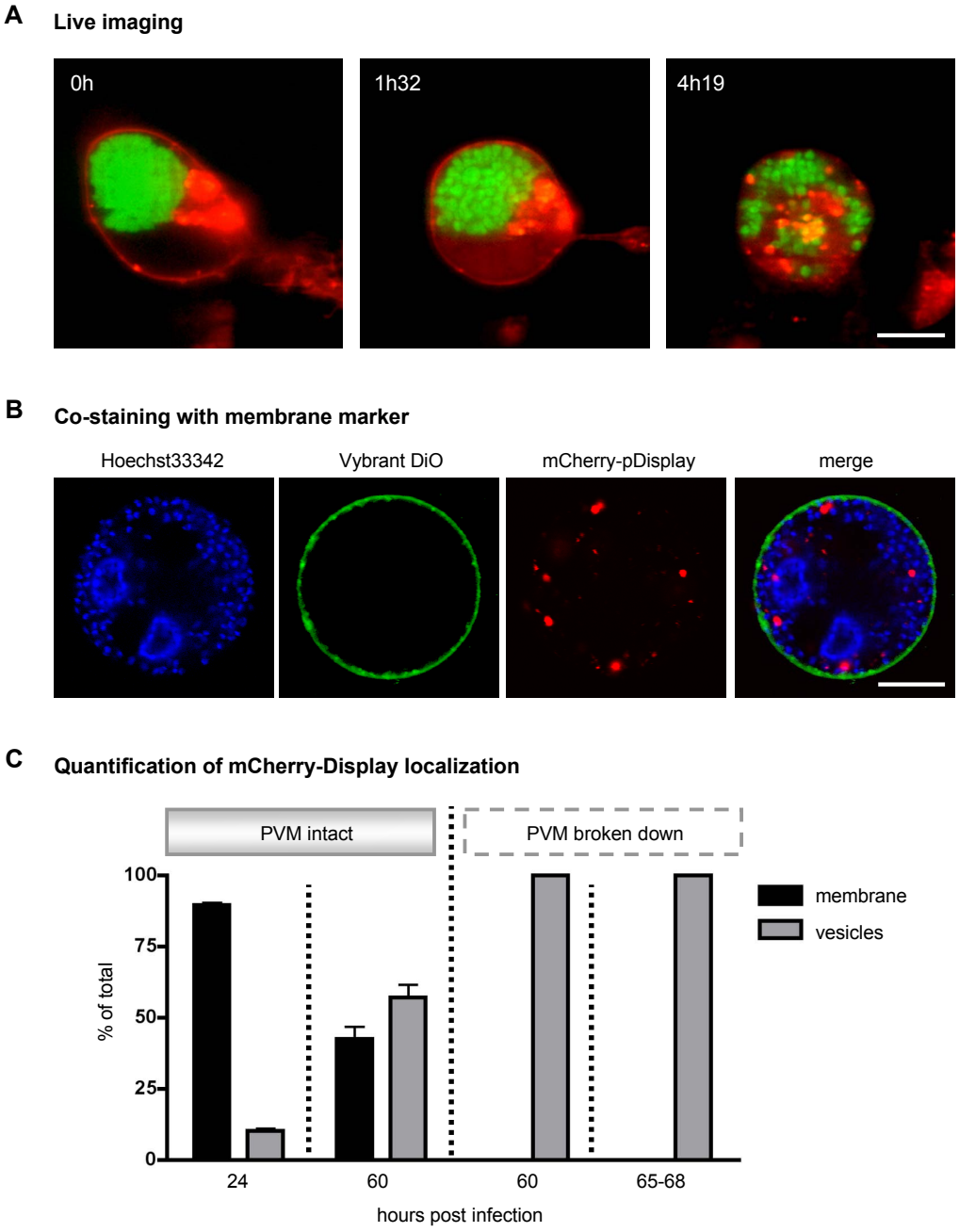

Figure 3.13: A host cell membrane protein was rapidly lost upon PVM breakdown (© S. Gräwe)
A HepG2 cells were transfected with pDisplay-mCherry and infected with *P. berghei*-GFP parasites (green). At 62 hpi, infected cells were imaged every 15 minutes in a confocal time-lapse setup. Representative images are shown. Before PVM breakdown, the Display-mCherry protein (red) localized to the host cell membrane (0h). After PVM breakdown and during detachment of the host cell, though, the fusion protein disappeared from the membrane until it was only present in vesicular structures within the detached cell (1h32 and 4h19). n=3, bar = 10 µm, CLS.
B HepG2 cells were transfected with pDisplay-mCherry and infected with *P. berghei* wild type parasites. At 68 hpi, detached cells and merosomes were stained with Hoechst 33342 to visualize nuclei (blue) and Vybrant DiO to visualize the surrounding membrane (green) before confocal imaging. The overlay confirmed that the residual clusters of Display-mCherry protein (red) were within the cytosol of the detached cell and not within the membrane. n=13 from three independent experiments, bar = 10 µm, CPS.
C HepG2 cells were transfected with pDisplay-mCherry and infected with *P. berghei*-GFP parasites. At 24 and 60 hpi, cells were fixed and stained for immunofluorescence analysis with anti-GFP and anti-RFP antibody. Late stages were also stained with anti-Exp1 antibody to assess the state of the PVM. At 65-68
continued on next page

hpi, detached cells and merosomes were collected and observed live. For all time points, the distribution of Display-mCherry was quantified and the means + SEM of three independent experiments are shown. Before PVM breakdown, Display-mCherry localized partly to vesicles (black columns) and partly to membranes (grey columns). After PVM breakdown, it was only observed in vesicles. Total n for 24 hpi: 201, 60 hpi before PVM breakdown: 252, 60 hpi after PVM breakdown: 53, 65-68 hpi: 574.

found in the host cell membrane as expected, but upon PVM breakdown it immediately distributed in patches throughout the cytosol of the detached cell.

To confirm that these patches are indeed cytosolic and not remnants in the membrane of the detached cell, pDisplay-mCherry-transfected HepG2 cells were infected with *P. berghei* wild type parasites. Resulting detached cells and merosomes were collected and stained with the membrane marker Vybrant DiO and Hoechst 33342. An overlay of the confocal images showed that the clusters of Display-mCherry protein were only present in the cytosol of the detached cell (Figure 13B).

For quantification of this phenomenon, HepG2 cells were transfected with pDisplay-mCherry, infected with *P. berghei*-GFP sporozoites and fixed at 24 and 60 hpi. They were stained for immunofluorescence analysis with anti-RFP and anti-GFP antibody. Additionally, samples fixed at 60 hpi were stained with anti-Exp1 antibody to distinguish between parasites before and after PVM breakdown. Since immunofluorescence staining and artificial attachment of detached cells and merosomes to a surface (i.e. via cytospin) often leads to their rupture and causes artifacts, they were collected at 65 hpi from the supernatant of infected cells and examined directly. The localization of the Display-mCherry protein was divided into two categories: vesicular or plasma membrane-bound (Figure 13C). At the beginning of infection (24 hpi), the majority of infected cells showed a membrane localization. At 60 hpi, the distribution shifted towards a vesicular localization. Likely, this was a consequence of the transfection method used, which only led to a transient expression of the Display-mCherry protein. Still, 43% of the cells with an intact PVM continued to exhibit a membrane localization of the transgenic protein. After PVM breakdown, though, membrane localization was invariably lost both before and after detachment. This confirmed the previous observations from live imaging.

The question arose whether the vesicular structures the Display-mCherry protein localized to were lysosomes, targeting the protein for destruction. To test this hypothesis, HepG2 cells were infected with *P. berghei*-GFP sporozoites and stained with LysoTracker® Red DND-99 at 62hpi. Representative confocal images from a time-lapse are shown (Figure 14). In the beginning, numerous lysosomes could be seen within the host cell cytoplasm. During and after PVM breakdown, however, their number decreased until they were no longer detectable. The positive staining for lysosomes in neighbouring cells in the same field of view confirmed that this was not due to a loss of staining efficacy. Therefore, the loss of Display-mCherry protein from the membrane of the detached cell could not be due to an increased rate of internalization and destruction in lysosomes.

Another possible reason for the loss of membrane proteins would be an arrest of protein biosynthesis within the host cell. This could lead to a shortage of the Display-mCherry protein itself or affect proteins involved in its localization or both. To adress this question, *P. berghei*-infected HepG2 cells were treated with cycloheximide, which blocks translational elongation and therefore protein biosynthesis in eukaryotic cells (Schneider-Poetsch, Ju et al. 2010). If protein synthesis has

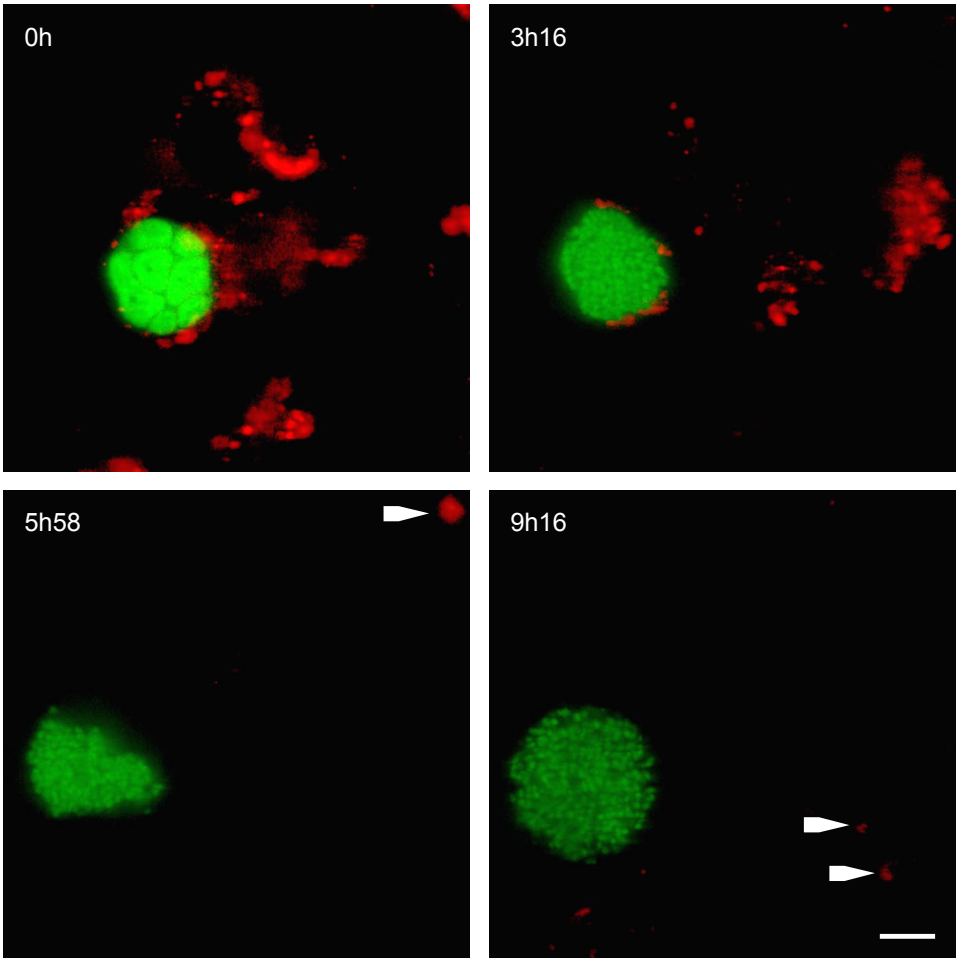

Figure 3.14: The number of host cell lysosomes did not increase upon PVM breakdown (© S. Gräwe)
HepG2 cells were infected with *P. berghei*-GFP parasites (green). At 62 hpi, they were stained with LysoTracker® Red DND-99 (red) to visualize lysosomes. During the cytomere stage, host cell lysosomes were clearly visible (0h). Upon breakdown of the PVM, though, the number of lysosomes decreased (3h16) until they were eventually no longer detectable in the detached cell (5h58 and 9h16). Some lysosomes could still be seen in adjacent cells (indicated by arrows), confirming that if present, lysosomes were still stained. n=17 from five independent experiments, bar = 10 µm, CLS.

indeed stopped in the late liver stage, treatment during 62-70 hpi should have no effect on parasite development and the formation of detached cells and merosomes. In addition, infected cells were treated during an earlier time period (36-44 and 36-70 hpi), when the parasite still actively replicates and protein biosynthesis is assumed to be crucial. Detached cells and merosomes from all treatment regimens were collected, counted and calculated as percentages of an untreated control (Figure 15A).
As expected, both short- and long-term treatment of infected cells during earlier liver stages led to a marked reduction in detached cells and merosomes. Samples treated during the late stage, in contrast, formed detached cells and merosomes at the same rate as the untreated control.

To confirm that the decrease in the formation of detached cells and merosomes after early treatment was not due to death of the host cells following cycloheximide treatment, cells were subjected to the long-term treatment regimen and stained with the Live/Dead reduced biohazard cell viability kit #1. It consists of a green fluorescence marker that enters all cells, living or dead,

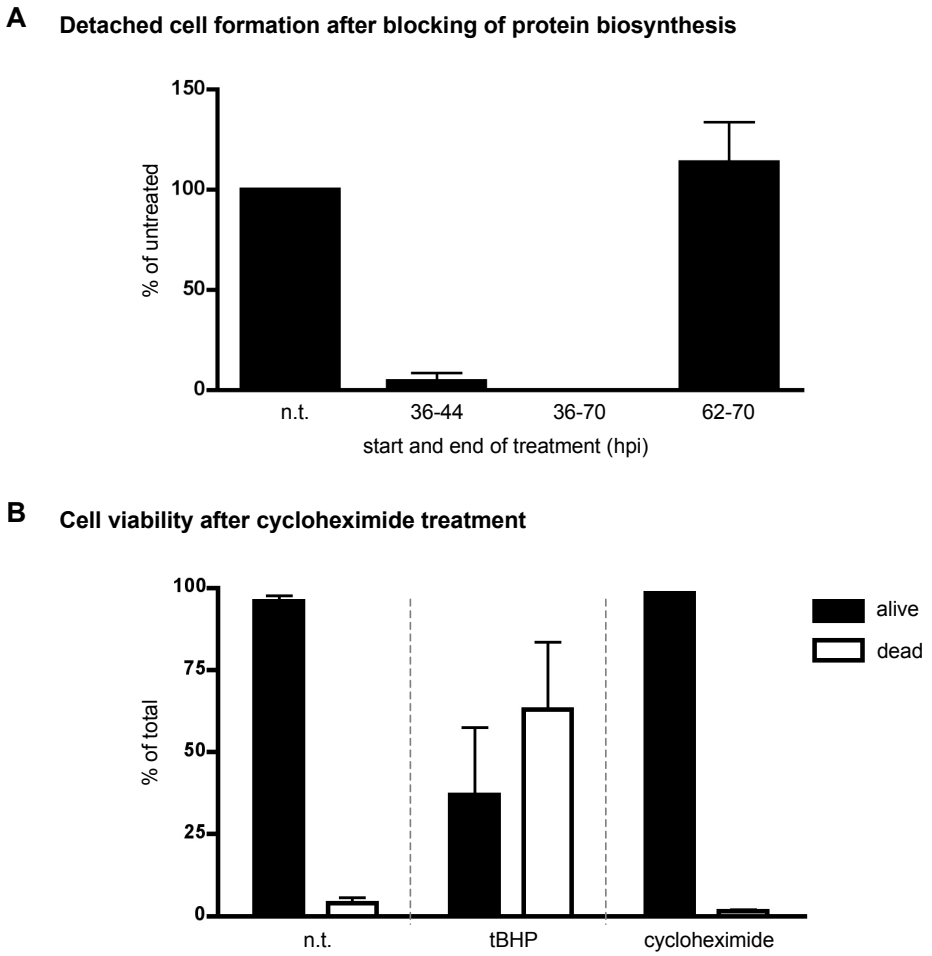

Figure 3.15: Protein biosynthesis appeared to stop after PVM breakdown (© S. Gräwe)
A HepG2 cells were infected with *P. berghei*-mCherry parasites. For different time periods during infection they were treated with 5 µg/ml cycloheximide. At 70 hpi, detached cells and merosomes were collected and counted. The number of detached cells and merosomes resulting from an untreated control infection (n.t.) was set to 100% and all other values were calculated in relation to it. The mean + SEM of three independent experiments is shown. Short- and long-term treatment that started early after infection resulted in a reduced number of detached cells and merosomes, whereas short-term treatment towards the end of liver stage development had no effect. Total n for untreated: 2435, 36-44 hpi: 32, 36-70 hpi: 0, 62-70 hpi: 2714.
B HepG2 cells were either left untreated (n.t.), treated with 10 µg/ml cycloheximide for 34 hours or 155 µM tBHP for 4 hours. They were then stained with the Live/Dead reduced biohazard cell viability kit #1 and both dead and alive cells were quantified. The total number of cells from each sample was set to 100% and the percentage of dead (white columns) versus alive (black columns) cells was calculated. The mean + SEM of three independent experiments is shown. Untreated cells showed a small portion of dead cells, whereas tBHP-treatment resulted in a large number of DeadRed-positive cells. Cycloheximide-treated cells exhibited no greater cell death rate than untreated cells, confirming that the observed drop in the number of detached cells was not the result of widespread host cell death. Total n for untreated: 189, tBHP-treated: 131, cycloheximide-treated: 810.

and a red fluorescence marker that will only stain dead cells. As a positive control, HepG2 cells were stained that had been treated with tBHP, a chemical agent causing cell death (Kim, Kang et al. 1998). Untreated, stained HepG2 cells served as a negative control and to get an impression of the base cell death rate in a normal culture. Living and dead cells were counted and calculated as percentages of the total amount of cells (Figure 15B). While more than 50% of the tBHP-treated cells were dead, the cycloheximide-treated cells showed viability comparable to untreated control HepG2 cells. The difference in the rates of detached cell and merosome formation between

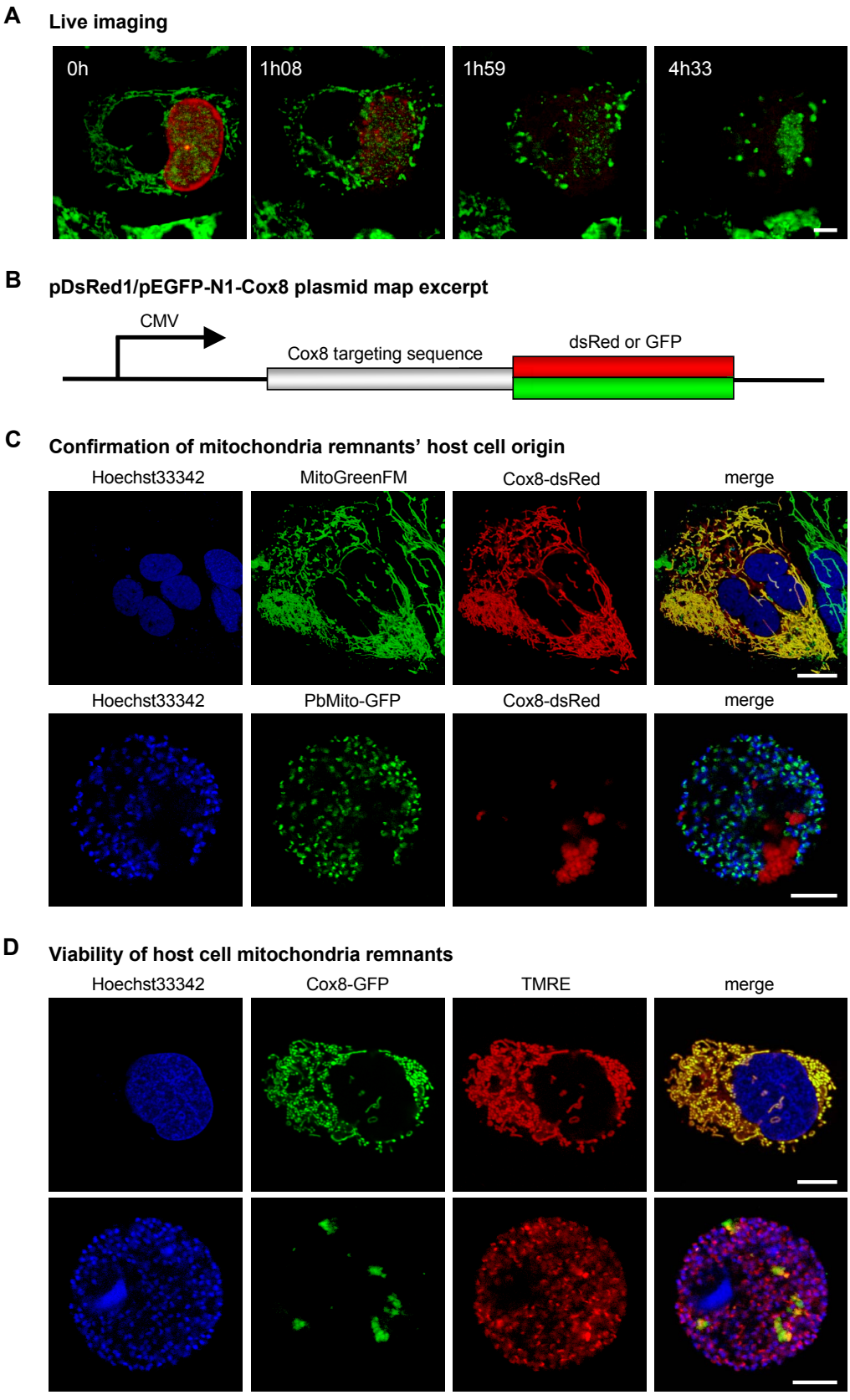

Figure 3.16: Host cell mitochondria quickly disintegrated after PVM breakdown (© S. Gräwe)
A HepG2 cells were infected with *P. berghei*-LLS-Exp1-mCherry parasites. At 62 hpi, cells were stained with MitoTracker® Green FM to visualize mitochondria (green) and imaged in a confocal time-lapse setup. While the PVM (red) was still intact, normal mitochondria staining could be observed (0h). After PVM breakdown, however, the host cell mitochondria began to draw together into clusters that exhibited bright fluorescence (1h08). As the host cell detached, the mitochondria disintegrated more and more (1h59) until
continued on next page

only a few clusters remained in the detached cell (4h33). n=17 from three independent experiments, bar = 10 µm, CLS.
B In the mammalian expression plasmids pDsRed1/pEGFP-N1-Cox8, either dsRed or GFP was fused to the targeting sequence of the mitochondrial Cox8 protein. Expression was driven by the constitutive CMV promoter. Kindly provided by Dr. Christina Deschermeier, Leonie Hecht and Frauke Bach (Bernhard Nocht Institute for Tropical Medicine, Hamburg, Germany).
C HepG2 cells were transfected with pDsRed1-N1-Cox8 and stained with MitoTracker® Green FM to visualize mitochondria (green) and Hoechst 33342 to visualize nuclei (blue). Representative confocal images are shown (top panel). The overlay image showed that DsRed-Cox8 protein (red) colocalized almost completely with the MitoTracker® Green FM fluorescence signal (green), confirming that the DsRed-Cox8 protein localizes to host cell mitochondria. Next, transfected HepG2 cells were infected with *P. berghei*-MitoGFP parasites. At 65hpi, detached cells and merosomes were collected and stained with Hoechst 33342 to visualize nuclei (blue). Representative confocal images are shown (bottom panel). In the overlay image, host cell mitochondria were seen in red and parasite mitochondria in green. All mitochondrial clusters exhibited red fluorescence only, confirming that they were of host cell origin. *P. berghei*-MitoGFP kindly provided by Dr. Rebecca Stanway (Bernhard Nocht Institute for Tropical Medicine, Hamburg, Germany). Bars = 10 µm, CPS.
D HepG2 cells were transfected with pEGFP-N1-Cox8 and stained with Hoechst 33342 to visualize nuclei (blue) and TMRE to visualize mitochondria with an active membrane potential (red). Representative confocal images are shown (top panel). The overlay image showed almost complete colocalization of TMRE and the Cox8-GFP protein, demonstrating that it localized to host cell mitochondria. Transfected HepG2 cells were also infected with *P. berghei* wild type parasites. At 65 hpi, detached cells and merosomes were collected and nuclei (blue) were stained with Hoechst 33342. The overlay image shows that only parts of the host cell mitochondria clusters retained their membrane potential. Bars = 10 µm, CPS.

early and late stage cycloheximide treatment could therefore only be explained by assuming that protein biosynthesis was still needed during early stages but had arrested or was dispensable during the late stages.

One reason why protein biosynthesis might stop could be a lack of energy in the host cell. To investigate this issue, HepG2 cells were infected with *P. berghei*-LLS-Exp1-mCherry parasites and mitochondria stained with MitoTracker® Green FM at 62 hpi. Representative confocal images from a time-lapse are shown (Figure 16A). Before the PVM broke down, the host cell mitochondria exhibited their normal morphology in the shape of a branched network. After PVM breakdown, however, they appeared to shrink and began to form highly fluorescent clusters. These clusters subsequently drew closer together and disintegrated until only a few remained in the detached cell. For a closer examination of these mitochondrial remnants, host cell mitochondria were visualized by transgenic expression of a fluorescent protein. For this, an expression plasmid was used that encoded either dsRed or GFP fused to the targeting sequence of the mitochondrial protein Cox8 (Figure 16B) (Partikian, Olveczky et al. 1998). Co-staining with either MitoTracker® Green FM or TMRE served to test the localization of the fusion proteins. HepG2 cells were transfected with the respective construct and then stained with the mitochondrial dye of the opposite color and Hoechst 33342. Representative confocal images are shown (Figure 16C and D, top rows). Overlaying the red and green fluorescence signals demonstrated almost complete colocalization, confirming that the fusion proteins marked host cell mitochondria. To verify that the mitochondrial remnants observed in live imaging were indeed of host cell and not parasite origin, Cox8-dsRed-transfected HepG2 cells were infected with *P. berghei*-MitoGFP parasites, which expressed GFP fused to the targeting sequence of PbHsp60 and therefore had green-fluorescent mitochondria. Detached cells and merosomes were collected, stained with Hoechst 33342 and imaged confocally (Figure 16C,

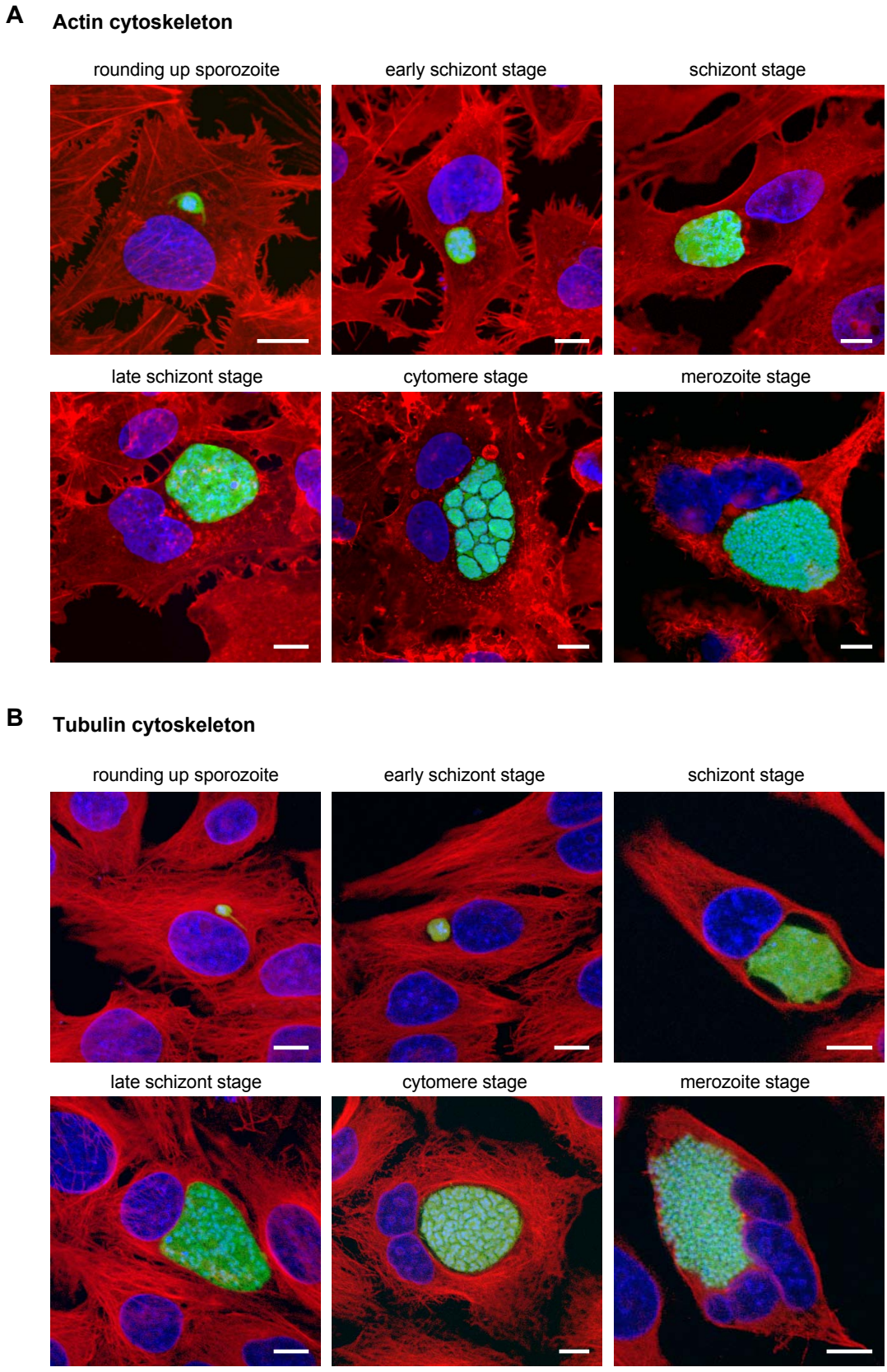

Figure 3.17: The liver stage development of the *Plasmodium* parasite before PVM breakdown was not accompanied by any specific changes in the actin or tubulin host cell cytoskeleton (© S. Gräwe)
A HepG2 cells were infected with *P. berghei*-GFP parasites. At 12, 24, 48 and 60 hpi, cells were fixed and stained for immunofluorescence analysis. Parasites (green) were visualized with anti-GFP antibody, nuclei (blue) with Dapi and the actin cytoskeleton (red) with Phalloidin 568. During all stages observed, no obvious changes in the actin host cell cytoskeleton were seen. Bars = 10 µm, CPS.
continued on next page

B HepG2 cells were infected with *P. berghei*-GFP parasites. At 12, 24, 48 and 60 hpi, cells were fixed and stained for immunofluorescence analysis. Parasites (green) are visualized via GFP, nuclei (blue) with Dapi and the tubulin cytoskeleton (red) with anti-tubulin antibody. At all developmental stages of the parasite that were examined, the tubulin cytoskeleton extends throughout the cell as a branched network and shows no specific changes. Bars = 10 µm, CPS.

bottom row). In the overlay, all remnants exclusively showed red fluorescence, confirming that they are of host cell origin.

Next, the viability of the host cell mitochondria remnants was tested. For this, Cox8-GFP-transfected HepG2 cells were infected with *P. berghei* wild type parasites. Detached cells and merosomes were collected and stained with TMRE and Hoechst 33342 for confocal imaging (Figure 16D, bottom row). As the overlay shows, only a subset of the green-fluorescent mitochondria remnants was still stained by TMRE. Since TMRE will only label mitochondria with an active membrane potential, this suggested a loss of their capability to produce ATP for intracellular synthesis processes. Therefore, a lack of energy might indeed be one of the causes why protein biosynthesis arrests during the late liver stage.

The observations above led us to question why the host cell mitochondria shrink rapidly after the breakdown of the PVM. Since mitochondria are known to be associated with the cytoskeleton (Rappaport, Oliviero et al. 1998), it is possible that they reacted to changes in it during the development of the parasite. These changes are likely to occur in the short time window between PVM breakdown and host cell detachment and might only be visible when imaged over time. Live observation would be ideal to resolve this question but unfortunately, the transgenic expression of several cytoskeleton proteins coupled to either GFP or mCherry failed to paint a clear picture. A potential reason is that the parasite distorted the infected cell into a spherical shape even before detachment. This could interfere with cytoskeletal imaging which works best in flat, extended cells. However, novel plasmid constructs will hopefully overcome this obstacle in the near future and deliver insights into cytoskeletal changes during detachment.

What could be shown here was that there were no significant changes in the host cell cytoskeleton before PVM breakdown, which correlated with the inconspicuous morphology of the mitochondria during this time. HepG2 cells were infected with *P. berghei*-GFP parasites, fixed at different time points after infection and stained for immunofluorescence analysis and confocal imaging of either the actin or tubulin cytoskeleton (Figure 17). In the actin cytoskeleton, minor changes occurred over time that are expected to happen during the rapid growth of any intracellular object (Figure 17A). These included stress fibers and an enrichment of filamentous actin at the cell edges and in focal adhesions. However, no specific changes were seen over the course of infection. The tubulin cytoskeleton extended as a branched network throughout the entire host cell at any time point observed (Figure 17B), and it also did not show any specific changes. While microtubuli appeared to surround the late schizont stage of the parasite, it is likely that this was due to spatial constraints rather than a targeted interaction.

CHAPTER 4: DISCUSSION

In this study a bright, photostable red-fluorescent protein was identified that could be expressed in *P. berghei* for microscopic long-term analysis. This protein was used to generate and study transgenic parasite strains to shed light on the events of the late liver stage. In particular, the origin of the membrane surrounding merosomes was determined and the parasite dependent host cell death was analyzed in detail.

The red-fluorescent mCherry protein allows long-term imaging of *Plasmodium* parasites without obvious photodamage

Of the three red-fluorescent parasite strains that were examined here, *P. berghei*-mCherry was by far the brightest. This finding is somewhat unexpected since previous studies indicated the opposite (Knop, Barr et al. 2002; Shaner, Campbell et al. 2004). However, these analyses have been performed on recombinant protein or in bacterial, yeast or mammalian expression systems, whereas in this study measurements were taken after expression in protozoan parasites. Both expression and brightness of the red-fluorescent proteins might vary depending on their host organism. This might make it impossible to compare data from different experimental setups.

Incongruity might also result from the use of different excitation light sources. While the data from Shaner *et al,* for example, were obtained using a Xenon arc lamp (Shaner, Campbell et al. 2004), in this study an HXP120 lamp or laser light were used. The fixed excitation wavelength of the laser line in particular may pose a problem, since not all fluorescent proteins will be excited equally. However, the laser used in this study emitted at 561 nm, which is much closer to the excitation maxima of RedStar and tdTomato (558 and 554 nm, respectively) than to that of mCherry (587 nm) (Knop, Barr et al. 2002; Shaner, Campbell et al. 2004). Therefore, if anything mCherry was excited to a lesser degree than RedStar and tdTomato and should have been less bright.

A more likely explanation for the superior brightness of mCherry might lie in its conformation. While RedStar and tdTomato are multimeric, mCherry is a monomer (Shaner, Campbell et al. 2004). It is possible that a multimeric state was difficult to reach in the *Plasmodium* expression system and therefore the overall fluorescence level remained low. Where multimeric folding is fully functional, RedStar and tdTomato might indeed be much brighter than mCherry.

Whatever the reason might be, for the *Plasmodium* expression system mCherry is unequivocally the best choice. In addition to being brighter than RedStar and tdTomato, it is also more photostable. It can only be speculated why this is the case since photobleaching is a complex and poorly understood process. From current knowledge the following model has been proposed (Ayers 2009; Eisemann, Oelsner et al. 2009; Leach 2009; Herman, Parry-Hill et al. 2010; Johnson and Davidson 2010; Sheffield Hallam University 2010): upon illumination at its excitation wavelength, the chromophore absorbs energy. It can then either discharge the superfluous energy as fluorescence or transition into an excited triplet state. This triplet state contains electrons that are no longer spin-paired and is thus highly reactive. It readily interacts with other molecules which

can lead to the covalent modification of the chromophore and therefore the permanent loss of its ability to fluoresce.

It is highly likely that oxygen plays a role during this process, since it often exists in a natural triplet state itself (Leach 2009). Fluorescent dyes containing aromatic carbon rings have been shown to bleach in the presence of oxygen (Renn, Seelig et al. 2006), and since the chromophores of the red-fluorescent proteins have such rings (Shu, Shaner et al. 2006), it is feasible that their loss of fluorescence occurs in a similar manner. Photobleaching involving oxygen is not just bothersome from an imaging point of view, but can also damage cells. Upon interaction with the triplet state chromophore, highly reactive singlet oxygen is formed that can induce DNA strand breakage (Yang, Wang et al. 1999), rapidly oxidize molecules containing carbon-carbon double bonds (Flors, Fryer et al. 2006) and ultimately trigger apoptosis (Kochevar, Lynch et al. 2000).

A modification of the chromophore after reaction with oxygen could explain why for all fluorescent proteins examined bleaching was far more pronounced in intravital than in *in vitro* imaging. Since oxygen is distributed via hemoglobin in the living organism, it should be relatively freely available within the liver tissue. In contrast, in cell culture oxygen mostly reaches the cells by passive diffusion through the culture medium (Camp and Capitano 2007). Under the culture conditions of this study, the oxygen concentration within the cells was likely low. As a result, chromophore-damaging reactions with triplet state oxygen might have occurred less often than in living tissue, thus leading to a reduced rate of photobleaching.

The triplet state theory behind bleaching also offers an explanation for the observation that photostability was higher in wide-field than in confocal imaging. In the latter, fluorescence is excited by a laser and this focused, high-energy light might allow formation of the triplet state more often than wide-field excitation. It is also possible that bleaching occurs at the same rate in both imaging types but is more readily detected in confocal imaging. Since only one focal plane is imaged, any loss of fluorescence will be immediately obvious, whereas in wide-field imaging some degree of bleaching might be masked by fluorescence from other focal planes.

While this explains why the same fluorescent protein behaves differently in varying imaging setups, it does not explain why the three red-fluorescent proteins differ in their photostabilities even in the same setup. Both tdTomato and mCherry are derived from mRFP and various mutations were introduced during their development (Shaner, Campbell et al. 2004). Little is known about how these changes affect the chromophore architecture in tdTomato, but the mCherry chromophore is distinctly distorted in comparison to the planar structure of mRFP (Shu, Shaner et al. 2006). This likely has an impact on the electron density distribution and might lead to steric changes. In combination these factors might hinder the ability of the chromophore to react with triplet state oxygen or other molecules and thus, photobleaching might occur to a lesser degree than for RedStar and tdTomato.

However, all this is mere speculation which further research into photodamage and photostability will have to prove or disprove. Independent of knowing the underlying molecular and physical mechanisms, the brightness and photostability of mCherry when expressed in *P. berghei* makes it a highly efficient tool to image parasite structures over long time periods.

After the PVM ruptures, the host cell membrane becomes the membrane of merosomes

Although the liver stage of *Plasmodium* infections is an attractive target for both treatment and vaccination, it is difficult to access for analysis and therefore still poorly understood (Rankin, Graewe et al. 2010). Therefore, several *P. berghei* parasite strains expressing mCherry either

cytosolically or targeted to specific locations were generated for *in vitro* live observation. A key question was the origin of the membrane surrounding detached cells and merosomes. As mentioned previously, both *in vivo* and *in vitro* merosomes derive directly from detached cells and thus share the same membrane (Sturm, Amino et al. 2006; Baer, Klotz et al. 2007). Therefore this study did not differentiate between detached cells and merosomes, but care was taken to confirm that the membranes of both exhibited the same phenotype.

Initially, common properties of the membrane in question were established. Staining with the general membrane marker Vybrant DiO confirmed the presence of a membrane in both newly formed and aging detached cells and merosomes. Using propidium iodide and pSIVA it was demonstrated that in early stages this membrane is intact and retains phosphatidylserine asymmetry. At later time points after formation, though, the membrane becomes permeable and phosphatidylserine is exposed in the outer membrane leaflet. This corroborated previous findings about both *in vitro* and *ex vivo* merosomes (Sturm, Amino et al. 2006; Baer, Klotz et al. 2007). However, some controversy had always remained on whether the exposure of phosphatidylserine might have been triggered by the change in culture conditions necessary for traditional annexin-based phosphatidylserine stainings. In the present study this could be excluded since the novel reagent pSIVA can be used in regular HepG2 cell culture medium (Kim, Chen et al. 2009). It is notable that membrane asymmetry and integrity are lost much faster in *P. yoelii ex vivo* than in *P. berghei in vitro* merosomes (Sturm, Amino et al. 2006; Baer, Klotz et al. 2007). This might be a result of the differing environmental conditions or a feature of the parasite strains themselves.

After this general characterization of the merosome membrane, the three membranes it could originate from were examined individually during the late liver stage. In agreement with a previous publication (Sturm, Graewe et al. 2009) the parasite membrane was shown to invaginate and to become the membrane of merozoites and could therefore be excluded as a possible source of the merosome membrane.

The PVM could be excluded as well because live imaging of a transgenic parasite strain expressing mCherry fused to the PVM marker protein Exp1 demonstrated that this membrane disintegrates entirely before detachment of the infected cell. This is in agreement with the circumstantial evidence delivered by a number of previous studies. Not only had a mixture of parasite and host cell material been observed in late liver stages (Meis, Verhave et al. 1985) but host cell organelles were also seen within intravital merosomes (Baer, Klotz et al. 2007). In addition, typical PVM proteins such as uis4 could not be detected on the membrane of merosomes (Baer, Klotz et al. 2007). As mentioned previously, imaging of living organisms can cause photodamage and therefore create artifacts (Yang, Wang et al. 1999; Kochevar, Lynch et al. 2000; Flors, Fryer et al. 2006). It is therefore a valid concern that the observed breakdown of the PVM is such an artifact. However, this can be excluded for several reasons. For one, the released merozoites continue to exhibit rapid movement after PVM breakdown. This is a marker of parasite viability since intravenous injection of detached cells and merosomes containing such merozoites into mice consistently results in blood stage infection (Stanway, Graewe et al. 2009). Interestingly, the merozoite movement becomes far more pronounced after the rupture of the PVM. This raises the possibility of active movement that has been confined by the PVM barrier. Another reason why accidental destruction of the PVM through phototoxicity can be ruled out is that the PVM is also absent in detached cells and merosomes that have developed without exposure to laser light. Moreover, in our hands photodamage virtually always resulted in developmental arrest and the

parasite exhibited either extensive vacuolization or undefined aggregates. Neither of those phenotypes were observed when the parasite strain expressing Exp1-mCherry in the late liver stage was analyzed.

So far it is still unknown how the breakdown of the PVM is triggered and executed. It can be prevented by the general protease inhibitor E64 and therefore proteases likely play a role (Sturm, Amino et al. 2006). However, definite executors are still unknown. Recently, the liver-specific protein 1 (LISP1) has been implicated in PVM disruption, but here also the exact mechanism is unclear (Ishino, Boisson et al. 2009). In *Toxoplasma gondii*, a pore-forming protein and changes in intracellular ion concentrations have been implicated (Moudy, Manning et al. 2001; Nagamune, Hicks et al. 2008; Kafsack, Pena et al. 2009). Such pore-forming proteins (PFPs) are a common means of vacuolar or cellular exit for a variety of intracellular pathogens. However, many of them cross a phagosomal membrane and therefore can control PFP activity via the ambient pH values as in *Trypanosoma cruzi* (Andrews 1990; Andrews, Abrams et al. 1990). In others, as in *T. gondii* and *Leishmania amazoniensis*, all surrounding membranes are lysed in quick succession (Noronha, Cruz et al. 2000; Moudy, Manning et al. 2001). In contrast to that, in the *Plasmodium* liver stage only the PVM was disrupted. Staining of the host cell membrane with Vybrant DiO revealed that it stays intact after the parasite has been released into the host cell cytoplasm. Upon detachment of the entire cell, it forms the membrane surrounding the cluster of exoerythrocytic merozoites, both in the main cell body and in subsequently budding merosomes. The formation of the latter can be blocked by protease inhibitors and has thus been suggested to occur through a protease-mediated destabilization of the detached cell membrane (Sturm, Amino et al. 2006).

In principle the situation is quite similar to the egress of blood stage merozoites. In both cases the parasite needs to cross two membranes before a new round of infection can occur. However, in contrast to the liver stage, where the host cell membrane ruptures much later than the PVM and only by physical force after the merosomes have reached the lung (Baer, Klotz et al. 2007), in the blood stage both membranes rupture in quick succession (Blackman 2008). To this day there is an ongoing debate on whether the PVM or the RBC membrane disintegrate first. Live imaging of parasites expressing GFP in the parasitophorous vacuole has shown that towards the end of the blood stage GFP fills the entire host cell (Wickham, Culvenor et al. 2003). This argues for a rupture of the PVM before the host cell membrane. However, another study reported extracellular clusters of merozoites that were tightly wrapped in the PVM, which indicates that the host cell membrane is first to dissolve (Soni, Dhawan et al. 2005). At present, no model has been suggested that can consolidate these conflicting observations.

All studies agree that a protease cascade is necessary for release of the parasite at the end of the blood stage (Yeoh, O'Donnell et al. 2007; Blackman 2008). It was found that the disruption of both PVM and RBC membrane could be specifically inhibited. While treatment with the broad-spectrum serine and cysteine protease inhibitors leupeptin and chymostatin prevented the rupture of the host cell membrane, degradation of the PVM could only be blocked by the cysteine protease-specific inhibitor E64 (Salmon, Oksman et al. 2001; Wickham, Culvenor et al. 2003; Soni, Dhawan et al. 2005). This implies that different sets of effector molecules exist. It is interesting that in both liver and blood stages the disintegration of the PVM is stopped by the same inhibitor (Salmon, Oksman et al. 2001; Wickham, Culvenor et al. 2003; Sturm, Amino et al. 2006), suggesting that the same mechanisms act in both stages. However, the set of effectors that breaks down the host cell membrane is either not expressed or not released in the liver stage.

Alternatively, it might be present, but inhibited by parasite factors such as the recently identified cysteine protease inhibitor PbICP (Rennenberg, Lehmann et al. 2010). While PbICP is not exclusive to the liver stage, it has been reported to undergo post-translational processing during the blood stage and this might alter its function or localization.

After breakdown of the PVM, the host cell undergoes a special kind of cell death that might result from aborted apoptosis due to energy depletion

The release of the parasite into the host cell cytoplasm has a profound effect on the host cell (summed up in Figure 4.1) and marks the beginning of a specialized kind of cell death (Sturm, Amino et al. 2006). This cell death might be triggered in several ways. For one, the cell could simply undergo an autophagy-like cell death after it has been depleted of its resources by the parasite. Two, the sheer mass of foreign protein that floods the cell after the PVM breakdown might cause the host cell to die as an unspecific effect. Or three, specific parasite proteins might be released upon PVM breakdown that orchestrate a parasite-dependent host cell death.

One of the first effects after PVM breakdown that was detected in this study was the deterioration of the mitochondrial network into small punctate structures. This is in contrast to a previous study where electron microscopy images of *in vivo* merosomes featured well-preserved mitochondria (Baer, Klotz et al. 2007). It is possible that these images coincidentally show one of the areas where here also membrane potential was still observed. Alternatively, this might reflect a general difference between *in vivo* and *in vitro* merosomes or even *P. berghei* and *P. yoelii*.

The mechanisms behind this degeneration are uncertain, but might involve the host cell cytoskeleton since mitochondrial fragmentation similar to the one seen here was also seen after the interruption of vimentin intermediate filaments (Tang, Lung et al. 2008). Both the morphology and the loss of membrane potential closely resemble mitochondria during apoptosis (Frank, Gaume et al. 2001).

Mitochondria play a key role in the apoptotic program, and often decide when it will be initiated (Kroemer and Reed 2000). It is not unlikely that host cell death after PVM rupture is also triggered via mitochondria. Several scenarios are conceivable that might act in combination. For one, mitochondria constantly integrate pro- and anti-apoptotic signals arriving from various cellular components (Kroemer and Reed 2000). Upon breakdown of the PVM, the host cell might simply be confronted with enough stress factors to shift the balance towards the induction of cell death. It is also possible that the parasite actively disrupts mitochondria. Various viruses and bacteria are already known to regulate host or target cell apoptosis at the mitochondrial level by producing either pore forming proteins (Muller, Gunther et al. 1999; Kozjak-Pavlovic, Dian-Lothrop et al. 2009) or homologs of pro-apoptotic host cell proteins (Boya, Roques et al. 2001). Parasite proteins could not only act on mitochondria, but also on other host cell organelles. For example, they could mediate the release of cathepsins from lysosomes. Cathepsins in turn are able to cause the release of cytochrome c from mitochondria and therefore to trigger apoptosis (Sturm and Heussler 2007). Any of these paths would lead to the rupture of the mitochondrial membrane and the release of apoptotic factors. Interestingly, the cell death seen during the late liver stage resembles the initial stages of apoptosis.

For one, cytochrome c is released into the host cell cytoplasm (Sturm, Amino et al. 2006). Under normal apoptotic circumstances it forms a complex with Apaf-1 (apoptotic protease activating factor), which then initiates the caspase cascade (Zou, Li et al. 1999). It has been demonstrated though, that caspases are not involved in this host cell death since caspase

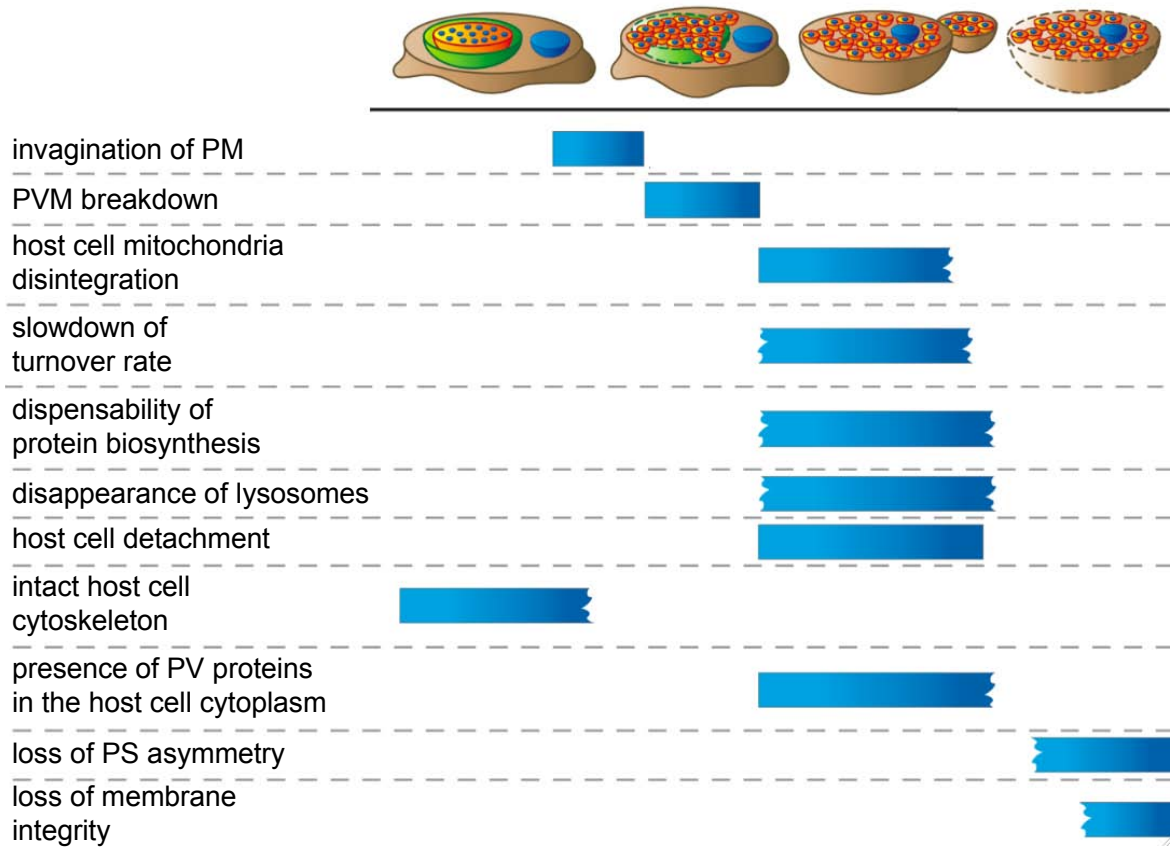

Figure 4.1: Alterations in host cell physiology during the late phase of *Plasmodium* hepatocyte infection (© S. Gräwe)
After invagination of the parasite membrane around merozoites, the PVM breaks down and parasite proteins are released into the host cell cytoplasm. This marks the beginning of several changes in host cell physiology. The mitochondria disintegrate, protein turnover appears to slow down and protein biosynthesis becomes dispensable. Lysosomes disappear and the host cell begins to detach. While the membrane surrounding the detached cells and merosomes is initially intact and phosphatidylserine-negative, both integrity and phosphatidylserine asymmetry are lost over time.

inhibitors had no effect on cellular development at this stage (Sturm, Amino et al. 2006). It is possible that the parasite actively blocks the caspase cascade. Also, host cell energy levels could play a role, since the formation of the apoptosome from cytochrome c and Apaf-1 requires ATP (Zou, Li et al. 1999). During its prolonged growth period the parasite exploits the cell‘s resources and is likely to put a strain on its energy supply. It is possible that this depletes the amount of available ATP to a level that is not sufficient for the full execution of the apoptotic program.

This would also explain why there is chromosomal condensation but not fragmentation (Sturm, Amino et al. 2006). Upon rupture of the mitochondria, apoptosis inducing factor (AIF) is released and translocates to the nucleus (Daugas, Susin et al. 2000). There, it activates DNAses and endonucleases which will then cut DNA strands. However, to do this they require energy in the form of ATP, which would not be available. Other nucleases would be stalled even earlier. They are usually activated by caspase 3 (Liu, Zou et al. 1997; Enari, Sakahira et al. 1998) which in turn is activated by caspase 9 (Kuida, Haydar et al. 1998). The inhibition or knock-out of caspases has repeatedly been shown to result in a loss or delay of DNA fragmentation (Kuida, Haydar et al. 1998; Petit, Arnoult et al. 2002; Essmann, Bantel et al. 2003; Zhou, Qian et al. 2005). Since caspase 9 is not activated here, its downstream effectors will also remain ineffective.

In addition to nuclear fragmentation, caspases have also been reported to be involved in the phosphatidylserine switch (Castedo, Hirsch et al. 1996; Martin, Finucane et al. 1996). The exact mode of action is not yet resolved but likely includes the downregulation of phospholipid translocases and the activation of a lipid scramblase that catalyzes a random bidirectional movement (Moreira and Barcinski 2004). In the absence of active caspases, this scramblase might not be switched on. Therefore, the active transport of phosphatidylserine to the outer membrane leaflet would be abolished. Without this mechanism, the flipping of lipids is slow and consequently membrane asymmetry is relatively stable. Phosphatidylcholine asymmetry, for example, decays with a half-time of six and a half hours (Kornberg and McConnell 1971). Therefore, the observed exposure of phosphatidylserine on the membrane of aging detached cells and merosomes might not be an active process but the result of passive diffusion over time. Interestingly, the treatment of merosomes with the calcium ionophore ionomycin resulted in phosphatidylserine exposure, indicating that the lipid scramblase can still be activated (Sturm, Amino et al. 2006). However, the mechanism underlying ionomycin-dependent asymmetry loss has been reported to differ from the one observed during apoptosis. While it still involves the lipid scramblase (Gonzalez, Gibbons et al. 2009), it is independent of mitochondrial depolarization (Arachiche, Kerbiriou-Nabias et al. 2009). Therefore, ionomycin might activate the lipid scramblase in a manner that is caspase- and ATP-independent and consequently circumvent the block caused by energy depletion. Once activated, the scramblase itself does not appear to require ATP to execute its function (Sulpice, Zachowski et al. 1994; Bevers, Comfurius et al. 1998).

In combination, the following model is suggested (Figure 4.2): during parasite replication the host cell is depleted of much of its ATP resources. Upon rupture of the PVM, mitochondria rupture and oxidative phosphorylation is uncoupled which aggravates the lack of available energy. At the same time, factors are released from the mitochondria that initiate apoptotic cell death. They proceed in their usual manner until they or their downstream effectors require major amounts of ATP. Then, they are stalled, which leads to an aborted version of apoptosis.

The overall standstill of processes that need energy would also explain why protein biosynthesis arrests during the late liver stage and why membrane proteins are lost from the host cell membrane. Especially proteins which have a high turnover rate are expected to be affected very quickly. While enough energy might be left for internalization, the synthesis of new protein might already have stopped, and this might be the reason why ASGR1 (asiaglycoprotein receptor) is not detectable anymore by the time merosomes form (Baer, Klotz et al. 2007).

However, the cell death observed in the late liver stage differs from oncosis, the standard death program that often occurs after the loss of energy. It is characterized by an increased membrane permeability that goes along with swelling and eventually blebbing and rupture of the cell (Fink and Cookson 2005; Malhi, Gores et al. 2006). Especially in hepatocytes various combinations of cell death types are often observed (Jaeschke and Lemasters 2003) which makes an exact classification difficult. Perhaps the remaining energy store within the cell is sufficient to tip the balance towards the initiation of apoptosis instead of necrosis. Also, the parasite might manipulate host cell death to a phenotype that suits it. Observations from avirulent *Toxoplasma gondii* infections make this a likely scenario. The PVM of these parasites has been shown to be disrupted by host IRG proteins (interferon-inducible immunity-related GTPases) (Zhao, Khaminets et al. 2009). While this kills the parasite, it also leads to the release of the contents of the parasitophorous vacuole into the host cell, which is similar to the situation after *Plasmodium* PVM

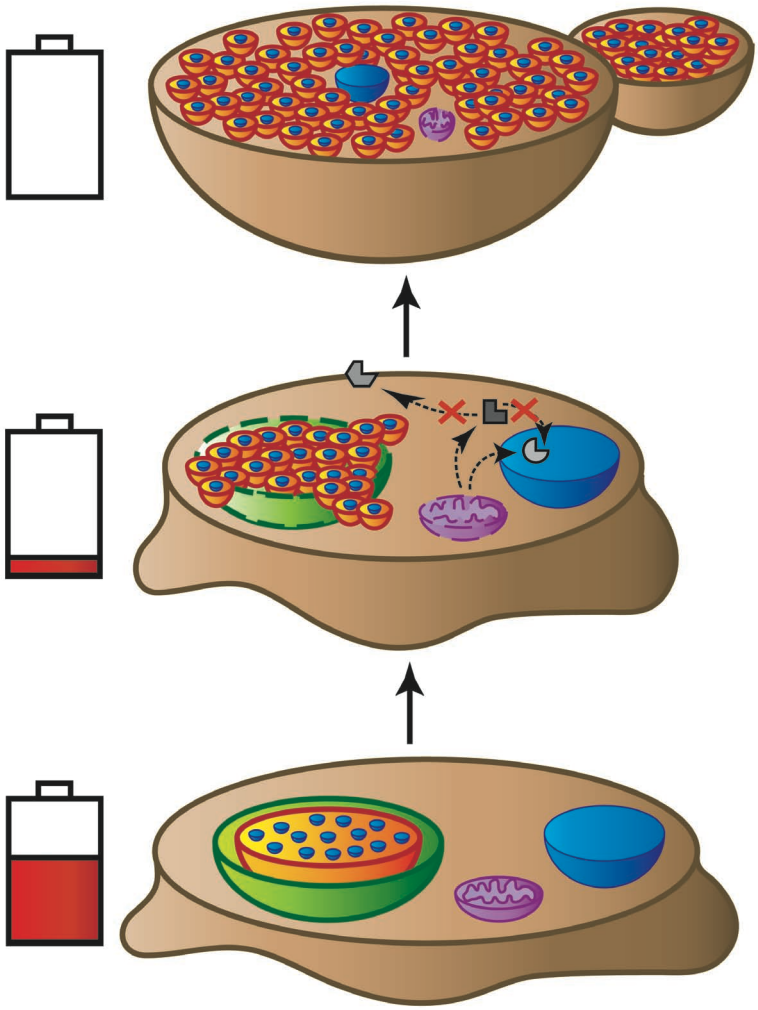

Figure 4.2: Energy depletion might lead to an aborted apoptosis program at the end of the *Plasmodium* liver stage (© S. Gräwe)
While the *Plasmodium* parasite (orange) grows inside its host hepatocyte (brown), it exploits its resources and likely puts a strain on the ATP supply (indicated by the battery symbol on the left). Otherwise, the cell is morphologically inconspicuous, both mitochondria (purple) and nucleus (blue) do not differ from uninfected cells (bottom panel). Once the PVM (green) breaks down, the host cell mitochondria begin to disintegrate and release various apoptotic factors (grey square and circle) such as cytochrome c and AIF (middle panel). They localize to their target structures but cannot activate their downstream effectors since the cellular ATP level has been further depleted. Neither chromosomal fragmentation nor caspase activation take place. Since the latter is necessary for activation of the phosphatidylserine scramblase (grey hexagon), membrane asymmetry is maintained while the cell undergoes an aborted version of apoptosis. Eventually, the host cell detaches and is merely a shell surrounding the merozoites (top panel). Since most mitochondrial remnants have lost their membrane potential at this point, the ATP level in the host cell is expected to be close to zero.

rupture. Just as in *Plasmodium* late liver stages, a caspase-independent host cell death results. However, while in *Plasmodium* infections this death is comparatively slow and immunologically inconspicuous, the release of *T. gondii* proteins causes a very rapid decay involving membrane permeabilization and the release of inflammatory proteins (Zhao, Khaminets et al. 2009). Clearly, a dismantling of the host cell to this extent would be unfavorable for *Plasmodium* and it might have developed specific inhibitory mechanisms to shift the host cell death after PVM rupture to a less drastic outcome.

Several such mechanisms have been tentatively identified. As mentioned above, the cysteine protease inhibitor PbICP was recently found to be secreted into the host cell upon PVM breakdown and might act on a variety of host cell cysteine proteases (Rennenberg, Lehmann et al. 2010). In addition, in *P. falciparum* blood stages the parasite has been shown to hijack host calpain-1 to egress from its host cell (Chandramohanadas, Davis et al. 2009). The precise mechanism is yet unknown, but appears to involve activation by an intracellular rise in calcium levels and a subsequent remodelling of the cytoskeleton. It has been suggested that similar events might occur in the liver stage of *Plasmodium*, but that the uptake of calcium by merozoites limits the activity of calpain, leading to detachment instead of lysis of the host cell (Heussler, Rennenberg et al. 2010). Here also, depletion of energy might play a role. So far the analysis of fixed specimen has not revealed any obvious changes in the host cell cytoskeleton. However, alterations are likely to occur during a short time period after PVM breakdown and might only be observable when imaged in a time-lapse. Hopefully, live imaging of cells with fluorescent cytoskeleton components will yield more information in the near future.

Parasite-dependent changes in the host cell cytoskeleton are also interesting in regard to merosome formation since several intracellular bacteria were shown to manipulate the cytoskeleton to wrap themselves in host cell membrane upon exiting. In *Chlamydia* infections, an egress mode termed extrusion was observed where clusters of bacteria are packaged into host cell membrane and subsequently released (Hybiske and Stephens 2007). While the underlying molecular mechanisms are not yet understood, the inhibition of actin polymerization and nucleation has been shown to block this process. In contrast to merosome formation, extrusion is not inhibited by protease inhibitors (Sturm, Amino et al. 2006; Hybiske and Stephens 2007). However, while *Plasmodium* is released into the host cell during the late liver stage, *Chlamydia* that exit via extrusion remain within their intracellular vacuole during their entire development. It is therefore possible that both pathogens target similar host cell structures, but have evolved different ways to do so. Interestingly, *Chlamydia* can alternatively exit host cells by lysing first their inclusion membrane and then the host cell membrane (Hybiske and Stephens 2007). As for *Plasmodium*, treatment with the protease inhibitor E64 inhibits the disruption of the vacuolar membrane (Sturm, Amino et al. 2006; Hybiske and Stephens 2007). Perhaps, if egress via extrusion is chosen, a bacterial protease inhibitor is produced that prevents breakdown of the inclusion membrane but also requires formation of extrusion vesicles via a mechanism that is independent of proteases. In *Plasmodium*, where breakdown of the PVM does not need to be blocked, this is not necessary and merosome formation can be initiated by proteases.

The exit mode of *Orientia tsutsugamushi* is morphologically similar to *Chlamydia* extrusion and might therefore also involve the host cell cytoskeleton (Hybiske and Stephens 2008). After intracellular replication, individual bacteria extrude from the cell and eventually pinch off into buds covered by plasma membrane (Schaechter, Bozeman et al. 1957). These buds are subsequently phagocytosed by new host cells (Ewing, Takeuchi et al. 1978; Urakami, Tsuruhara et al. 1983).

A slightly different pathway of exploiting the cytoskeleton is used by *Listeria monocytogenes*. Like *Plasmodium*, it initially disrupts a surrounding vacuole, in this case the phagosomal membrane, without disrupting the host cell membrane (Tilney and Portnoy 1989). This is mediated by the pore-forming protein listeriolysin O and bacterial phospholipases (Gaillard, Berche et al. 1987; Smith, Marquis et al. 1995). After replicating, *Listeria* uses actin filaments to push into a cellular extension that is covered by host cell membrane and ultimately taken up by the next host

cell (Tilney and Portnoy 1989). Considering the rapid movement that merozoites exhibited upon PVM breakdown, the formation of merosomes in a similar manner would be feasible if the necessary energy was supplied by the parasite itself.

The specialized host cell death likely protects the parasite from the host immune response

While many of the specifics are still unclear, the advantages *Plasmodium* draws from its particular exit mode are obvious. While it egresses from the liver into blood vessels, it needs to bypass the numerous Kupffer cells that line the sinusoids (Crispe 2009). By remaining inside an intact membrane that is derived from the host cell it masks the parasite antigens that are exposed on the merozoite surface. To phagocytes the merosomes appear to be self and they will therefore not initiate an immune response against them. The surrounding membrane additionally renders the exoerythrocytic merozoites inaccessible to components of the humoral immune response. When the merozoites are eventually released in the lung capillaries (Baer, Klotz et al. 2007), they almost immediately invade an RBC and find shelter within the next host cell membrane.

Besides safe passage to the lungs, this Trojan horse strategy might also mediate a long-term protective effect from the immune response. It has been demonstrated that some parasite material remains in the liver after the formation of merosomes (Sturm, Amino et al. 2006; Baer, Klotz et al. 2007) and that immune cells are recruited to these sites (van de Sand, Horstmann et al. 2005; Baer, Klotz et al. 2007). If the host cell membrane simply ruptured towards the end of the liver stage, necrotic material would be released that could activate an inflammatory immune response (Savill 1998; Scaffidi, Misteli et al. 2002; Shi, Evans et al. 2003). In contrast, a host cell membrane that initially remains intact and only slowly begins to expose phosphatidylserine will appear apoptotic to immigrating immune cells. Unless significant danger signals are present, the uptake of antigen from apoptotic cells leads to the release of anti-inflammatory mediators such as the transforming growth factor beta (TGF-β) and prostaglandin E2 (PGE_2) (Fadok, Bratton et al. 1998; Savill, Dransfield et al. 2002; Cvetanovic and Ucker 2004). Tolerance is promoted and in consequence an immune response against parasite antigens might be limited. It is not completely abolished because some protective immunity involving IFN-γ-producing T cells and intracellular parasite killing via nitric oxide arises after liver stage infection (Nussler, Renia et al. 1993; Klotz, Scheller et al. 1995; Doolan and Hoffman 2000; Doolan and Martinez-Alier 2006; Frevert and Nardin 2008). However, together with the suppressive effect of the parasite blood stages (Orjih and Nussenzweig 1979; Orengo, Wong et al. 2008) these mechanisms might keep the immune response to a minimum and therefore aid subsequent infections with *Plasmodium*.

It remains to be seen to what extent the parasite actively orchestrates this outcome. The identification of parasite proteins involved in the regulation of the specialized kind of host cell death is an ongoing research effort. If they can be blocked, a more necrotic host cell death might result that could ultimately strengthen the protective immune response. At the same time, the parasite might be unable to transition to the blood stage. To further understand the specifics of the host cell death and to test the proposed model of energy depletion, host cell ATP levels should be determined at different time points during late liver stage parasite development. Since death of the host cell only occurs after the parasite has been released into the host cell, it is also of great interest to understand the mechanisms behind this process. It would be interesting to know if calcium signalling plays a role in host cell death or, as in *T. gondii*, in triggering the rupture of the PVM (Moudy, Manning et al. 2001). Furthermore, live imaging could be employed to observe when

the dismantling of the host cell cytoskeleton takes place and how it allows the formation of merosomes.

In conclusion, this study demonstrates that after the invagination of the parasite membrane around merozoites the membrane of the parasitophorous vacuole breaks down. Merozoites are released into the host cell cytoplasm and distinct changes occur in the host cell. Among other effects mitochondrial disintegration, the loss of membrane proteins and an arrest of protein biosynthesis are observed. It is proposed that the release of the parasite from the parasitophorous vacuole triggers apoptosis which is then arrested at an early stage due to energy depletion. During this process the membrane of the detaching host cell retains integrity and phosphatidylserine asymmetry. It forms the membrane of budding merosomes and thereby shields the parasite from the host immune response on its way to the lung. This simultaneously marks the final step in the exploitation of the hepatocyte by the *Plasmodium* parasite and the first step towards the blood stage.

CHAPTER 5: REFERENCES

Adak, T., V. P. Sharma, et al. (1998). "Studies on the Plasmodium vivax relapse pattern in Delhi, India." Am J Trop Med Hyg **59**(1): 175-9.

Alonso, P. L., J. Sacarlal, et al. (2004). "Efficacy of the RTS,S/AS02A vaccine against Plasmodium falciparum infection and disease in young African children: randomised controlled trial." Lancet **364** (9443): 1411-20.

Aly, A. S., S. A. Mikolajczak, et al. (2008). "Targeted deletion of SAP1 abolishes the expression of infectivity factors necessary for successful malaria parasite liver infection." Mol Microbiol **69**(1): 152-63.

Amino, R., D. Giovannini, et al. (2008). "Host cell traversal is important for progression of the malaria parasite through the dermis to the liver." Cell Host Microbe **3**(2): 88-96.

Amino, R., S. Thiberge, et al. (2006). "Quantitative imaging of Plasmodium transmission from mosquito to mammal." Nat Med **12**(2): 220-4.

Andrews, N. W. (1990). "The acid-active hemolysin of Trypanosoma cruzi." Exp Parasitol **71**(2): 241-4.

Andrews, N. W., C. K. Abrams, et al. (1990). "A T. cruzi-secreted protein immunologically related to the complement component C9: evidence for membrane pore-forming activity at low pH." Cell **61**(7): 1277-87.

Arachiche, A., D. Kerbiriou-Nabias, et al. (2009). "Rapid procoagulant phosphatidylserine exposure relies on high cytosolic calcium rather than on mitochondrial depolarization." Arterioscler Thromb Vasc Biol **29**(11): 1883-9.

Aurrecoechea, C. (2008). "PlasmoDB: a functional genomic database for malaria parasites." Nucleic Acids Research **Oct 31**.

Ayers, A. (2009). "Molecular Light Absorbance and Fluorescence." suite101: http://biology.suite101.com/article.cfm/molecular_light_absorbance_and_fluorescence.

Baer, K., C. Klotz, et al. (2007). "Release of hepatic Plasmodium yoelii merozoites into the pulmonary microvasculature." PLoS Pathog **3**(11): e171.

Bano, N., J. D. Romano, et al. (2007). "Cellular interactions of Plasmodium liver stage with its host mammalian cell." Int J Parasitol **37**(12): 1329-41.

Bejon, P., J. Lusingu, et al. (2008). "Efficacy of RTS,S/AS01E vaccine against malaria in children 5 to 17 months of age." N Engl J Med **359**(24): 2521-32.

Bevers, E. M., P. Comfurius, et al. (1998). "Regulatory mechanisms of transmembrane phospholipid distributions and pathophysiological implications of transbilayer lipid scrambling." Lupus **7 Suppl 2**: S126-31.

Bhanot, P., K. Schauer, et al. (2005). "A surface phospholipase is involved in the migration of plasmodium sporozoites through cells." J Biol Chem **280**(8): 6752-60.

Blackman, M. J. (2008). "Malarial proteases and host cell egress: an 'emerging' cascade." Cell Microbiol **10** (10): 1925-34.

Boya, P., B. Roques, et al. (2001). "New EMBO members' review: viral and bacterial proteins regulating apoptosis at the mitochondrial level." Embo J **20**(16): 4325-31.

Camp, J. P. and A. T. Capitano (2007). "Induction of zone-like liver function gradients in HepG2 cells by varying culture medium height." Biotechnol Prog **23**(6): 1485-91.

Carrolo, M., S. Giordano, et al. (2003). "Hepatocyte growth factor and its receptor are required for malaria infection." Nat Med **9**(11): 1363-9.

Carter and Diggs (1977). "Plasmodia of rodents." Parasitic Protozoa **3**: 359-465.

Carter, R. (2001). "Transmission blocking malaria vaccines." Vaccine **19**(17-19): 2309-14.

Castedo, M., T. Hirsch, et al. (1996). "Sequential acquisition of mitochondrial and plasma membrane alterations during early lymphocyte apoptosis." J Immunol **157**(2): 512-21.

CDC, C. f. D. C. (2009). "Malaria." CDC website: www.cdc.gov/malaria/.

Chandramohanadas, R., P. H. Davis, et al. (2009). "Apicomplexan parasites co-opt host calpains to facilitate their escape from infected cells." Science **324**(5928): 794-7.

Chattopadhyay, R., D. Rathore, et al. (2003). "PfSPATR, a Plasmodium falciparum protein containing an altered thrombospondin type I repeat domain is expressed at several stages of the parasite life cycle and is the target of inhibitory antibodies." J Biol Chem **278**(28): 25977-81.

Chen, C. H., H. Huang, et al. (2007). "A synthetic maternal-effect selfish genetic element drives population replacement in Drosophila." Science **316**(5824): 597-600.

Coppi, A., C. Pinzon-Ortiz, et al. (2005). "The Plasmodium circumsporozoite protein is proteolytically processed during cell invasion." J Exp Med **201**(1): 27-33.

Coppi, A., R. Tewari, et al. (2007). "Heparan sulfate proteoglycans provide a signal to Plasmodium sporozoites to stop migrating and productively invade host cells." Cell Host Microbe **2**(5): 316-27.

Corby-Harris, V., A. Drexler, et al. (2010). "Activation of Akt signaling reduces the prevalence and intensity of malaria parasite infection and lifespan in Anopheles stephensi mosquitoes." PLoS Pathog **6**(7): e1001003.

Cowman, A. F. and B. S. Crabb (2006). "Invasion of red blood cells by malaria parasites." Cell **124**(4): 755-66.

Cox-Singh, J., T. M. Davis, et al. (2008). "Plasmodium knowlesi malaria in humans is widely distributed and potentially life threatening." Clin Infect Dis **46**(2): 165-71.

Crispe, I. N. (2009). "The liver as a lymphoid organ." Annu Rev Immunol **27**: 147-63.

Cvetanovic, M. and D. S. Ucker (2004). "Innate immune discrimination of apoptotic cells: repression of proinflammatory macrophage transcription is coupled directly to specific recognition." J Immunol **172**(2): 880-9.

Daugas, E., S. A. Susin, et al. (2000). "Mitochondrio-nuclear translocation of AIF in apoptosis and necrosis." Faseb J **14**(5): 729-39.

Doolan, D. L. and S. L. Hoffman (2000). "The complexity of protective immunity against liver-stage malaria." J Immunol **165**(3): 1453-62.

Doolan, D. L. and N. Martinez-Alier (2006). "Immune response to pre-erythrocytic stages of malaria parasites." Curr Mol Med **6**(2): 169-85.

Eisemann, S., S. Oelsner, et al. (2009). "UV/Vis spectroscopy II." Virtuelles Analytiklabor, Department of Pharmacy and Molecular Biotechnology, University of Heidelberg: http://www.pharmaziestudenten-hd.de/analytik/uv-vis2/entheorie.html.

Enari, M., H. Sakahira, et al. (1998). "A caspase-activated DNase that degrades DNA during apoptosis, and its inhibitor ICAD." Nature **391**(6662): 43-50.

Essmann, F., H. Bantel, et al. (2003). "Staphylococcus aureus alpha-toxin-induced cell death: predominant necrosis despite apoptotic caspase activation." Cell Death Differ **10**(11): 1260-72.

Ewing, E. P., Jr., A. Takeuchi, et al. (1978). "Experimental infection of mouse peritoneal mesothelium with scrub typhus rickettsiae: an ultrastructural study." Infect Immun **19**(3): 1068-75.

Fadok, V. A., D. L. Bratton, et al. (1998). "Macrophages that have ingested apoptotic cells in vitro inhibit proinflammatory cytokine production through autocrine/paracrine mechanisms involving TGF-beta, PGE2, and PAF." J Clin Invest **101**(4): 890-8.

Fidock, D. A., E. Bottius, et al. (1994). "Cloning and characterization of a novel Plasmodium falciparum sporozoite surface antigen, STARP." Mol Biochem Parasitol **64**(2): 219-32.

Fink, S. L. and B. T. Cookson (2005). "Apoptosis, pyroptosis, and necrosis: mechanistic description of dead and dying eukaryotic cells." Infect Immun **73**(4): 1907-16.

Flegel, K. M. (1976). "Symptoms and signs of malaria." Can Med Assoc J **115**(5): 409-10.

Flors, C., M. J. Fryer, et al. (2006). "Imaging the production of singlet oxygen in vivo using a new fluorescent sensor, Singlet Oxygen Sensor Green." J Exp Bot **57**(8): 1725-34.

Foley, M. and L. Tilley (1998). "Protein trafficking in malaria-infected erythrocytes." Int J Parasitol **28**(11): 1671-80.

Frank, S., B. Gaume, et al. (2001). "The role of dynamin-related protein 1, a mediator of mitochondrial fission, in apoptosis." Dev Cell **1**(4): 515-25.

Frevert, U., S. Engelmann, et al. (2005). "Intravital observation of Plasmodium berghei sporozoite infection of the liver." PLoS Biol **3**(6): e192.

Frevert, U. and E. Nardin (2008). "Cellular effector mechanisms against Plasmodium liver stages." Cell Microbiol **10**(10): 1956-67.

Gaillard, J. L., P. Berche, et al. (1987). "In vitro model of penetration and intracellular growth of Listeria monocytogenes in the human enterocyte-like cell line Caco-2." Infect Immun **55**(11): 2822-9.

Genton, B. (2008). "Malaria vaccines: a toy for travelers or a tool for eradication?" Expert Rev Vaccines **7**(5): 597-611.

Gollin, D. and C. Zimmermann (2007). "Malaria: Disease impacts and long-run income differences." Institute for the study of labor website(http://ftp.iza.org/dp2997.pdf).

Gonzalez, L. J., E. Gibbons, et al. (2009). "The influence of membrane physical properties on microvesicle release in human erythrocytes." PMC Biophys **2**(1): 7.

Graewe, S., S. Retzlaff, et al. (2009). "Going live: a comparative analysis of the suitability of the RFP derivatives RedStar, mCherry and tdTomato for intravital and in vitro live imaging of Plasmodium parasites." Biotechnol J **4**(6): 895-902.

Greenwood, B. M., K. Bojang, et al. (2005). "Malaria." Lancet **365**(9469): 1487-98.

Haldar, K., S. C. Murphy, et al. (2007). "Malaria: mechanisms of erythrocytic infection and pathological correlates of severe disease." Annu Rev Pathol **2**: 217-49.

Herman, B., M. J. Parry-Hill, et al. (2010). "Photobleaching." Olympus Microscopy Resource Center: http://www.olympusmicro.com/primer/java/fluorescence/photobleaching/index.html.

Heussler, V., A. Rennenberg, et al. (2010). "Host cell death induced by the egress of intracellular Plasmodium parasites." Apoptosis **15**(3): 376-85.

Hoffman, S. L., L. M. Goh, et al. (2002). "Protection of humans against malaria by immunization with radiation-attenuated Plasmodium falciparum sporozoites." J Infect Dis **185**(8): 1155-64.

Hybiske, K. and R. S. Stephens (2007). "Mechanisms of host cell exit by the intracellular bacterium Chlamydia." Proc Natl Acad Sci U S A **104**(27): 11430-5.

Hybiske, K. and R. S. Stephens (2008). "Exit strategies of intracellular pathogens." Nat Rev Microbiol **6**(2): 99-110.

Ishino, T., B. Boisson, et al. (2009). "LISP1 is important for the egress of Plasmodium berghei parasites from liver cells." Cell Microbiol **11**(9): 1329-39.

Ishino, T., Y. Chinzei, et al. (2005). "A Plasmodium sporozoite protein with a membrane attack complex domain is required for breaching the liver sinusoidal cell layer prior to hepatocyte infection." Cell Microbiol **7**(2): 199-208.

Ishino, T., Y. Chinzei, et al. (2005). "Two proteins with 6-cys motifs are required for malarial parasites to commit to infection of the hepatocyte." Mol Microbiol **58**(5): 1264-75.

Ishino, T., K. Yano, et al. (2004). "Cell-passage activity is required for the malarial parasite to cross the liver sinusoidal cell layer." PLoS Biol **2**(1): E4.

Ito, J., A. Ghosh, et al. (2002). "Transgenic anopheline mosquitoes impaired in transmission of a malaria parasite." Nature **417**(6887): 452-5.

Jaeschke, H. and J. J. Lemasters (2003). "Apoptosis versus oncotic necrosis in hepatic ischemia/reperfusion injury." Gastroenterology **125**(4): 1246-57.

Janse, C. J., J. Ramesar, et al. (2006). "High-efficiency transfection and drug selection of genetically transformed blood stages of the rodent malaria parasite Plasmodium berghei." Nat Protoc **1**(1): 346-56.

Jensen, A. T., P. Magistrado, et al. (2004). "Plasmodium falciparum associated with severe childhood malaria preferentially expresses PfEMP1 encoded by group A var genes." J Exp Med **199**(9): 1179-90.

Jethwaney, D., T. Lepore, et al. (2005). "Fetuin-A, a hepatocyte-specific protein that binds Plasmodium berghei thrombospondin-related adhesive protein: a potential role in infectivity." Infect Immun **73**(9): 5883-91.

Jobe, O., G. Donofrio, et al. (2009). "Immunization with radiation-attenuated Plasmodium berghei sporozoites induces liver cCD8alpha+DC that activate CD8+T cells against liver-stage malaria." PLoS One **4**(4): e5075.

Jobe, O., J. Lumsden, et al. (2007). "Genetically attenuated Plasmodium berghei liver stages induce sterile protracted protection that is mediated by major histocompatibility complex Class I-dependent interferon-gamma-producing CD8+ T cells." J Infect Dis **196**(4): 599-607.

Johnson, I. D. and M. W. Davidson (2010). "Jablonski Energy Diagram." Olympus Microscopy Resource Center: http://www.olympusmicro.com/primer/java/jablonski/jabintro/index.html.

Kafsack, B. F., J. D. Pena, et al. (2009). "Rapid membrane disruption by a perforin-like protein facilitates parasite exit from host cells." Science **323**(5913): 530-3.

Kaiser, F. H., K. A. Bienz, et al. (1998). "Medizinische Mikrobiologie." (Georg Thieme Verlag).

Kaiser, K., N. Camargo, et al. (2004). "A member of a conserved Plasmodium protein family with membrane-attack complex/perforin (MACPF)-like domains localizes to the micronemes of sporozoites." Mol Biochem Parasitol **133**(1): 15-26.

Kappe, S., T. Bruderer, et al. (1999). "Conservation of a gliding motility and cell invasion machinery in Apicomplexan parasites." J Cell Biol **147**(5): 937-44.

Kariu, T., T. Ishino, et al. (2006). "CelTOS, a novel malarial protein that mediates transmission to mosquito and vertebrate hosts." Mol Microbiol **59**(5): 1369-79.

Karnasuta, C., K. Pavanand, et al. (1995). "Complete development of the liver stage of Plasmodium falciparum in a human hepatoma cell line." Am J Trop Med Hyg **53**(6): 607-11.

Kim, J. A., Y. S. Kang, et al. (1998). "Role of Ca2+ influx in the tert-butyl hydroperoxide-induced apoptosis of HepG2 human hepatoblastoma cells." Exp Mol Med **30**(3): 137-44.

Kim, Y. E., J. Chen, et al. (2009). "Engineering a polarity-sensitive biosensor for time-lapse imaging of apoptotic processes and degeneration." Nat Methods **7**(1): 67-73.

Klotz, C. and U. Frevert (2008). "Plasmodium yoelii sporozoites modulate cytokine profile and induce apoptosis in murine Kupffer cells." Int J Parasitol **38**(14): 1639-50.

Klotz, F. W., L. F. Scheller, et al. (1995). "Co-localization of inducible-nitric oxide synthase and Plasmodium berghei in hepatocytes from rats immunized with irradiated sporozoites." J Immunol **154**(7): 3391-5.

Knop, M., F. Barr, et al. (2002). "Improved version of the red fluorescent protein (drFP583/DsRed/RFP)." Biotechniques **33**(3): 592, 594, 596-8 passim.

Kochevar, I. E., M. C. Lynch, et al. (2000). "Singlet oxygen, but not oxidizing radicals, induces apoptosis in HL-60 cells." Photochem Photobiol **72**(4): 548-53.

Kornberg, R. D. and H. M. McConnell (1971). "Inside-outside transitions of phospholipids in vesicle membranes." Biochemistry **10**(7): 1111-20.

Kozjak-Pavlovic, V., E. A. Dian-Lothrop, et al. (2009). "Bacterial porin disrupts mitochondrial membrane potential and sensitizes host cells to apoptosis." PLoS Pathog **5**(10): e1000629.

Krishna, S., S. Pulcini, et al. (2008). "Artemisinins and the biological basis for the PfATP6/SERCA hypothesis." Trends Parasitol.

Kroemer, G. and J. C. Reed (2000). "Mitochondrial control of cell death." Nat Med **6**(5): 513-9.

Kuida, K., T. F. Haydar, et al. (1998). "Reduced apoptosis and cytochrome c-mediated caspase activation in mice lacking caspase 9." Cell **94**(3): 325-37.

Kumar, K. A., P. Baxter, et al. (2009). "Conserved protective mechanisms in radiation and genetically attenuated uis3(-) and uis4(-) Plasmodium sporozoites." PLoS One **4**(2): e4480.

Kumar, K. A., C. R. Garcia, et al. (2007). "Exposure of Plasmodium sporozoites to the intracellular concentration of potassium enhances infectivity and reduces cell passage activity." Mol Biochem Parasitol **156**(1): 32-40.

Labaied, M., A. Harupa, et al. (2007). "Plasmodium yoelii sporozoites with simultaneous deletion of P52 and P36 are completely attenuated and confer sterile immunity against infection." Infect Immun **75**(8): 3758-68.

Leach, M. R. (2009). "Diradical Chemistry." The Chemogenesis web book: http://www.meta-synthesis.com/webbook/16_diradical/diradical.html.

Leiriao, P., S. S. Albuquerque, et al. (2005). "HGF/MET signalling protects Plasmodium-infected host cells from apoptosis." Cell Microbiol **7**(4): 603-9.

Liu, X., H. Zou, et al. (1997). "DFF, a heterodimeric protein that functions downstream of caspase-3 to trigger DNA fragmentation during apoptosis." Cell **89**(2): 175-84.

Lopez, R., J. Garcia, et al. (2003). "Identification of specific Hep G2 cell binding regions in Plasmodium falciparum sporozoite-threonine-asparagine-rich protein (STARP)." Vaccine **21**(19-20): 2404-11.

Malhi, H., G. J. Gores, et al. (2006). "Apoptosis and necrosis in the liver: a tale of two deaths?" Hepatology **43**(2 Suppl 1): S31-44.

MAP, M. A. P. (2007). Malaria Atlas Project website: http://www.map.ox.ac.uk/.

Martin, S. J., D. M. Finucane, et al. (1996). "Phosphatidylserine externalization during CD95-induced apoptosis of cells and cytoplasts requires ICE/CED-3 protease activity." J Biol Chem **271**(46): 28753-6.

Matuschewski, K. (2006). "Vaccine development against malaria." Curr Opin Immunol **18**(4): 449-57.

Matuschewski, K. and H. Schuler (2008). "Actin/myosin-based gliding motility in apicomplexan parasites." Subcell Biochem **47**: 110-20.

Meis, J. F., P. H. Jap, et al. (1983). "Ultrastructural studies of a vesicle system associated with endoplasmic reticulum in exo-erythrocytic forms of Plasmodium berghei." J Protozool **30**(1): 111-4.

Meis, J. F., J. P. Verhave, et al. (1985). "Fine structure of exoerythrocytic merozoite formation of Plasmodium berghei in rat liver." J Protozool **32**(4): 694-9.

Mendis, K., B. J. Sina, et al. (2001). "The neglected burden of Plasmodium vivax malaria." Am J Trop Med Hyg **64**(1-2 Suppl): 97-106.

Merzlyak, E. M., J. Goedhart, et al. (2007). "Bright monomeric red fluorescent protein with an extended fluorescence lifetime." Nat Methods **4**(7): 555-7.

Mitchell, G. H., A. W. Thomas, et al. (2004). "Apical membrane antigen 1, a major malaria vaccine candidate, mediates the close attachment of invasive merozoites to host red blood cells." Infect Immun **72**(1): 154-8.

Morahan, B. J., L. Wang, et al. (2009). "No TRAP, no invasion." Trends Parasitol **25**(2): 77-84.

Moreira, M. E. and M. A. Barcinski (2004). "Apoptotic cell and phagocyte interplay: recognition and consequences in different cell systems." An Acad Bras Cienc **76**(1): 93-115.

Mota, M. M., J. C. Hafalla, et al. (2002). "Migration through host cells activates Plasmodium sporozoites for infection." Nat Med **8**(11): 1318-22.

Mota, M. M., G. Pradel, et al. (2001). "Migration of Plasmodium sporozoites through cells before infection." Science **291**(5501): 141-4.

Moudy, R., T. J. Manning, et al. (2001). "The loss of cytoplasmic potassium upon host cell breakdown triggers egress of Toxoplasma gondii." J Biol Chem **276**(44): 41492-501.

Mueller, A. K., N. Camargo, et al. (2005). "Plasmodium liver stage developmental arrest by depletion of a protein at the parasite-host interface." Proc Natl Acad Sci U S A **102**(8): 3022-7.

Mueller, A. K., M. Deckert, et al. (2007). "Genetically attenuated Plasmodium berghei liver stages persist and elicit sterile protection primarily via CD8 T cells." Am J Pathol **171**(1): 107-15.

Mueller, A. K., M. Labaied, et al. (2005). "Genetically modified Plasmodium parasites as a protective experimental malaria vaccine." Nature **433**(7022): 164-7.

Muller, A., D. Gunther, et al. (1999). "Neisserial porin (PorB) causes rapid calcium influx in target cells and induces apoptosis by the activation of cysteine proteases." Embo J **18**(2): 339-52.

Nagamune, K., L. M. Hicks, et al. (2008). "Abscisic acid controls calcium-dependent egress and development in Toxoplasma gondii." Nature **451**(7175): 207-10.

Noronha, F. S., J. S. Cruz, et al. (2000). "Macrophage damage by Leishmania amazonensis cytolysin: evidence of pore formation on cell membrane." Infect Immun **68**(8): 4578-84.

Nussenzweig, R. (1980). "Use of radiation-attenuated sporozoites in the immunoprophylaxis of malaria." Int J Nucl Med Biol **7**(2): 89-96.

Nussler, A. K., L. Renia, et al. (1993). "In vivo induction of the nitric oxide pathway in hepatocytes after injection with irradiated malaria sporozoites, malaria blood parasites or adjuvants." Eur J Immunol **23**(4): 882-7.

Ocana-Morgner, C., M. M. Mota, et al. (2003). "Malaria blood stage suppression of liver stage immunity by dendritic cells." J Exp Med **197**(2): 143-51.

Ocana-Morgner, C., K. A. Wong, et al. (2007). "Role of TGF-beta and PGE2 in T cell responses during Plasmodium yoelii infection." Eur J Immunol **37**(6): 1562-74.

Ono, T., L. Cabrita-Santos, et al. (2008). "Adenylyl cyclase alpha and cAMP signaling mediate Plasmodium sporozoite apical regulated exocytosis and hepatocyte infection." PLoS Pathog **4**(2): e1000008.

Orengo, J. M., K. A. Wong, et al. (2008). "A Plasmodium yoelii soluble factor inhibits the phenotypic maturation of dendritic cells." Malar J **7**: 254.

Orjih, A. U. and R. S. Nussenzweig (1979). "Plasmodium berghei: suppression of antibody response to sporozoite stage by acute blood stage infection." Clin Exp Immunol **38**(1): 1-8.

Pandey, A. V., B. L. Tekwani, et al. (1999). "Artemisinin, an endoperoxide antimalarial, disrupts the hemoglobin catabolism and heme detoxification systems in malarial parasite." J Biol Chem **274**(27): 19383-8.

Partikian, A., B. Olveczky, et al. (1998). "Rapid diffusion of green fluorescent protein in the mitochondrial matrix." J Cell Biol **140**(4): 821-9.

Pasquetto, V., D. A. Fidock, et al. (1997). "Plasmodium falciparum sporozoite invasion is inhibited by naturally acquired or experimentally induced polyclonal antibodies to the STARP antigen." Eur J Immunol **27**(10): 2502-13.

Petit, F., D. Arnoult, et al. (2002). "Productive HIV-1 infection of primary CD4+ T cells induces mitochondrial membrane permeabilization leading to a caspase-independent cell death." J Biol Chem **277**(2): 1477-87.

Pinder, J., R. Fowler, et al. (2000). "Motile systems in malaria merozoites: how is the red blood cell invaded?" Parasitol Today **16**(6): 240-5.

Pinzon-Charry, A. and M. F. Good (2008). "Malaria vaccines: the case for a whole-organism approach." Expert Opin Biol Ther **8**(4): 441-8.

Pinzon-Ortiz, C., J. Friedman, et al. (2001). "The binding of the circumsporozoite protein to cell surface heparan sulfate proteoglycans is required for plasmodium sporozoite attachment to target cells." J Biol Chem **276**(29): 26784-91.

Plebanski, M., E. Locke, et al. (2008). "Malaria vaccines: into a mirror, darkly?" Trends Parasitol **24**(12): 532-6.

Pradel, G. and U. Frevert (2001). "Malaria sporozoites actively enter and pass through rat Kupffer cells prior to hepatocyte invasion." Hepatology **33**(5): 1154-65.

Pradel, G., S. Garapaty, et al. (2002). "Proteoglycans mediate malaria sporozoite targeting to the liver." Mol Microbiol **45**(3): 637-51.

Prudencio, M., A. Rodriguez, et al. (2006). "The silent path to thousands of merozoites: the Plasmodium liver stage." Nat Rev Microbiol **4**(11): 849-56.

Purcell, L. A., S. K. Yanow, et al. (2008). "Chemical attenuation of Plasmodium berghei sporozoites induces sterile immunity in mice." Infect Immun **76**(3): 1193-9.

Rankin, K. E., S. Graewe, et al. (2010). "Imaging liver-stage malaria parasites." Cell Microbiol **12**(5): 569-79.

Rappaport, L., P. Oliviero, et al. (1998). "Cytoskeleton and mitochondrial morphology and function." Mol Cell Biochem **184**(1-2): 101-5.

Reeder, J. C. and G. V. Brown (1996). "Antigenic variation and immune evasion in Plasmodium falciparum malaria." Immunol Cell Biol **74**(6): 546-54.

Renn, A., J. Seelig, et al. (2006). "Oxygen-dependent photochemistry of fluorescent dyes studied at the single molecule level." Molecular Physics **104**(3): 409-414.

Rennenberg, A., C. Lehmann, et al. (2010). "Exoerythrocytic Plasmodium parasites secrete a cysteine protease inhibitor involved in sporozoite invasion and capable of blocking cell death of host hepatocytes." PLoS Pathog **6**(3): e1000825.

RKI, R. K. I. (2010). "SurvStat." SurvStat website: www3.rki.de/SurvStat/.

Ro, D. K., E. M. Paradise, et al. (2006). "Production of the antimalarial drug precursor artemisinic acid in engineered yeast." Nature **440**(7086): 940-3.

Rosenthal, P. J. and S. R. Meshnick (1996). "Hemoglobin catabolism and iron utilization by malaria parasites." Mol Biochem Parasitol **83**(2): 131-9.

Rowe, J. A., J. M. Moulds, et al. (1997). "P. falciparum rosetting mediated by a parasite-variant erythrocyte membrane protein and complement-receptor 1." Nature **388**(6639): 292-5.

Sachs, J. and P. Malaney (2002). "The economic and social burden of malaria." Nature **415**(6872): 680-5.

Salmon, B. L., A. Oksman, et al. (2001). "Malaria parasite exit from the host erythrocyte: a two-step process requiring extraerythrocytic proteolysis." Proc Natl Acad Sci U S A **98**(1): 271-6.

Savill, J. (1998). "Apoptosis. Phagocytic docking without shocking." Nature **392**(6675): 442-3.

Savill, J., I. Dransfield, et al. (2002). "A blast from the past: clearance of apoptotic cells regulates immune responses." Nat Rev Immunol **2**(12): 965-75.

Scaffidi, P., T. Misteli, et al. (2002). "Release of chromatin protein HMGB1 by necrotic cells triggers inflammation." Nature **418**(6894): 191-5.

Schaechter, M., F. M. Bozeman, et al. (1957). "Study on the growth of Rickettsiae. II. Morphologic observations of living Rickettsiae in tissue culture cells." Virology **3**(1): 160-72.

Schneider-Poetsch, T., J. Ju, et al. (2010). "Inhibition of eukaryotic translation elongation by cycloheximide and lactimidomycin." Nat Chem Biol **6**(3): 209-217.

Shakibaei, M. and U. Frevert (1996). "Dual interaction of the malaria circumsporozoite protein with the low density lipoprotein receptor-related protein (LRP) and heparan sulfate proteoglycans." J Exp Med **184**(5): 1699-711.

Shaner, N. C., R. E. Campbell, et al. (2004). "Improved monomeric red, orange and yellow fluorescent proteins derived from Discosoma sp. red fluorescent protein." Nat Biotechnol **22**(12): 1567-72.

Sheffield Hallam University, B. D. (2010). "UV-Vis Luminescence Spectroscopy, Theoretical principles." Biosciences Division, Faculty of Health and Well-being, Sheffield Hallam University: http://teaching.shu.ac.uk/hwb/chemistry/tutorials/molspec/lumin1.htm.

Sherman, I. W. (2005). "Molecular approaches to malaria." (ASM Press).

Shi, Y., J. E. Evans, et al. (2003). "Molecular identification of a danger signal that alerts the immune system to dying cells." Nature **425**(6957): 516-21.

Shililu, J. I., G. M. Tewolde, et al. (2003). "Efficacy of Bacillus thuringiensis israelensis, Bacillus sphaericus and temephos for managing Anopheles larvae in Eritrea." J Am Mosq Control Assoc **19**(3): 251-8.

Shorte, S. L. and F. Frischknecht (2007). "Imaging cellular and molecular biological functions." (Springer): 354 ff.

Shu, X., N. C. Shaner, et al. (2006). "Novel chromophores and buried charges control color in mFruits." Biochemistry **45**(32): 9639-47.

Silvie, O., J. F. Franetich, et al. (2004). "A role for apical membrane antigen 1 during invasion of hepatocytes by Plasmodium falciparum sporozoites." J Biol Chem **279**(10): 9490-6.

Silvie, O., K. Goetz, et al. (2008). "A sporozoite asparagine-rich protein controls initiation of Plasmodium liver stage development." PLoS Pathog **4**(6): e1000086.

Silvie, O., E. Rubinstein, et al. (2003). "Hepatocyte CD81 is required for Plasmodium falciparum and Plasmodium yoelii sporozoite infectivity." Nat Med **9**(1): 93-6.

Sinnis, P. and A. Coppi (2007). "A long and winding road: the Plasmodium sporozoite's journey in the mammalian host." Parasitol Int **56**(3): 171-8.

Smith, G. A., H. Marquis, et al. (1995). "The two distinct phospholipases C of Listeria monocytogenes have overlapping roles in escape from a vacuole and cell-to-cell spread." Infect Immun **63**(11): 4231-7.

Soldati-Favre, D. (2008). "Molecular dissection of host cell invasion by the apicomplexans: the glideosome." Parasite **15**(3): 197-205.

Soni, S., S. Dhawan, et al. (2005). "Characterization of events preceding the release of malaria parasite from the host red blood cell." Blood Cells Mol Dis **35**(2): 201-11.

Stanway, R. R., S. Graewe, et al. (2009). "Highly efficient subcloning of rodent malaria parasites by injection of single merosomes or detached cells." Nat Protoc **4**(10): 1433-9.

Stanway, R. R., T. Witt, et al. (2009). "GFP-targeting allows visualization of the apicoplast throughout the life cycle of live malaria parasites." Biol Cell **101**(7): 415-30, 5 p following 430.

Stewart, M. J. and J. P. Vanderberg (1991). "Malaria sporozoites release circumsporozoite protein from their apical end and translocate it along their surface." J Protozool **38**(4): 411-21.

Sturm, A., R. Amino, et al. (2006). "Manipulation of host hepatocytes by the malaria parasite for delivery into liver sinusoids." Science **313**(5791): 1287-90.

Sturm, A., S. Graewe, et al. (2009). "Alteration of the parasite plasma membrane and the parasitophorous vacuole membrane during exo-erythrocytic development of malaria parasites." Protist **160**(1): 51-63.

Sturm, A. and V. Heussler (2007). "Live and let die: manipulation of host hepatocytes by exoerythrocytic Plasmodium parasites." Med Microbiol Immunol **196**(3): 127-33.

Sullivan, D. J. (2002). "Theories on malarial pigment formation and quinoline action." Int J Parasitol **32**(13): 1645-53.

Sulpice, J. C., A. Zachowski, et al. (1994). "Requirement for phosphatidylinositol 4,5-bisphosphate in the Ca (2+)-induced phospholipid redistribution in the human erythrocyte membrane." J Biol Chem **269**(9): 6347-54.

Tang, H. L., H. L. Lung, et al. (2008). "Vimentin supports mitochondrial morphology and organization." Biochem J **410**(1): 141-6.

Thiberge, S., S. Blazquez, et al. (2007). "In vivo imaging of malaria parasites in the murine liver." Nat Protoc **2**(7): 1811-8.

Tilney, L. G. and D. A. Portnoy (1989). "Actin filaments and the growth, movement, and spread of the intracellular bacterial parasite, Listeria monocytogenes." J Cell Biol **109**(4 Pt 1): 1597-608.

Trampuz, A., M. Jereb, et al. (2003). "Clinical review: Severe malaria." Crit Care **7**(4): 315-23.

Urakami, H., T. Tsuruhara, et al. (1983). "Penetration of Rickettsia tsutsugamushi into cultured mouse fibroblasts (L cells): an electron microscopic observation." Microbiol Immunol **27**(3): 251-63.

Usynin, I., C. Klotz, et al. (2007). "Malaria circumsporozoite protein inhibits the respiratory burst in Kupffer cells." Cell Microbiol **9**(11): 2610-28.

van de Sand, C., S. Horstmann, et al. (2005). "The liver stage of Plasmodium berghei inhibits host cell apoptosis." Mol Microbiol **58**(3): 731-42.

van Dijk, M. R., B. Douradinha, et al. (2005). "Genetically attenuated, P36p-deficient malarial sporozoites induce protective immunity and apoptosis of infected liver cells." Proc Natl Acad Sci U S A **102**(34): 12194-9.

van Schaijk, B. C., C. J. Janse, et al. (2008). "Gene disruption of Plasmodium falciparum p52 results in attenuation of malaria liver stage development in cultured primary human hepatocytes." PLoS One **3**(10): e3549.

Vincke, I. H. and M. Lips (1948). "Un noveau plasmodium d'un rongeur sauvage du Congo: Plasmodium berghei n. sp." Annales de la Societe Belge de Medecine Tropicale **28**: 97-104.

Walther, M. (2006). "Advances in vaccine development against the pre-erythrocytic stage of Plasmodium falciparum malaria." Expert Rev Vaccines **5**(1): 81-93.

Wang, J., L. Huang, et al. (2010). "Artemisinin directly targets malarial mitochondria through its specific mitochondrial activation." PLoS One **5**(3): e9582.

WHO (2008). "World Malaria Report." WHO website: www.who.int/malaria/wmr2008/

WHO (2010). "Economic costs of malaria." Roll back malaria website: http://www.rollbackmalaria.org/cmc_upload/0/000/015/363/RBMInfosheet_10.pdf.

WHO (2010). "Fact Sheet Malaria." WHO website **94**: www.who.int/mediacentre/factsheets/fs094/en/.

Wickham, M. E., J. G. Culvenor, et al. (2003). "Selective inhibition of a two-step egress of malaria parasites from the host erythrocyte." J Biol Chem **278**(39): 37658-63.

Yang, J. L., L. C. Wang, et al. (1999). "Singlet oxygen is the major species participating in the induction of DNA strand breakage and 8-hydroxydeoxyguanosine adduct by lead acetate." Environ Mol Mutagen **33** (3): 194-201.

Yeoh, S., R. A. O'Donnell, et al. (2007). "Subcellular discharge of a serine protease mediates release of invasive malaria parasites from host erythrocytes." Cell **131**(6): 1072-83.

Ying, P., M. Shakibaei, et al. (1997). "The malaria circumsporozoite protein: interaction of the conserved regions I and II-plus with heparin-like oligosaccharides in heparan sulfate." Exp Parasitol **85**(2): 168-82.

Zhao, Y. O., A. Khaminets, et al. (2009). "Disruption of the Toxoplasma gondii parasitophorous vacuole by IFNgamma-inducible immunity-related GTPases (IRG proteins) triggers necrotic cell death." PLoS Pathog **5**(2): e1000288.

Zhou, P., L. Qian, et al. (2005). "Nitric oxide inhibits caspase activation and apoptotic morphology but does not rescue neuronal death." J Cereb Blood Flow Metab **25**(3): 348-57.

Zhou, Z., L. Xiao, et al. (2002). "Antibody responses to repetitive epitopes of the circumsporozoite protein, liver stage antigen-1, and merozoite surface protein-2 in infants residing in a Plasmodium falciparum-hyperendemic area of western Kenya. XIII. Asembo Bay Cohort Project." Am J Trop Med Hyg **66**(1): 7-12.

Zou, H., Y. Li, et al. (1999). "An APAF-1.cytochrome c multimeric complex is a functional apoptosome that activates procaspase-9." J Biol Chem **274**(17): 11549-56.

ACKNOWLEDGEMENTS

I would like to thank Prof. Dr. Volker Heussler for supervising my PhD study and for agreeing to review it. Thank you that your door was always open for questions, advice and discussion - even when at the end that door was a country away.

I would also like to express my gratitude to Prof. Dr. Iris Bruchhaus for her advice and for agreeing to review this study.

A number of people contributed to making this study possible by kindly providing various reagents. I would like to thank Prof. Dr. Roger Y. Tsien from the University of California San Diego (USA) for the mFruit cDNA constructs, Prof. Dr. Anthony Holder from the National Institute for Medical Research (London, UK) for the α-MSP-1 antibody, Dr. Yujin Kim from the University of Southern California (USA) for pSIVA and Prof. Dr. Isabelle Tardieux from the Universite Paris Descartes (France) for the pDisplay-mCherry plasmid construct.

To all past and present members of the Heussler Lab: thank you for being such great colleagues! I had lots of fun working with you and am looking forward to coming back in November!

I very much appreciate that Dr. Kathleen Rankin and Ben Mulhall proofread this thesis and made sure it complied with the rules of the English language. Thanks guys!

Last but not least and more than anything I would like to thank my family and friends, without whom I could not have done this. Thanks for always being there when I need you!

Drinks on me after this is done!